MRI and Computational Modeling of In Vivo Muscle-Tendon Architecture and Function

---

A Dissertation

Presented to

the faculty of the School of Engineering and Applied Science

University of Virginia

---

in partial fulfillment

of the requirements for the degree

Doctor of Philosophy

by

Geoffrey Gale Handsfield

December

2014

APPROVAL SHEET

The dissertation

is submitted in partial fulfillment of the requirements

for the degree of

Doctor of Philosophy

AUTHOR

The dissertation has been read and approved by the examining committee:

Silvia S. Blemker

Advisor

Craig Meyer

Shayn Peirce-Cottler

Jeffrey Holmes

Joseph Hart

Mark Abel

Accepted for the School of Engineering and Applied Science:

Dean, School of Engineering and Applied Science

December

2014

Abstract

Musculoskeletal tissues have an incredible structure-function relationship. The size and shape of skeletal muscles and tendons are closely related to their functional capacity. Understanding the function and mechanics of these tissues begins with a strong foundational understanding of their size and shape. The current knowledge of human muscle architecture is based on cadaver dissection which is limited by the old age, poor health, and limited subject pool of cadaver donors. Modern medical imaging avoids these limitations and allows for muscle architecture data to be obtained *in vivo* from healthy subjects ranging in size. Medical imaging can be extended to the muscles of pathological populations such as cerebral palsy and elite athletic populations such as sprint runners. Coupled with knowledge of the muscle sizes in healthy subjects *in vivo*, these assessments can be used to quantify muscle impairments for pathological populations or quantify muscle hypertrophy patterns due to exercise for athletic populations. Additionally, modern medical imaging approaches allow for the determination of tendon architecture *in vivo* which can be used to create computational finite element models to simulate and probe the mechanics of tendon function. In the case of the Achilles tendon, these sophisticated approaches may be used to elucidate previously unexplained observations of complex, non-uniform tendon deformations. In this dissertation, I utilize non-Cartesian magnetic resonance imaging (MRI) to generate a comprehensive data set of muscle lengths and volumes in the lower limbs of 24 healthy subjects. Using these data, I explore size scaling relationships in the human lower limb, develop a metric for assessing muscle sizes in populations of interest, and extend this to two populations: subjects with cerebral palsy and competitive collegiate sprinters. I go on to use non-Cartesian MRI and finite element modeling to explore the effects of Achilles tendon morphology on non-uniform tendon displacements in the Achilles.

Acknowledgments

When I began the journey of my doctoral education five years ago, I had only vague ideas about what would be in store for me. This path that I have taken has given me the opportunity to explore the muscles of the human body in new ways, to undertake advanced imaging approaches, to build models and come to new insights, and to learn from great scientific minds in my teachers and peers at the University of Virginia. It has also given me moments of anxiety, misunderstanding, heartache, and doubt. I have been fortunate that these moments have been brief and have always been interspersed with bright moments: joy at undertaking research worth pursuing, the happy constancy of progressive work toward a goal, and the sheer elation of discovering something new. The greatest joy in science, however, is to simply gain an understanding of something fundamental about the world we live in. In these moments of new understanding, science reveals itself to the scientist and one cannot help but see consistencies across ideas, a heightened understanding of things previously learned, and the great interconnectedness of science and the world. It is these moments as a scientist that make the path well worth traveling. For showing me this path and for giving me the opportunity to travel it, I have many people to whom I owe gratitude.

First and foremost, I would like to thank my research adviser, mentor, and friend Dr. Silvia Blemker. It is hard to imagine what Silvia saw in me when I applied for graduate study in her lab at UVA. I held a bachelor's degree in physics and mathematics but had very little exposure to the field of biomedical engineering. I like to think that Silvia saw in me a raw interest in imaging and muscles and a fundamental desire to learn. Whatever it was, Silvia's accepting me into her lab and mentoring me along the way—teaching me biomechanics, allowing me to chart a course through my research, fostering my teaching skills, shaping my perspectives on the importance of clinical questions in biomechanics research, and generally striking an ideal balance between independence and supervision of my graduate work—has been much appreciated. I would not be where I am now without Silvia's guidance and support. Silvia, working with you has been a privilege.

I would like to thank my committee members for agreeing to supervise the progress of this dissertation. To Craig Meyer, thank you for teaching me imaging, for supporting my very first graduate research project, for mentoring my teaching efforts on the path to becoming a professor, and for your open-mindedness on applying imaging to crazy and not-so-crazy musculoskeletal projects. To Shayn Peirce-Cottler, thanks for your perspectives on the role of modeling in biomedical research and for help with random animal experiments along the way. It was a pleasure and a privilege to work with you on graduate recruiting efforts. Thanks for keeping it fun! To Jeff Holmes, thanks for teaching me physiology, biomechanical modeling, and for shaping my perspectives on how one should approach biomedical science. To Joe Hart, the casual conversations that we've had on muscular anatomy and function have been more helpful than you probably realized. Thanks for helping me learn muscles and for your support in navigating protocols and in our shared research projects in general. To Mark Abel, thank you for your critical feedback on the role of imaging information in cerebral palsy. If biomedical engineering is a synthesis between technology and clinical need, you have

been the reasoned voice of clinical needs and pragmatism. Thank you for serving in this role and for giving me opportunities to become more clinically aware.

To co-authors Wilson Miller, Katie Knaus, Nic Fiorentino, Laura Slane, and Darryl Thelen- thanks for your willingness to collaborate and to teach me new concepts. Biomedical engineering is both a 'team sport' and an inter-disciplinary field. I am grateful to each of you for your help and all of the work that you've done toward understanding the muscles and tendons of the lower limb!

I would like to thank the faculty of the Department of Biomedical Engineering and, more broadly, the School of Engineering and Applied Science at the University of Virginia. Your passion for teaching and willingness to interact with students has been a major benefit to my education. Specifically I owe gratitude to the commitment to teaching of the following professors: Jason Papin, Kevin Janes, Rich Kent, Jeff Crandall (and the CAB lab in general), Ed Botchwey, Jeff Saucerman, and Ed Hall. Thanks for the extra efforts that you've made and for the commitment to students; it has definitely been noticed and appreciated.

I would be remiss to not acknowledge members of the Multiscale Muscle Mechanics lab, past and present, for engaging with me in all of the fun biomechanics discussions, thought experiments, and heated debates. Bahar Sharafi, Nic Fiorentino, Mike Rehorn, Chris Zirker, and Shawn Russell- thanks for being the face of the lab when I joined UVA. You have taught me a great deal and hold a special place in my heart as my very first graduate lab mates. Hon Fai Choi, Josh Inouye, and Xiao Hu- thanks for teaching me what you have about modeling. I have learned a great deal through conversations and modeling sessions with each of you. Kelley Virgilio, Katie Knaus, Katie Pelland, and John Miller- thanks for each of your contributions as lab members, friends, and colleagues.

Lastly, I would like to thank friends and family for their love and support over the last five years. While I regret that I cannot individually thank all of the people in the UVA and Charlottesville communities that have made the last five years fantastic, I would like to acknowledge the students of the Biomedical Engineering Dept. and the School of Engineering and Applied Sciences for walking this path of biomedical education with me. I like to think that we're all students of the same class, but with some phase shifts in there. To members of the University of Virginia Club Water Polo team, thanks for a lot of great playing. I had a lot of fun. To members of Dr. T.J. Eckleberg's 22% Vegan Cookin' Book Lookin' Think and Drink Solution, thanks for being a part of the best book club in Central VA. You were a welcome distraction from graduate research. To my wife and best friend, Lydia, thank you for supporting me in my goal to obtain a Ph.D. It wasn't always easy but you were always there supporting and encouraging me. Thanks for everything!

-Geoff

December 2014

Charlottesville, VA

Contents

List of Tables

List of Figures

MRI and Computational Modeling of In Vivo Muscle-Tendon Architecture and Function

By Geoffrey Gale Handsfield

“There are some things in this science worth reading.”

-Thomas Jefferson

Chapter 1

Introduction

1.1 Overview

Anatomical structure is the foundation for biological function. In both healthy and diseased cases, a firm understanding of anatomy grounds the study of physiology and mechanics. In the case of skeletal muscle, muscle size and orientation largely determine its functional capacity. Unique in its role as actuator of human motion, skeletal muscle can grow, shrink, lengthen, and shorten in response to stimulus. As humans range in size, shape, age, activity level, and state of health, so skeletal muscles range in size, shape, and quality. The array of skeletal muscle differences across humans provides a fascinating area of study that has captivated scientists for several centuries (Borelli et al., 1743). Furthermore, muscle interacts with its surrounding tissues, especially tendons and bones, suggesting a role for skeletal muscle in the mechanics of these tissues in health and disease. For these musculoskeletal tissues, determining anatomy is a key step in understanding function.

Medical imaging offers the opportunity to look inside the body and determine anatomy non-invasively. The advent of medical imaging over a century ago represented a paradigm shift for medicine. The more recent development of magnetic resonance imaging (MRI) greatly advanced soft tissue imaging. MRI has been used increasingly over the last 40 years to understand anatomical structure and function in a variety of organs in health and disease.

Despite the remarkable capabilities of medical imaging, the vast majority of information on the size and shape of skeletal muscles has come from cadaver dissection. These data are used as the basis for our understanding of muscle anatomy in clinical research and are input into computational models of musculoskeletal function for populations ranging from healthy humans to subjects with muscle and gait impairments and elite athletes. This is in spite of the facts that cadaver donors are typically elderly and ill before death and undergo chemical processes that affect their muscles after death. Needless to say, it is doubtful that the muscles from a cadaver represent

the muscles from healthy, living humans. Furthermore, it is not clear how muscle sizes and orientations in pathological populations differ from the muscle data acquired from cadavers and how elite athlete populations' muscles differ from cadaver data.

Tendon function, especially for the Achilles tendon, has suffered from a lack of *in vivo* anatomical information. Conventional understanding of Achilles tendon function reflects this lack of detailed anatomical information, with most Achilles models treating the tendon as a single nonlinear spring. Recent work has suggested the importance of Achilles tendon fascicles[*] in Achilles mechanics. In not capturing this meso-scale[†] structure of the Achilles tendon, previous models of the Achilles tendon have not been able to explain the observed phenomena of non-uniform tissue displacements in the tendon. An adequate understanding of these experimental results requires more advanced models of the tendon.

In this dissertation, I couple advanced MRI approaches with state-of-the-art image processing and modeling techniques to explore the *in vivo* structure and function of human muscles and tendons. By focusing on the skeletal muscles of the lower limb in normal, pathological, and athletic populations, this work aims to understand how muscle sizes differ across functionally different populations. I go on to use MRI and finite element modeling approaches to understand the deformation patterns of the human Achilles tendon and its relationship to muscle function. The research presented here represents the first comprehensive database of muscle sizes in typical healthy humans and an extension from this to populations with cerebral palsy and a population of collegiate sprint runners. Additionally, this dissertation proposes a non-isometric scaling approach for skeletal muscle, a novel metric which captures the functional capacity of the lower limb muscles, and the first image-based finite element modeling approach to include the meso-scale structure of the Achilles tendon.

---

[*] Tendon fascicles are the substructure of the tendon immediately smaller than the whole tendon (Screen et al., 2004). In the case of the Achilles, the fascicles are believed to move freely and slide independently of one another, giving rise to motion that is not explained by conventional models (see Ch. 5).

[†] Meso-scale refers to the length scale between micro-scale and macro-scale and is on the order of 100s of microns to millimeters. In this case, tendons are on the macro-scale and fascicles are on the meso-scale.

1.2 Outline of this Dissertation

The remaining chapters of the dissertation are as follows. Chapter 2 provides background information. Chapters 3-6 represent the four main bodies of work that each translate to published or prepared journal publications. Chapter 3 is an analysis of muscle sizes and scaling relationships in 24 healthy, normal subjects. This work has been published in the *Journal of Biomechanics* with co-authors Joseph Hart, Mark Abel, Craig Meyer, and Silvia Blemker. Chapter 4 is an extension of this work to the muscles of children with cerebral palsy for which a normative database is a valuable key to determining muscle size abnormalities in pathological populations. This work has been submitted to *Muscle and Nerve* with co-authors Mark Abel, Craig Meyer, and Silvia Blemker. Chapter 5 is an extension of muscle volume determination techniques to a population of collegiate sprinters. This work is in preparation for submission to *Medicine and Science in Sports and Exercise* with co-authors Katherine Knaus, Niccolo Fiorentino, Craig Meyer, and Silvia S. Blemker. Chapter 6 contains an image-based finite element modeling approach for understanding non-uniform deformation patterns of the Achilles tendon. This chapter is in preparation for submission to the *Journal of Biomechanics* with co-authors Joshua Inouye, Laura Slane, Darryl Thelen, Wilson Miller, and Silvia Blemker. Finally, I conclude with a summary chapter that explains the overall contributions of this body of work to the field of biomechanics as well as provides my perspective on the exciting next steps of this line of work.

Chapter 2

Background

"The earliest books containing the concepts of biomechanics were probably the Greek classic *On the Parts of Animals* by Aristotle (384-322 B.C.), and the Chinese book, *Nei Jing*… written by anonymous authors in the Warring Period (472-221 B.C.)."

-Y.C. Fung

2.1 Muscle Biomechanics and Anatomy

Muscle is well suited for study with medical imaging as it has a well-defined structure-function relationship. Muscle is force-generating. For a given muscle fiber type, the force a muscle is capable of generating is proportional to its cross-sectional area. Additionally, the length of a muscle is a determinant of its range of motion (Fig. 2.1). The relationship between peak muscle force, its length, and contraction velocity is well-established (Blemker et al., 2005; Hill, 1938). For these reasons, determination of optimal length of a muscle and its physiological cross-sectional area* offer a great deal of information on the muscle's functional capacity.

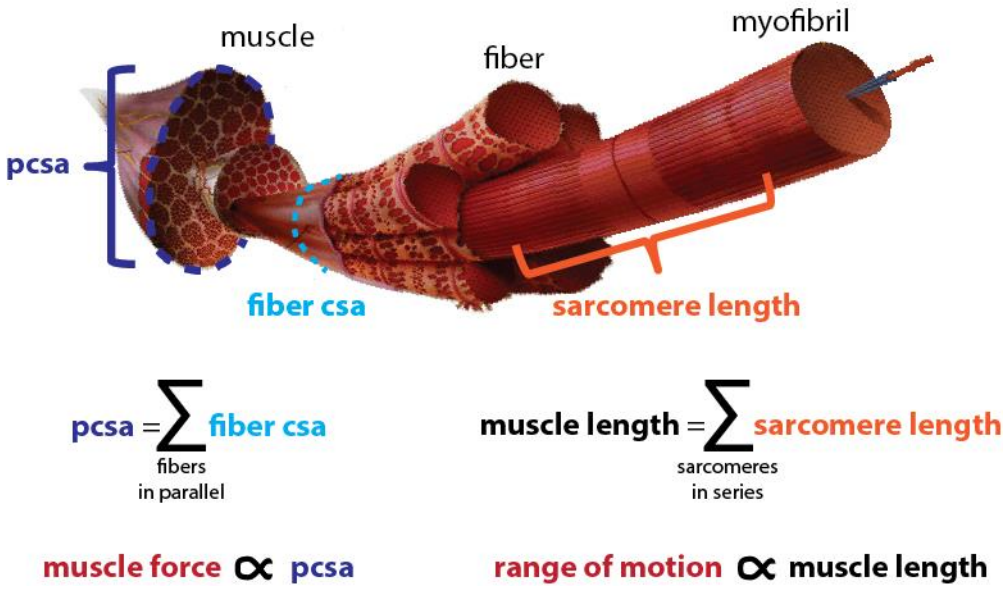

Figure 2.1: The macro-scale structure of muscle directly indicates its micro-scale structure which determines functional capacity such as force and range of motion

PCSA or physiological cross sectional area is the sum of the cross sectional areas (csa) of all of the fibers in parallel. Muscle force is proportional to pcsa. Muscle length is the sum of the lengths of the sarcomeres in series. Range of motion is proportional to muscle length. Figure adapted from (Anderson et al., 2000)

* Physiological cross-sectional area, or PCSA, is defined as the sum of the cross-sectional areas of all of the muscle fibers within a muscle. In other words, it is the cross-sectional area of the muscle in a plane perpendicular to the muscle's fibers. Since muscle fibers are seldom oriented perpendicular to the conventional anatomical planes, a distinction is made between PCSA and anatomical cross-sectional area (aCSA) of the muscle. PCSA is the measurement that determines a muscle's force-generating capacity (Lieber, 2002).

The clear structure-function relationship of muscle has motivated modeling approaches. In rigid body musculoskeletal modeling, physics-based computer models are built from known musculoskeletal size and orientation data. By combining equations of motion with equations of muscle force-generation based on anatomical and physiological principles, these simulations can determine muscle, tendon, and joint loads and are used to predict injury and to better understand human movement. As recently as five years ago, dissection of cadavers was the state-of-the-art for determining the muscle parameters of cross-sectional area, length, and fiber direction (Arnold et al., 2010; Ward et al., 2009).

The reliance on cadaver muscle data in simulations of living subjects has been acknowledged as a limitation of musculoskeletal models (Blemker et al., 2007; Narici, 1999). Cadaver donors are typically older and/or suffer from illness before death. Aging and illness are associated with loss of muscle mass through the processes of sarcopenia[*] (Frontera et al., 2000) and cachexia[†] (Tisdale, 2010). The immobility related to terminal illness also leads to muscle loss due to disuse atrophy. Additionally, the process of *rigor mortis* and chemical fixation for preserving cadaver tissue with formalin alter the structure of muscle from its *in vivo* state. These *ante*- and *postmortem* processes suggest that muscles from cadaver donors do not represent normal subjects. Additionally, cadaver muscle will not be representative of the muscle of human subjects with specific musculoskeletal pathologies.

In this dissertation, I present an imaging-based approach for determining muscle architectural parameters in different populations. Equations for estimating muscle architectural parameters from image sets are provided in Appendix I.

---

[*] Sarcopenia is the natural process of muscle loss with aging. It is thought that sarcopenia arises from an increase in the rate of damage to the muscle and/or a decrease in the rate of muscle repair at the cellular level.

[†] Cachexia is the pathological process of muscle loss with disease. Cachexia is believed to be caused by a pathological and significant increase in proteolysis of muscle tissue. This increase in proteolysis is so large that it cannot be balanced by physiological muscle synthesis.

2.2 Muscle Allometry and Scaling of Muscle Volumes

Humans vary in both size and shape. Across a wide range of masses and heights, human biomechanics are similar. In other words, humans of very different sizes and shapes perform relatively similar tasks. This raises the question: how do muscle sizes scale with body size such that the muscles of differently sized people produce similar movements?

Previous work on this question has generally settled on a linear relationship between body mass and muscle volume, referred to as isometric scaling. While this scaling relationship works reasonably well empirically, especially across species varying in size (Biewener, 1989), previous researchers have questioned the sensibility of this relationship. Isometric scaling of muscles implies geometric similarity of organisms, suggesting that organisms are proportionately scaled with respect to one another. Geometric similarity does not generally hold in humans (Kramer and Sylvester, 2013) and a previous seminal work in quadrupeds reported small but significant deviations from isometric scaling across species (Alexander et al., 1981). Biomechanists in the past have argued that a mechanical principle, such as prevention of buckling in tree trunks (McMahon, 1973) or quadruped torsos (Rashevsky, 1955), is more sensible than a geometric principle for scaling in biology.

The product of body mass and height is a simple metric that combines a measure of size (mass) with a measure of shape (height) and grossly represents the torque imposed on the musculoskeletal system by the human body. It may be that this metric works well as a scaling parameter for muscle volumes in the lower limb while also satisfying the need for a mechanically-based, non-isometric scaling parameter. Acquisition of an *in vivo* dataset of muscle volumes across a population of humans varying in size will allow the exploration of this parameter as a scaling metric.

2.3 Study Populations: Normal, Cerebral Palsy, and Collegiate Sprinters

Skeletal muscle is among the most plastic tissues in the body, meaning it remodels in response to certain stimuli (Lieber, 2002; Wisdom et al., 2014). Muscle responds to mechanical overload by building additional muscle, a process referred to as hypertrophy. When muscle is under-utilized, it responds by proteolyzing its tissue and decreasing its mass: referred to as atrophy (Wisdom et al., 2014). Because of the plasticity of skeletal muscle, muscle size varies greatly across populations. Healthy, active humans have more muscle mass than sedentary humans. Subjects with musculoskeletal pathology such as cerebral palsy (CP)[*] have less muscle mass than normal humans. Athletes have greater muscle mass than normal or pathological populations. Thus, there may be a general relationship between the functional capacity of these three study populations and their muscle mass.

Although it would be expected that total lower limb muscle mass varies across these populations, the individual muscles may not scale uniformly up or down in size compared to a reference population of normal humans. For example, every lower limb muscle of subjects with CP may not be reduced in size by the same amount compared to normal subjects. Instead, it may be that the neural aspects of CP affects different muscles differently, leading to non-uniform atrophy[†] of the lower limb muscles. Similarly, collegiate sprinters may not stimulate all muscles equally during training; the muscles may also not respond equally to training. In the case of elite athletes and subjects with cerebral palsy, hypertrophy and atrophy respectively may not present uniformly across lower limb muscles.

---

[*] Cerebral palsy is a diverse category of pathologies caused by a central neural lesion occurring at or near birth. This neural lesion leads to abnormal development of the musculoskeletal system, neuromuscular spasticity, functionally weakened muscles, and impaired gait. See Chapter 4 or additional sources for further reading.

[†] In the case of cerebral palsy, it is not clear whether small muscles result from loss of muscle mass or failure to develop sufficient muscle mass. In this dissertation, I make no distinction between these two causes and I use the term "atrophy" to refer to deficiency of muscle mass in general.

For subjects with cerebral palsy, the identification of non-uniformly atrophied muscles may have implications for correcting gait impairments and for improving surgical decision making. If the muscles are not uniformly atrophied, then some muscles will contribute more to functional weakness than others and will benefit the most from targeted strength training. Alternatively, the knowledge that certain muscles are preferentially small may add valuable information to the decision whether to perform muscle-tendon lengthening or muscle-tendon transfer surgeries. For collegiate sprinters, the presence of non-uniformly hypertrophied muscles may explain higher rates of musculoskeletal injury among athletes compared to the general population and may suggest that targeted strength training can be more effective than general strength training. For subjects with cerebral palsy and for athletes, musculoskeletal modeling approaches will be improved by determination of *in vivo* muscle sizes which not only capture gross atrophy or hypertrophy compared to normal populations, but also capture the subtle effects of non-uniform atrophy or hypertrophy across individual muscles.

2.4 Magnetic Resonance Imaging

Magnetic resonance imaging (MRI) is an imaging technique that utilizes magnetic fields and radiofrequency pulses to image tissues in the body. Tissues are distinguished based on their T1 and T2 decay characteristics[*]: the chemical properties concerning the rates of magnetic interaction at the atomic level which differ across tissues. Tissues are spatially distinguished in MRI by the application of gradient magnetic fields, which apply spatially-varying magnetization during the scanning sequence. MRI data is acquired in spatial frequency space, also known as k-space, which is related back to the image through the Fourier transform[†]. A number of different acquisition strategies or trajectories (Fig. 2.2) are used to sample k-space, and each strategy has advantages and disadvantages in terms of acquisition time, image reconstruction complexity, and other factors.

Recent advancements in MRI have led to sequences that make rapid image acquisition feasible through their k-space trajectories. Conventional MRI has typically used k-space sampling approaches that vary only one gradient magnetic field at a time, producing a k-space trajectory that follows the lines of the x-coordinate direction in k-space (Fig. 2.2). This sampling, referred to as Cartesian sampling, is not sensitive to magnetic field inhomogeneities; however, it is time-consuming. Non-Cartesian sampling, such as radial or spiral sampling (Fig. 2.2), utilizes simultaneous variation of two or more gradient magnetic fields. Among other advantages, some

[*] T1 is a rate constant related to how quickly the protons in a tissue align with an external magnetic field; this process is referred to as spin-lattice relaxation. T2 is a rate constant related to how quickly protons in a tissue de-phase via proton-proton interactions; this process of de-phasing among spinning protons is referred to as spin-spin relaxation. For further reading, refer to (Nishimura, 2010)

[†] The Fourier transform is a mathematical transform function that maps functions in a given domain (e.g., time) to their corresponding function in the inverse domain (e.g. time^{-1} or frequency). In MRI, the image domain is the spatial domain. Its inverse domain (k-space) is called spatial frequency. The Fourier transform is given by:

$$F(\varepsilon) = \int_{-\infty}^{\infty} f(x) e^{-\tau i x \varepsilon} dx,$$

where $F(\varepsilon)$ is the transformed function and domain, $f(x)$ is the initial function and domain, and $\tau = 2\pi$.

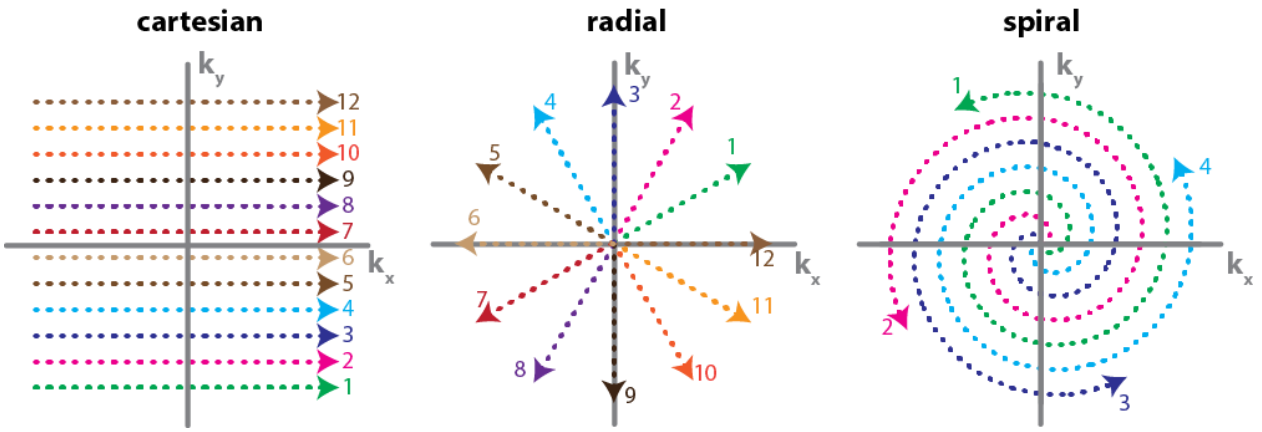

Figure 2.2: Three different k-space acquisition trajectories

Each numbered line represents a sequence repetition in a 2D k-space coordinate system, the length of each line indicates the relative length of time required for sampling of one repetition. Cartesian sampling acquires data on a single line of k-space per sequence repetition. Radial sampling may utilize shorter repetitions than Cartesian sequences. Spiral trajectories often utilize a smaller number of repetitions that are typically longer than in radial.

non-Cartesian approaches, such as spiral, allow image data to be acquired with fewer repetitions, yielding a more rapid acquisition of image data. Other non-Cartesian sequences, such as radial spokes, are proving to be useful for imaging tissues with very short T2 times, such as tendon and cortical bone, for which Cartesian sampling would not be able to collect sufficient image data before MR signal decay.

Table 2.1: Comparison of Cartesian, radial, and spiral acquisition*

Sequence	Reconstruction Complexity	Sensitivity to Magnetic Field Inhomogeneity	Typical Sampling Time per Repetition compared to Cartesian	Number of Repetitions compared to Cartesian	Imaging Time compared to Cartesian
cartesian	Simple	Insensitive	--	--	--
radial	More Complex	More Sensitive	Shorter	Fewer	Shorter
spiral	Most Complex	Most Sensitive	Longer	Fewest	Shorter

Non-Cartesian sequences, such as radial and spiral, have scan time advantages over traditional Cartesian sequences.

* It should be noted that particular spiral or radial sequences may be engineered to have properties different than those listed in this table. For example, spiral sequences may utilize repetitions with low curvature; these sequences would have shorter sampling time per repetition than Cartesian sequences.

While MRI has been used to image biological tissues as small as tens of microns in size (Infantolino, 2012), most MRI hardware and pulse sequences are best suited for imaging structures on the scale of millimeters or greater. In this dissertation, I make use of several non-Cartesian MRI approaches to determine the morphology and function of muscle and tendon structures in the lower limbs of living humans.

2.5 Finite Element Modeling of Musculoskeletal Tissues

Musculoskeletal tissues generate and transmit forces in order to produce movement. While the fundamental phenomena of force generation and transmission in the musculoskeletal system are generally understood, the complex shapes and orientations of musculoskeletal tissues make it difficult to resolve equations of motion analytically. Finite element modeling, a technique developed for solving differential equations over complex geometries in the aerospace industry, has been used in the past to understand the mechanics of muscles, ligaments, and bones (Blemker et al., 2005; Donahue et al., 2002; Fiorentino and Blemker, 2013; Rehorn and Blemker, 2010; Sharafi et al., 2011; Weiss et al., 1996).

Until now, finite element modeling of tendons has been extremely limited. Despite the obvious importance of the Achilles tendon in storing elastic energy and transmitting forces for motion, only two recent finite element models of the Achilles tendon have been published (Shim et al., 2014; Von Forell and Bowden, 2014). The Achilles tendon is a particularly important tendon as it is the primary energy-storing tendon in standing, walking, and running.

The Achilles tendon, the thickest tendon in the body, is susceptible to various pathologies in different populations. For example, the Achilles tendon is susceptible to catastrophic rupture which requires surgical repair (Maffulli, 1999). Lengthening surgeries of the Achilles tendon are common in subjects with cerebral palsy and other gait impairments (Abel et al., 1999). Achilles

tendinopathy*, a chronic condition, is common among aging subjects and runners, although the mechanisms causing it are not well understood (Maffulli et al., 2004) .

The Achilles tendon is unique in its structure. The Achilles tendon is actuated by three different muscles†, each with notable differences in size, orientation, and fiber-type composition (Fig. 2.3). Research has suggested that these three muscles each operate on different fascicles of the tendon, implying that changes in the muscles will lead to altered deformation patterns within the tendon. Other studies have revealed additional complexities in the structure of the tendon as well as tendon deformation patterns that are not as yet fully understood.

Finite element modeling is attractive for study of the Achilles tendon as it allows for individual aspects of the tendon, such as muscle forces, material behavior, and motion, to be manipulated independently. In this dissertation, I present a finite element model of the Achilles tendon to elucidate the interactions between the plantar-flexor muscles and the Achilles tendon in order to better understand the function and deformation patterns of this major tendon.

* Achilles tendinopathy is defined as a general non-inflammatory degradation of the tendon. Lack of inflammation distinguishes tendinopathy from the acute conditions of tendinosis/tendinitis.

† The primary plantarflexor muscles—the medial gastrocnemius, lateral gastrocnemius, and soleus—are collectively referred to as the triceps surae muscle complex. All three of these muscles insert into the Achilles tendon, but the sizes, force-generating capacities, and activation profiles of these muscles differ.

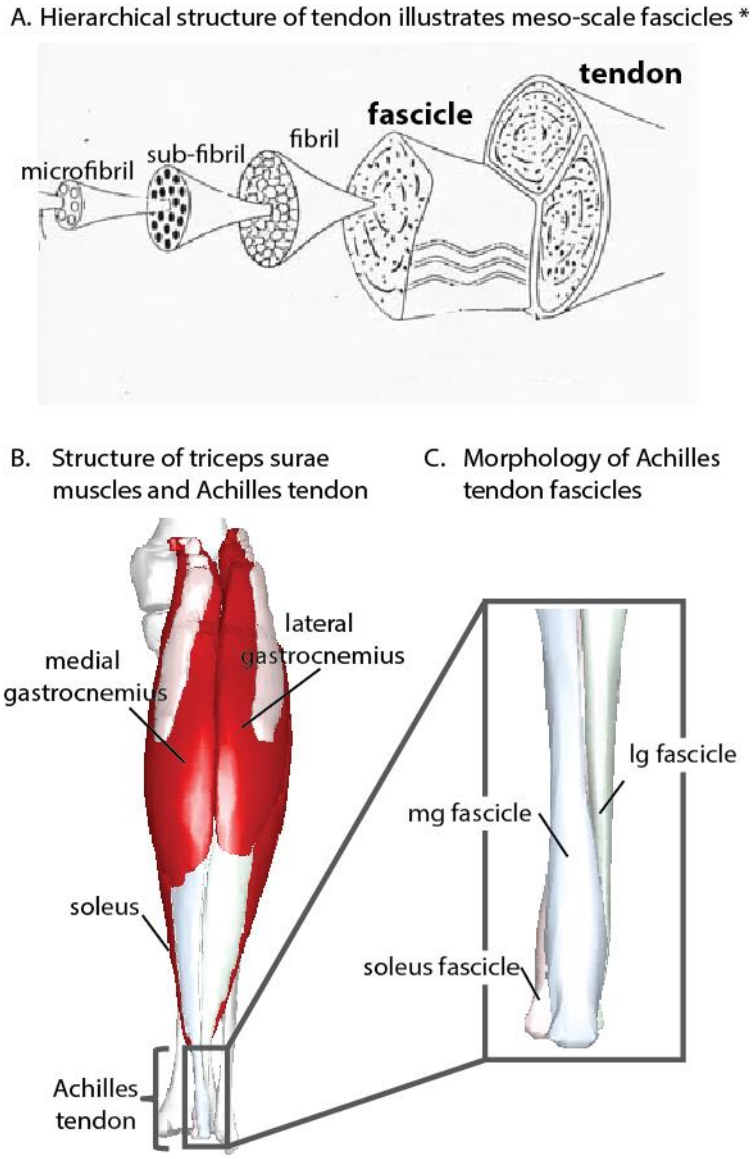

Figure 2.3: The hierarchical structure of the Achilles tendon gives rises to fascicles that are each controlled by a different triceps surae muscle

A: Tendon has a hierarchical structure. The meso-scale substructure is the tendon fascicle. *adapted from (Kastelic et al., 1978). B: The triceps surae muscle group is composed of three muscles that insert into the Achilles tendon. C: The Achilles tendon is composed of fascicles associated with the three triceps surae muscles.

Chapter 3

Relationships of 35 Lower Limb Muscles to Height and Body Mass Quantified Using MRI

"The shape of any organism is determined by the requirements of performing certain mechanical and physiological functions."

-Nicolas Rashevsky

"Everything should be made as simple as possible, but not simpler."

-Albert Einstein

3.1 Abstract

Skeletal muscle is the most abundant tissue in the body and serves various physiological functions including the generation of movement and support. Whole body motor function requires adequate quantity, geometry, and distribution of muscle. This raises the question: how do muscles scale with subject size in order to achieve similar function across humans? While much of the current knowledge of human muscle architecture is based on cadaver dissection, modern medical imaging avoids limitations of old age, poor health, and limited subject pool, allowing for muscle architecture data to be obtained *in vivo* from healthy subjects ranging in size. The purpose of this study was to use novel fast-acquisition MRI to quantify volumes and lengths of 35 major lower limb muscles in 24 young, healthy subjects and to determine if muscle size correlates with bone geometry and subject parameters of mass and height. It was found that total lower limb muscle volume scales with mass (R^2=0.85) and with the height-mass product (R^2=0.92). Furthermore, individual muscle volumes scale with total muscle volume (median R^2=0.66), with the height-mass product (median R^2=0.61), and with mass (median R^2=0.52). Muscle volume scales with bone volume (R^2=0.75), and muscle length relative to bone length is conserved (median s.d.=2.1% of limb length). These relationships allow for an arbitrary subject's individual muscle volumes to be estimated from mass or mass and height while muscle lengths may be estimated from limb length. The dataset presented here can further be used as a normative standard to compare populations with musculoskeletal pathologies.

3.2 Introduction

Skeletal muscle is the most abundant tissue in the human body and is essential for movement. Muscle volume is an important determinant of muscle functional capacity. For example, physiological cross sectional area (PCSA) correlates with peak isometric force (Gans, 1982; Sacks and Roy, 1982) and can be computed from muscle volume and optimal fiber length (Brand et al., 1986; Lieber and Friden, 2000). Additionally, muscle volume has been related to the energetic capacity of muscle (Roberts et al., 1998) and to a muscle's joint torque-generating capacity (Fukunaga et al., 2001; Holzbaur et al., 2007a; Trappe et al., 2001). These relationships between muscle PCSA and peak muscle force, and between muscle volume and peak muscle torque motivate the study of muscle volumes and lengths across healthy humans varying in size.

To date, the most comprehensive muscle volume data in humans is based on cadaveric measurements (Friederich and Brand, 1990; Ward et al., 2009; Wickiewicz et al., 1983). While cadaver dissection is attractive in its directness of measurement, old age and poor health among cadaver donors confounds applying cadaver data to young, healthy populations (Doherty, 2003; Narici et al., 2003; Vidt et al., 2011). Furthermore, other limitations of cadaver studies have generally prevented muscle scaling relationships from being assessed.

Imaging modalities, on the other hand, have been used in the upper limb to obtain *in vivo* muscle architectures in subjects ranging in age and health condition (Holzbaur et al., 2007b; Vidt et al., 2011) and in the lower limb to quantify volumes of large muscles and muscle groups in subject populations of interest (Correa and Pandy, 2011; Fukunaga et al., 1992; Gopalakrishnan et al., 2010; Kawakami et al., 2000; LeBlanc et al., 2000). Prolonged imaging times have impeded the scanning of large limbs with high resolution. In this study, we use advanced high-speed MRI, which makes it possible to quickly scan the entire lower limb in high resolution, facilitating a thorough assessment of the individual muscles in the lower limb.

Quantifying healthy muscle volumes with *in vivo* approaches enables several important questions to be answered. First: are relative muscle volumes and lengths preserved across differently sized healthy individuals? Subject-specificity of anatomy has been discussed in biomechanical modeling (Duda et al., 1996; White et al., 1989). A finding of consistent scaling for muscle volumes and lengths would suggest that anatomical variability is small in healthy individuals and would also provide a normative basis of comparison for individuals with musculoskeletal impairments. Second: how do bones and muscles scale with each other? Muscles and bones are mechanically linked in structure and function. Previous authors have investigated how bone strength scales with size in general and in various animal species and humans (Alexander et al., 1979; Biewener, 1989; Ferretti et al., 2001; Frost, 2000). The relationship between muscle and bone volumes and lengths has not been explored in healthy humans *in vivo*. A finding that muscle lengths and bone lengths scale would lend further confidence to anthropometric scaling of the musculoskeletal system (Brand et al., 1982; White et al., 1989). A finding of a volumetric relationship between muscle and bone may also serve as a normative standard for evaluating gross age- and activity-related bone loss such as osteoporosis or bone resorption during space flight.

A comprehensive *in vivo* assessment of muscles from differently sized subjects would also allow for the exploration of how muscle volumes scale with body size. Geometric similarity has been used as a principle for muscle scaling but has been questioned by previous authors studying muscles of animals (Alexander et al., 1981) and humans (Nevill et al., 2004). Other authors have used many subject parameters (e.g. limb girth, age, gender, body weight, and waist size) to predict muscle volume (Chen et al., 2011; Lee et al., 2000). It may be that a two-component parameter, the height-mass product, can predict human muscle volume variation with high accuracy.

In this study, we used a fast non-Cartesian MRI sequence to rapidly scan the entire lower limb and comprehensively assess 35 lower limb muscles of 24 healthy males and females ranging

in height by 28 cm and in mass by 51 kg. **The goals of this study were to *(i)* determine relative volumes and lengths of lower limb muscles in this population, *(ii)* determine how muscles and bones scale with each other, and *(iii)* determine how lower limb muscle volume scales with the subject parameters of mass and height.**

3.3 Methods

Twenty-four active, healthy subjects (8 females and 16 males with the following subject characteristics (mean ± s.d. [range]): age: 25.5 ± 11.1 [12-51] years, height: 171 ± 10 [145-188] cm, body mass: 71.8 ± 14.6 [47.5-107.0] kg, body mass index (BMI): 24.3 ± 4.0 [18.9-35.1] kg/m^2) all with no history of lower limb injury, were provided informed consent and selected for this study (Table 3.1). Subject selection and study protocol were approved by the University of Virginia's Institutional Review Board. Subjects were scanned on a 3T Siemens (Munich, Germany) Trio MRI Scanner using a 2D multi-slice sequence utilizing spiral gradient echo (Meyer et al., 1992). Scan time was approximately 20 minutes per subject. The scanning parameters used were: TE/TR/α: 3.8 ms/ 800 ms/ 90°, field of view: 400 mm × 400 mm, slice thickness: 5 mm, in plane spatial resolution: 1.1 mm × 1.1 mm. A Chebyshev approximation was applied for semi-automatic off-resonance correction (Chen et al., 2008). Axial images were obtained contiguously from the iliac crest* to the ankle joint in acquisition sets of 20 images. The table was moved 100 mm through the scanner after each acquisition and scanning was repeated.

Sets of axial images were registered and each of 35 muscles (Table 3.2, Appendix) in the 24 subjects' lower limbs was segmented (Fig. 3.1) using in-house segmentation software written in Matlab (The Mathworks Inc., Natick, MA, USA). The segmentation technique is similar to others in the literature (Akima et al., 2000; Fukunaga et al., 1992; Holzbaur et al., 2007b) and required users to specify 2-D contours defining the perimeter of a structure in each axial image. Voxels inside each of the 2-D contours were assigned a value of one, while external voxels were assigned a zero value. To filter contour noise generated by small user errors in each slice, the

* For four subjects, scans were acquired from the 12th thoracic vertebra (T12) to the ankle joint. The psoas volume and length reported in this chapter represent the muscle from T12 to femoral insertion obtained from the four subjects whose scans extended to T12. The volume and length for other subjects was extrapolated to include the virtual T12 to iliac crest so that comparisons across subjects would be consistent.

voxelated volume was smoothed by convolving with an averaging filter of 3x3x3 voxels. Following this smoothing procedure, the 3D anatomical structure was reconstructed as an isosurface by selecting an isovalue of half the maximum value present in the volume after smoothing. The smoothing process has a very minimal (<1%) effect on computed volumes and reproduces more realistic 3-D muscle architectures which are smooth *in vivo*.

Table 3.1: Subject data for normal, healthy subjects

Subject	Age (years)	Height (cm)	Mass (kg)	BMI (kg/m^2)	Total Muscle Volume (cm^3)	Limb Length (cm)
Female 1	20	165	56.7	21	6157	82.8
Female 2	22	173	65.8	22	6427	86.6
Female 3	26	160	56.3	22	4951	73.6
Female 4	27	173	56.7	19	6185	82.5
Female 5	30	166	59	21	5912	79
Female 6	31	178	70.5	22	6449	87
Female 7	40	163	61.4	23	6002	79.8
Female 8	41	170	75	26	6866	79.8
Male 1	12	145	47.5	23	3979	71.6
Male 2	13	168	83.5	30	7307	85.6
Male 3	13	161	56	22	5795	78.4
Male 4	14	178	65.7	21	7059	88.6
Male 5	14	167	56.3	20	6104	81.9
Male 6	15	165	63.6	23	6587	84.3
Male 7	15	178	77.6	24	7584	88.1
Male 8	17	170	76.8	27	7690	82.3
Male 9	20	185	81.7	24	8242	86.5
Male 10	23	188	81.7	23	9266	89
Male 11	25	180	74.8	23	8330	84.7
Male 12	28	175	81.7	27	7729	85.7
Male 13	32	180	83.9	26	8683	89.3
Male 14	41	178	106.8	34	10064	84.7
Male 15	42	165	95.5	35	8493	84.2
Male 16	51	183	87.7	26	8922	89.5

Age, height, mass, total muscle volume of the lower limb, and combined length of the tibia and femur are reported for the twenty-four subjects included in this study.

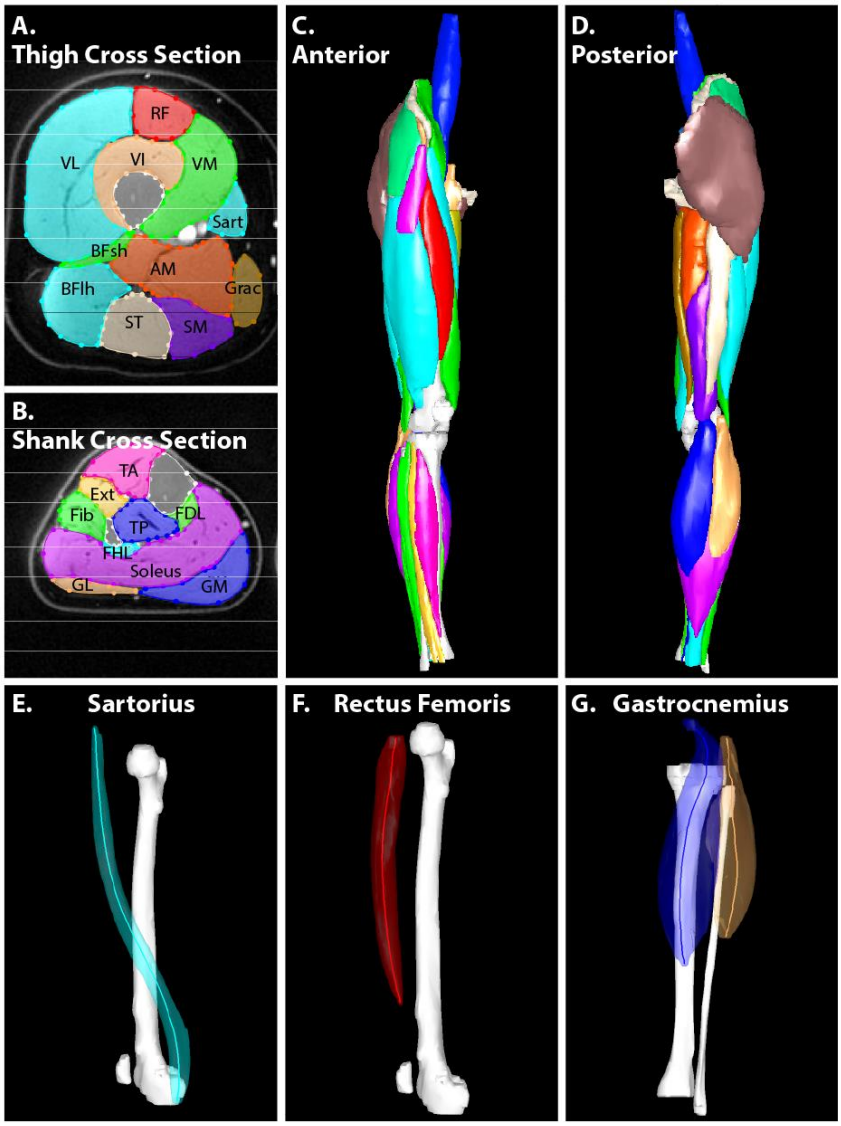

Figure 3.1: Illustration of segmentation, reconstruction, and volume and length determination

Muscles and bones were segmented in axial MR Images (A and B) and reconstructed in 3-D (C and D) to obtain volumes. Muscle belly lengths were determined by following the axial centroids in 3-D space, yielding the muscle belly line-of-action length (E-G).

Segmentations were performed by a team of eleven trained users who utilized a detailed slice-by-slice muscle segmentation atlas created from one of our data sets. A single highly trained user evaluated and refined all segmentations before further analysis to ensure consistency across users. User input time was approximately 25 hours per limb. Total lower limb muscle volume was found by summing the volumes of all 35 segmented muscles. A muscle's volume fraction was defined as its volume divided by the total lower limb muscle volume.

The anatomical length of each muscle was determined using axial centroids. The centroid of each muscle was computed in each axial slice. The 3D Euclidean distance between adjacent-slice centroids was calculated and all inter-slice distances were summed to yield muscle length. By defining muscle length using centroids, lengths represent the anatomical line-of-action lengths, incorporating the muscle's curved shape and complex wrapping (Fig. 1, E-G). For the obturator externus, the small external rotators, the quadratus femorus, and the piriformis, the centroid path was inconsistent with the line-of-action. For these muscles, linear distances along the line of action were used for muscle length (see Supplementary Text).

The linear length of bones was determined along the anatomical long axis oriented in the superior-inferior direction. Limb length was defined as the sum of the tibia and femur lengths. To compare muscle lengths between subjects, muscle belly lengths were normalized by limb length.

A cylindrical water phantom of known volume was imaged and segmented to estimate accuracy, revealing a volume error of less than 0.5%. This may underestimate errors associated with complex muscle shapes. A previous study reported errors of less than 3% for imaging and segmentation of more complex imaging phantoms (Mitsiopoulos et al., 1998).

3.4 Results

Within narrow standard deviations, muscle volume fractions for the 35 muscles included in this study are conserved for this population (Fig. 3.2A). Standard deviations are on the order of 1% of total lower limb musculature. The ratio of muscle belly length to bone length in the lower limb is conserved for this population (Fig. 3.2B). The average standard deviation of muscle belly length was 3.2% of bone length.

Volumes of individual muscles scale linearly with total limb muscle volume (Fig. 3.3 and Appendix Table 3.3; see Appendix Table 3.2 for coefficients of best fit). The highest coefficients of determination (R^2) between total lower limb muscle volume and individual muscle volume are in large muscles associated with knee extension ($0.48 \leq R^2 \leq 0.85$), knee flexion and hip extension ($0.52 \leq R^2 \leq 0.76$), hip flexion ($0.55 \leq R^2 \leq 0.78$), and ankle plantarflexion ($0.45 \leq R^2 \leq 0.73$). In contrast, R^2 values were lower in the smaller hip external rotator muscles ($0.16 \leq R^2 \leq 0.41$). All volume correlations were significant ($p<0.05$) except for those of the obturator externus. All length correlations were significant ($p<0.05$) except for several hip-crossing muscles: the small external rotators, obturator muscles, quadratus femoris, piriformis, and pectineus.

Muscles grouped into functional groups scale more tightly than individual muscles (Fig. 3.4). The muscle groups that scale the best with total lower limb muscle volume are the hip flexors and extensors ($R^2=0.88$, $R^2=0.95$, Fig. 3.4A), the hip adductors ($R^2=0.90$, Fig. 3.4B), and the knee flexors and extensors ($R^2=0.90$, $R^2=0.91$, Fig. 3.4C). The ankle dorsiflexors and plantarflexors and hip abductors also scale well with total lower limb muscle volume ($R^2=0.83$, $R^2=0.79$, $R^2=0.78$, Fig. 3.4B, 3.4D) while the hip external rotators display the lowest R^2 values ($R^2=0.43$, Fig. 3.4B).

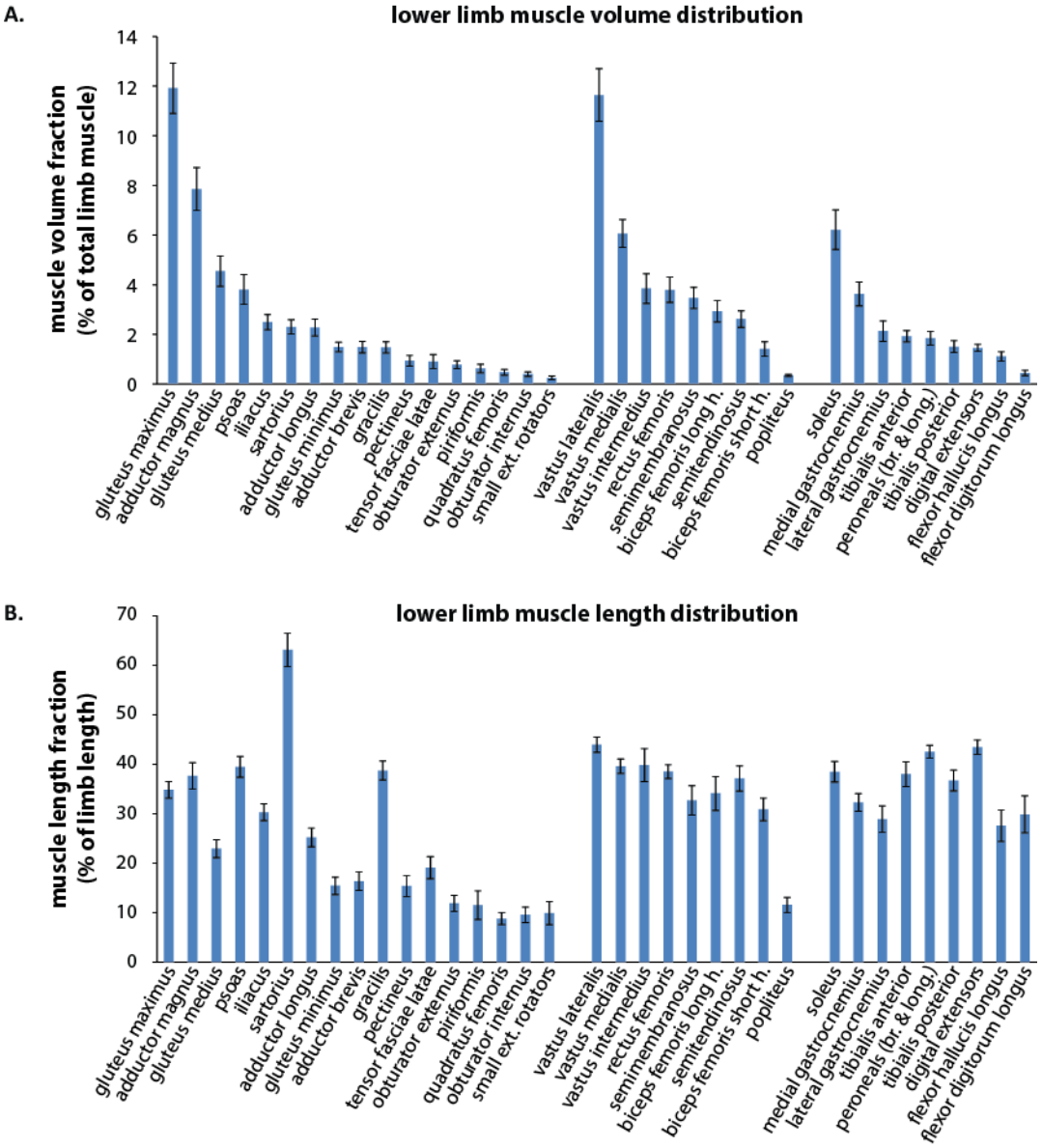

Figure 3.2: Muscle volume and length distributions in healthy humans

A: Muscle volume fraction (muscle volume divided by total limb muscle volume) means and standard deviations for muscles crossing the hip, knee, and ankle. B: Muscle length fraction (muscle belly length divided by limb length) means and standard deviations.

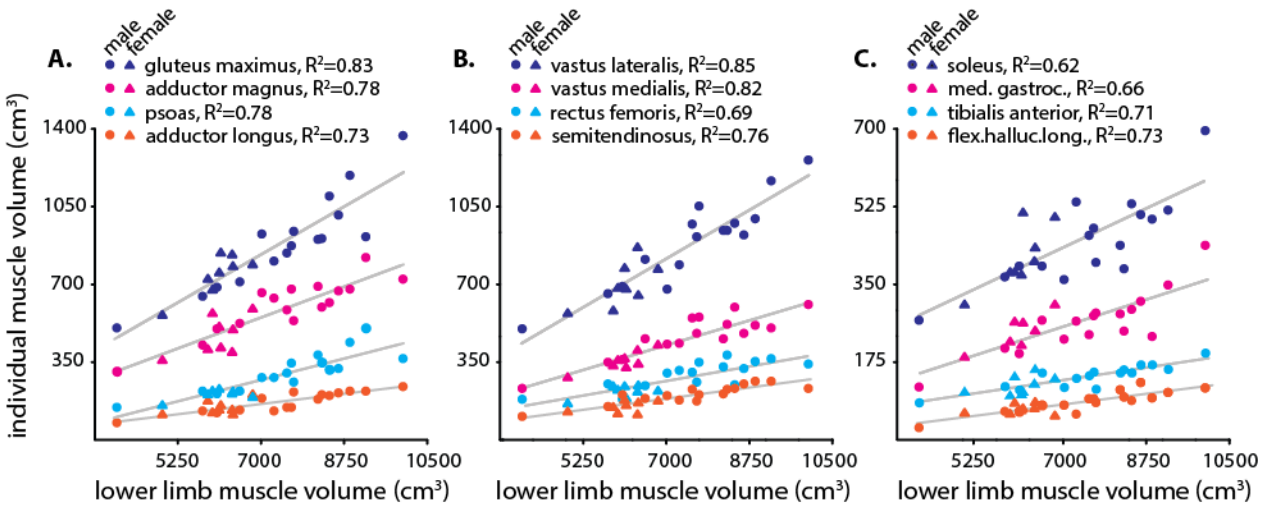

Figure 3.3: Individual muscle volumes scale with lower limb muscle volume

Muscles crossing the hip (A), knee (B), and ankle (C) illustrate that lower limb muscle volume is a good predictor of volumes of muscles ranging in size for both males (●) and females (▲).

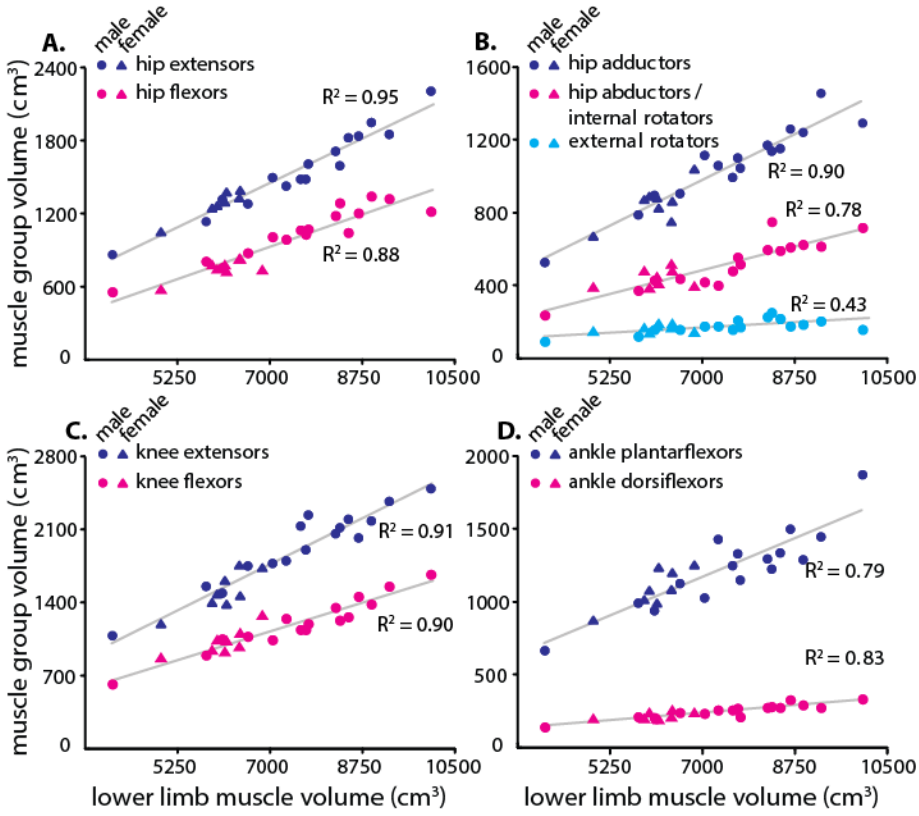

Figure 3.4: Volumes of functional muscle groups scale with lower limb muscle volume

Total lower limb muscle volume scaled with the product of height and mass (Fig. 3.5A, R^2=0.92). This scaling relationship was higher than a relationship based on mass (Fig. 3.5B, R^2=0.85) or height (Fig. 3.5C, R^2=0.64). The effectiveness of height-mass scaling of lower limb muscle volume did not reach significance compared to mass scaling (p=0.28, two-tailed t-test of Fisher transformation) although it was significantly more effective than height scaling (p=0.007). The coefficient of determination for height-mass scaling was also higher than that for scaling based on the limb length-mass product (R^2=0.90) although this difference was not significant. In addition to predicting total lower limb muscle volume, the height-mass product is also a good predictor of individual muscle volumes (Appendix II, Table 3.3), especially for muscles involved in hip flexion and extension ($0.48 \leq R^2 \leq 0.82$), knee flexion and extension ($0.45 \leq R^2 \leq 0.79$), and the large muscles crossing the ankle joint ($0.47 \leq R^2 \leq 0.77$). The height-mass product predicted individual muscle volumes with a greater R^2 than mass for all but one muscle (App. II, Table 3.3), with a mean increase in R^2 of 0.05. As a predictor of individual muscle volumes in the lower limb, height-mass scaling is significantly more effective than mass scaling ($p<0.05$, t-test of R values in 35 muscles).

The total lower limb muscle volume reported previously in a comprehensive cadaver dissection study (Ward et al., 2009) is half as large as the value predicted by our linear model for subjects of the same height and mass (square marker, Fig. 3.5). Despite the overall small muscle sizes reported for cadavers, the muscle volume fractions computed from Ward et al. were mostly consistent with those found in this study, with a few exceptions. The computed cadaver muscle volume fractions for the gluteus medius, psoas, and vastus lateralis muscles were significantly different from this study's healthy muscle volume fractions (App. II, Table 3.4, 95% Confidence Interval). Values for absolute physiological cross sectional area (PCSA) of the cadaver muscles reported in Ward et al. are also small compared to healthy subjects' computed PCSAs (App. II, Table 3.4) although normalization by total PCSA reduces these differences.

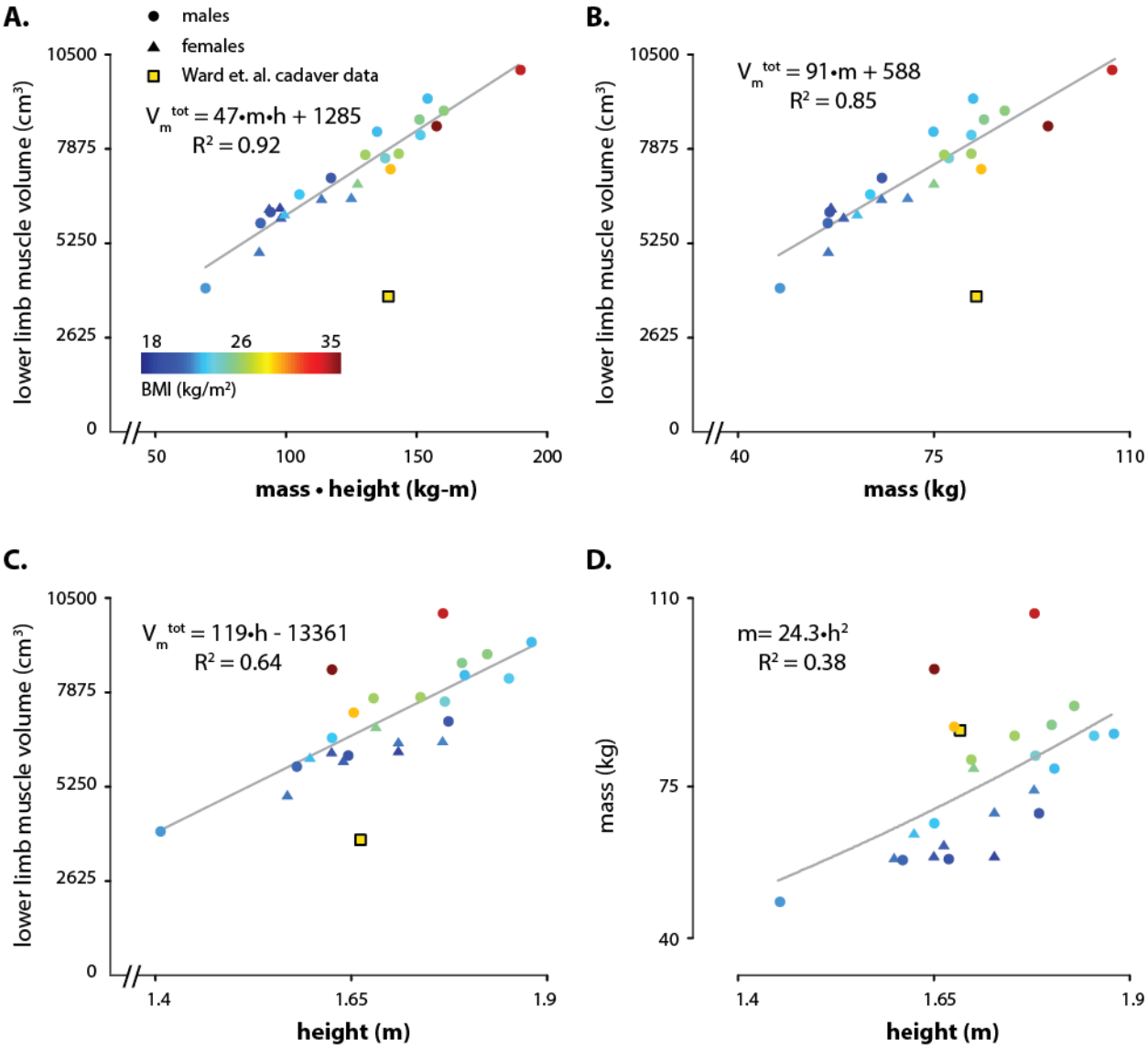

Figure 3.5: Scaling relationships for total lower limb muscle volume and body size parameters

The product of mass and height is the best predictor of lower limb muscle volume for subjects ranging in BMI, compared to mass or height alone. Cadaver muscle volume (■, (Ward et al., 2009)) is significantly smaller than the muscle volume of a healthy subject. A. Lower limb muscle volume scales well with height*mass. B. Lower limb muscle volume scales slightly less well with body mass alone. C. Height alone is the worst predictor of lower limb muscle volume. D. The relationship between mass and height is not strong for subjects ranging in BMI, motivating the use of mass and height as covariates.

A linear relationship between the total bone volume in the lower limb (the summed volumes of the patella, tibia, fibula, and femur) and the total muscle volume in the lower limb was found. One outlier was found using a two-sided Grubbs' test (α=0.01) of total bone volume and was omitted from this analysis. Within the remaining population, 75% of the variation in muscle volume is accompanied by a commensurate variation in bone volume (Fig. 3.6).

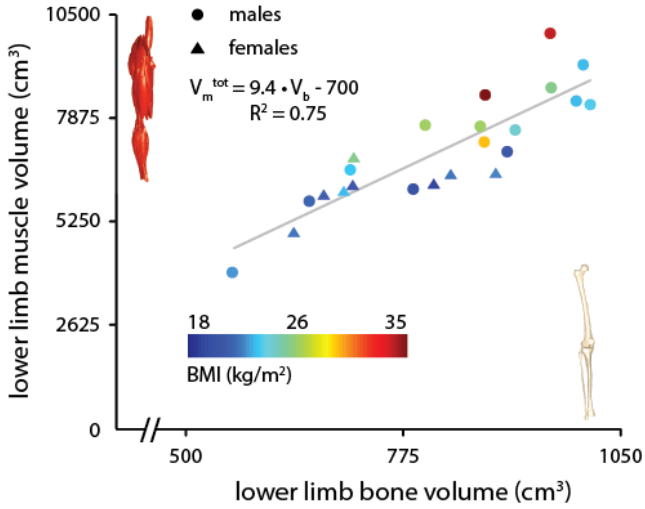

Figure 3.6: Scaling relationship between lower limb muscle volume and bone volume.

Total lower limb muscle volume scales well with the total bone volume in the lower limb—summed volume of the femur, tibia, fibula, and patella. Variation in bone volume predicts 75% of the variation in lower limb muscle volume.

3.5 Discussion

The purpose of this study was to determine muscle volumes and lengths for a cohort of healthy subjects *in vivo* in order to determine how muscles, bones, and subject parameters scale together. Our results revealed that: *(i)* muscle volumes consistently scale relative to total muscle volume, and muscle lengths consistently scale relative to bone length for healthy individuals varying in size and age; *(ii)* bone volume and muscle volume in the lower limb scale together, and *(iii)* total lower limb muscle volume scales with the product of height and mass for healthy subjects ranging in size, gender, and age.

In our healthy subject population, 92% of the variability in lower limb muscle volume was predicted by variations in the height-mass product while 85% of the variability was explained by mass alone. The inclusion of height as a covariate with body mass thus improved the linear predictive model by 7%. As a covariate relationship, body mass seems to dominate lower limb muscle volume while height offers a small predictive improvement. This difference did not reach statistical significance for total lower limb muscle volume; however, height-mass was significantly better than mass alone as a predictor of individual muscle volumes.

The possible role of height in lower limb muscle scaling may suggest that body stature, and not just size, has a role in intraspecific variation of muscle volume in humans. There are both geometric/energetic and mechanical explanations of this hypothesis. In a study on the energetics of bipedal runners, Roberts et al. show that the cost of running is greater for bipeds than for quadrupeds of a similar mass (Roberts et al., 1998). The authors suggest that longer muscles in the taller bipeds contribute to larger muscle volumes. It is possible that the inclusion of height explains small intraspecific variations in muscle length that contribute to total muscle volume. A separate mechanical argument can be made that the function of muscle volume is to provide torque to balance and control the body. Indeed, muscle volume has been shown to correlate with maximum

torque-generating capacity (Fukunaga et al., 2001; Holzbaur et al., 2007a; Trappe et al., 2001). With arbitrary increases in either height or mass, muscle volume in general must increase in order to maintain torque-balance.

Previous authors have hypothesized that inclusion of a body stature parameter (i.e. height) as a covariate with body mass could account for mass-independent increases in muscle mass in taller human subjects (Kramer and Sylvester, 2013; Nevill, 1994). Our results are consistent with these hypotheses although the effect of including height in the model was small. Future assessments with larger and more extremely varying human subjects may determine the extent and mechanisms underlying height-mass scaling for lower limb muscle volumes.

In addition to predicting total lower limb muscle volume, the height-mass product predicted individual muscle volumes as well or better than body mass for 34 of the 35 muscles (App. II, Table 3.3). This result was statistically significant. Strong correlations between the height-mass product and muscle volume occur in hip extensors, knee extensors, knee flexors, and the ankle plantarflexors, muscle groups that consist of large muscles that are functionally significant in bipedal support and mobility (Liu et al., 2006; Winter, 1980).

Comparisons between this study's results and previous cadaveric measurements reveal a significant disparity in the muscle volumes of these young, healthy and recreationally active subjects compared to cadavers. In a comprehensive dissection study (Ward et al., 2009), the average cadaver presents a total muscle volume 50% smaller than this study's results for a given body size. Thus, cadaver muscles are generally small even when normalized by body size. This may result from pre-mortem sarcopenia (Doherty, 2003), inactivity (Bloomfield, 1997; Kawakami et al., 2001, 2000), or disease-related atrophy (Tisdale, 2010). These differences call into question using cadaver measurements for applications to young, healthy subjects. One previous study (Arnold et al., 2010) which built a musculoskeletal model from values reported in Ward et al. used

high specific tension values compared to literature (61 N/cm^2 compared to 20-30 N/cm^2) to achieve the movements of a healthy adult (Erskine et al., 2011; Fukunaga et al., 1996; Maganaris et al., 2001). The same effect would have been achieved from larger muscle sizes, rather than altering specific tension. Minor inconsistencies in muscle volume fraction between the present data and cadaver data may be explained by preferential atrophy accompanying disease states (Ramsay et al., 2011) or aging (Brooks and Faulkner, 1994; Brown et al., 1992; Buford et al., 2012). The fact that the data presented here are from young, healthy subjects implies that the linear model for total muscle volume cannot be generalized to all living humans. Just as cadaver data was distinct from the healthy model presented, it is also expected that elderly, obese, or inactive populations will not have the same muscle volume per height and mass as the healthy subjects presented here but will fall below the regression line presented.

A linear relationship was observed between muscle and bone volume in the lower limb. This finding reinforces the mechanical relationship between muscle and bone. Scaling between muscle architecture and bone dimensions have been explored in the past in animals and humans (Alexander et al., 1979; Biewener, 1989; Ferretti et al., 2001). Our result is consistent with previous claims that muscle loads are among the most dominant factors that influence bone modeling and remodeling (Biewener, 1989; Frost, 1997; Robling, 2009; Schoenau, 2005; Wetzsteon et al., 2011). Since our imaging sequence did not distinguish between cortical and trabecular bone, subtler relationships regarding cortical bone density (Barbour et al., 2010) could not be investigated here.

There are several limitations of this study. While we obtained a population of 24 subjects, only one-third of the population was women and there was a larger range of masses and heights for males. The present data cannot conclusively establish that male and female curves do not diverge at extreme heights and masses; it is promising though that the females in this study fell

along the same trend line as the males. Ethnic differences in muscle volume scaling could not be addressed as 21 of these subjects were of Caucasian descent and 3 did not report ethnicity. These data can be used as the foundation for future studies performing architectural comparisons across ethnicities. The two primary muscle parameters reported in this study are volume and anatomical length; the two parameters often used in computational biomechanical models are PCSA and optimal fiber length (Zajac, 1989). These parameters can be computed from volume and length using literature values for muscle length to optimal fiber length ratio (Ward et al., 2009). PCSA values computed thus are provided (App. II, Table 3.4). Small muscles in which the line of action was oriented parallel to our transverse imaging plane (e.g. hip external rotators) are susceptible to partial volume effects and segmentation errors. Future studies on these muscles should utilize a sagittal imaging plane to reduce these errors. In this study we analyzed the right legs of all subjects. While some of our subjects may have been left-leg dominant, none of our subjects routinely participated in distinctly single-leg recreational activities (e.g. soccer). For this reason we believe that stability and ambulation—both double leg dependent activities—dominated the muscle architecture of our subjects. Further studies are needed to investigate lower limb muscle symmetry in healthy subjects. Lastly, while muscle architecture is a major predictor of muscle function, there are many other factors involved in muscle function not investigated here.

In this study, we showed that muscle volumes and lengths scale with body size in healthy humans. While these parameters do not fully describe human muscle architecture—muscle fiber length and pennation angle, for example, cannot be derived from these data without further assumptions—they can serve as a foundation for further muscle architectural studies. The results described in this paper are not directly relevant to the study of local or global muscle pathologies where one would expect substantial deviations in the size and relative size of muscles. However, these data do provide a valuable normative foundation that can be used as a basis for identifying local or global deviations in muscle volumes in these patient populations. This will allow for the

identification of preferential atrophy, muscle size imbalances, and deviations of muscle distributions in a wide variety of clinical problems as well as in elderly and obese populations. Similarly, future studies aimed at identifying adaptations of muscle distributions in athlete populations are enabled by the comprehensive normative dataset presented here.

Chapter 4

Visualization of Abnormal Muscle Size Distributions In Children with Cerebral Palsy

"The heterogeneity of disorders covered by the term CP… led Mutch and colleagues to modify the definition of CP… This definition emphasized the motor impairment and acknowledged its variability."

-Statement from the Executive Committee on the Definition and Classification of Cerebral Palsy(Rosenbaum et al., 2007)

4.1 Abstract

Introduction: Cerebral palsy is treated with a variety of therapies including musculotendon surgeries. But current treatment planning modalities do not assess sizes of individual muscles, despite the fact that surgeries target individual muscles and tendons. The aim of this study is to present an imaging-based assessment of muscle size deficits in 35 lower limb muscles in individuals with cerebral palsy.

Methods: We scanned 10 subjects with cerebral palsy using MRI, segmented 35 lower limb muscles, and determined muscle volumes and lengths. Muscle parameters were normalized and Z-scores were computed using a recently published database of typically developed muscle sizes.

Results: Muscle volumes are reduced in subjects with cerebral palsy but muscle deficits differ between muscles and across subjects. The most affected muscles were the soleus, gastrocnemius, and tibialis anterior.

Discussion: The methods presented here may be used as a pre-surgical clinical assessment that complements the existing pre-treatment assessments for cerebral palsy.

4.2 Introduction

Cerebral palsy is a disorder associated with impaired motor control and other neurosensory deficits resulting from a developmental brain injury occurring in utero or around the time of birth (Bax, 1964; Bax et al., 2005; Mutch et al., 1992; Rosenbaum et al., 2007). The incidence has been approximately 2-5 per 1000 live births for the last 3 decades (Stanley et al., 2000). The clinical problems and movement deficits in these patients varies depending on the size and location of the brain lesions (Bax et al., 2005; Mutch et al., 1992; Narayanan, 2012). This heterogeneity has led to an array of treatment approaches to address the motor impairments including lengthening of muscle-tendon units (Abel et al., 1999), injections with neurotoxins (botulinum) (Boyd and Hays, 2001; Graham et al., 2000), oral tonus-affecting medications (Albright, 1996; Butler et al., 2000), and neurosurgical approaches including selective dorsal rhizotomy (McLaughlin et al., 2002, 2008; Wright et al., 2008). Physical therapies are perhaps the most commonly used modality since they are non-invasive (Damiano, 2006). The specific treatment used is dependent on defining the movement or gait abnormality and its cause. Physical exams, joint motion assessments, and observational or computerized gait analysis are the common means to define the sources of the problem and to plan treatments (Gage, 1994; Narayanan, 2007). These techniques are limited, however, in that none offers information about individual muscle architecture, despite the fact that the treatments, especially musculotendon surgery, are designed to affect individual muscles. An assessment tool that reveals information of individual muscles would thus be a valuable complement to the current set of pre-treatment assessments.

Muscle volumes and length measures may be obtained from medical imaging approaches and are important since these measures relate directly to muscular strength capacity and joint excursion (Akagi et al., 2009; Fukunaga et al., 2001; Holzbaur et al., 2007a; Lieber and Friden, 2000; Trappe et al., 2001). Imaging studies in cerebral palsy have made it clear that subjects with

cerebral palsy have less muscle volume on average than typically developed subjects (Barrett and Lichtwark, 2010; Elder et al., 2003; Fry et al., 2007; Malaiya et al., 2007; Noble et al., 2014; Oberhofer et al., 2010; Reid et al., 2014). These studies have focused only on a small number of lower limb muscles, leaving a gap in understanding about the spectrum of effects across all the muscles of the lower limb. Furthermore, previous studies report population means of muscle volume or volume deficit, which are not sufficient for understanding how an individual's specific muscle profile relates to a movement deficit. For surgical and treatment planning purposes, information on muscle volume abnormality would be more powerful if it were available on a subject-by-subject and a muscle-by-muscle basis in a way that compares individual subjects to a normative confidence interval.

In this study, we present an MRI-based approach for quantifying and visualizing individual muscle sizes in subjects with cerebral palsy. To assess individual muscle size deficit with respect to typically developed muscle, muscle size parameters in subjects with cerebral palsy were compared to a previously published *in vivo* dataset of muscle sizes (Ch. 3, Handsfield et al., 2014) using Z-scores. **The goal of this work was to apply this approach to a cohort of subjects with cerebral palsy and assess volume, length, and PCSA deficit across 35 muscles in each subject.** We believe the method presented here can be used to non-invasively identify abnormally small muscles in individual subjects and will complement the existing mobility and strength measures used for pre-treatment assessments in cerebral palsy.

4.3 Methods

Subject Characteristics

Ten children with cerebral palsy with the following subject characteristics (mean ± s.d. [range]): age: 13.9 ± 1.9 [11-17] years, height: 159.1 ± 12.6 [134.5-175.3] cm, body mass: 59.4 ± 16.7 [36.4-96.1] kg, body mass index: 23.2 ± 4.7 [17.6-31.5] kg/m^2 were selected for this study (Table 4.1). The cerebral palsy population is heterogeneous and included hemiplegic and diplegic subjects ranging in GMFCS score from I to III. Also, many subjects previously had surgical interventions including hamstrings release, Achilles lengthening, hamstrings lengthening, and dorsal rhizotomy. Subject inclusion criteria were: age between 11 and 17 years, the ability to ambulate, and the ability to remain motionless in the MRI scanner for the duration of the imaging time. Subjects were recruited from University of Virginia clinics; those who could safely undergo an MRI were included in the study until we reached the budget number of 10 subjects. All subjects and their legal guardians provided informed consent and all methods were approved by the University of Virginia Institutional Review Board. A subset of 8 age-matched typically developing subjects was selected from a previously published dataset of *in vivo* muscle lengths and volumes (Ch. 3, Handsfield et al., 2014). The subject parameters of this subset were: age: 14.0 ± 1.5 [12-17], height: 165.7 ± 10.1 [145.4-178.4] cm, body mass: 64.9 ± 12.1 [47.5-83.5] kg, body mass index: 23.5 ± 3.0 [20.2-29.7] kg/m^2.

Tables 4.1 a/b: Subject data for subjects with cerebral palsy

Subject	1	2	3	4	5
GMFCS	1	1	2	2	2
Gender	m	m	m	m	m
Age	14	15	15	12	13
Ethnicity	white	white	white	white	white
Mass (kg)	41.5	54.6	65.1	63.1	60
Height (m)	1.535	1.753	1.625	1.534	1.544
BMI(kg/m^2)	17.6	17.8	24.7	26.8	25.2
CP Aetiology	placenta previa	stroke	prematurity	stroke	stroke
CP subtype	diplegia	hemiplegia	diplegia	hemiplegia	hemiplegia
Most Affected Side	left	right	right	right	right
Surgical History	none	none	hamstring release, previous botox	gastroc-soleus-achilles lengthening	none
Gait	foot dragging	equinovarus	crouch	equinus, crouch	equinus
Orthosis Use	over-the-counter arch supports	none	over-the-counter arch supports	posterior shell ankle-foot-orthosis	articulated ankle-foot-orthosis

Subject	6	7	8	9	10
GMFCS	2	2	2	2	3
Gender	m	f	m	f	m
Age	17	13	16	11	13
Ethnicity	white	other	white	white	white
Mass (kg)	96.1	53.6	52.2	36.4	71.5
Height (m)	1.748	1.499	1.698	1.345	1.632
BMI(kg/m^2)	31.5	23.9	18.1	20.1	26.8
CP Aetiology	unknown	prematurity	hemorrhage/ infarct	prematurity	stroke / hemorrhage
CP subtype	diplegia	hemiplegia	hemiplegia	hemiplegia	diplegia
Most Affected Side	right	right	right	left	left
Surgical History	gastroc-soleus-achilles lengthening	femoral osteotomy, gastroc-soleus-achilles lengthening	gastroc-soleus-achilles lengthening	gastroc-soleus-achilles lengthening	hamstring lengthening, dorsal rhizotomy
Gait	claw toe, bilateral cavus feet	in-toeing, equinus	equinovalgus	equinus	crouch
Orthosis Use	none	ankle-foot-orthosis	right side articulated ankle-foot-orthosis	over-the-counter arch supports	loftstrand crutch, bilateral floor reaction ankle-foot-orthoses, Left thigh cuff

Imaging and Segmentation

Subjects were scanned on a 3T Siemens (Munich, Germany) Trio MRI Scanner using a 2D multi-slice gradient-echo pulse sequence with an interleaved spiral k-space trajectory (Meyer et al., 1992). The scanning parameters used were: TE/TR/α: 3.8 ms/ 800 ms/ 90°; FOV: 400 mm × 400 mm; slice thickness: 5 mm; in plane spatial resolution: 1.1 mm × 1.1 mm; body receiver coil; and 4 signal averages. Spectral-spatial excitation pulses were used for fat suppression (Meyer et al., 1990). Additionally, a Chebyshev approximation was applied for semi-automatic off-resonance correction to compensate for spatial variations of the magnetic field (Chen and Meyer, 2008). Contiguous axial images were obtained from the iliac crest to the ankle joint. Scan time was approximately 20 minutes per subject.

Each of 35 muscles in the paretic limb for hemiplegic subjects and the most affected limb for diplegic subjects was segmented using in-house segmentation and image processing software written in Matlab (The Mathworks Inc., Natick, MA, USA). Segmentations were performed by a team of 4 trained individuals, each provided with a detailed slice-by-slice segmentation atlas created from one of our data sets. A single highly trained user evaluated and refined all segmentations before further analysis to ensure consistency across users. After segmentation, the volume of each muscle was calculated by summing all of the slice-wise voxel volumes for each muscle. Total lower limb muscle volume was computed as the sum of all of the 35 muscles segmented for each subject (muscle volume reconstructions shown in Fig. 4.1).

Muscle length, which has been shown to influence joint range of motion (Lieber and Friden, 2000), and muscle physiological cross sectional area (PCSA), which has been shown to influence muscle strength (Lieber and Friden, 2000), were determined from imaging volumes. Muscle lengths along the muscle's line-of-action were computed from the 3D path of the centroids calculated at each imaging slice (Ch. 3, Handsfield et al., 2014). PCSA was computed by dividing

muscle volume by optimal fiber length, where the optimal fiber length was estimated by scaling muscle length by the optimal fiber length – to – muscle length ratios (L_m/L_f^0) found in the literature (Ward et al., 2009) (Appendix I, Eq. A1). Use of PCSA over a standard cross-sectional area metric controls for differences in fiber direction between muscles in estimating muscular strength capacity (Lieber and Friden, 2000). Computation of PCSA and length distinguishes muscle volume deficits as relating to strength impairments (PCSA deficit) or range-of-motion impairments (length deficit).

Data Analysis

To remove the effects of body size on muscle size differences, muscle volumes were normalized by the product of height and mass (App. I, Eq. A2). It has been found that lower limb muscle volumes of healthy subjects are better predicted by this product than by mass alone (Ch. 3, Handsfield et al., 2014). Normalizing by this product yields a functional metric—muscle volume per height-mass—that accounts for both size (body mass) and stature (height) in assessing muscle size. Muscle length was normalized by limb length (App. I, Eq.A3) as these parameters have been found to scale together (Ch. 3, Handsfield et al., 2014) and PCSA was normalized by height·mass and limb length (App. I, Eq. A4.1).

To assess the normality of individual muscles in subjects with cerebral palsy we computed Z-scores for each muscle in each subject with cerebral palsy. A Z-score is the difference between an individual parameter and the mean of a reference population divided by the standard deviation of the reference population:

$$Z = \frac{normalized\ volume_{CP} - mean(normalized\ volume_{TD})}{st.dev.(normalized\ volume_{TD})} \quad (1)$$

where *normalized volume$_{CP}$* is the volume per height-mass of a muscle for subjects with CP, *mean(normalized volume$_{TD}$)* is the population mean of volume per height-mass in the typically

developed group, and *st.dev.(normalized volume$_{TD}$)* is the typically developed standard deviation of volume per height-mass. In this case, Z-score is a measure of how many TD standard deviations (σ) a CP muscle is away from the TD mean. Use of Z-scores provides a statistically meaningful measure of volume deviation relative to typically developed muscles. Z-scores were computed for height-mass normalized muscle volumes for each of the 35 muscles. Z-scores greater than 2 or less than -2 were considered to be markedly abnormal since these limits fall outside of the 95% confidence interval of the TD data. For all statistical tests on normalized parameters, the Wilcoxon Rank-Sum test was used.

4.4 Results

A visualization of the Z-scores of muscle volumes per height-mass mapped onto subject-specific limb reconstructions (Fig. 4.1) reveals the array of muscle size impairments across the lower limbs from subjects with cerebral palsy. By colorcoding muscles that fall outside of 2σ of the typically developed mean, the illustration highlights regions of the limb that are the most impaired. Deficits can be visually noted in the calf for all subjects, the thigh for approximately half the subjects, and across the hip in some subjects.

A Z-score myoarray (Fig. 4.2A) allows inspection of patterns of individual muscle size deficits across muscles and across CP subjects. Individual muscles, listed in order of proximal to distal, are displayed on the horizontal axis while subjects are on the vertical axis. Despite the heterogeneity of the present CP population, several patterns are evident. Abnormally small muscles are concentrated more distally than proximally and the plantarflexors and dorsiflexors are small in all subjects. Hamstrings and quadriceps are often small across the population. Tabulation of the number of subjects with Z-scores less than -2σ for each muscle reveals population-wide individual muscle trends (Fig. 4.2B). The soleus, medial gastrocnemius, tibialis anterior, semimembranosus, and the digital extensors (combined volumes of the EDL and EHL muscles) are each abnormally small in at least 8 of the 10 subjects. Of the 350 muscles assessed in subjects with CP, 117 muscles (33%) are outside of the 2σ confidence interval and 78 of these muscles (22%) are more than 2.5σ smaller than the mean. Twenty-three muscles in the cerebral palsy cohort are more than 4σ smaller than the mean, indicating a severe degree of muscle size impairment.

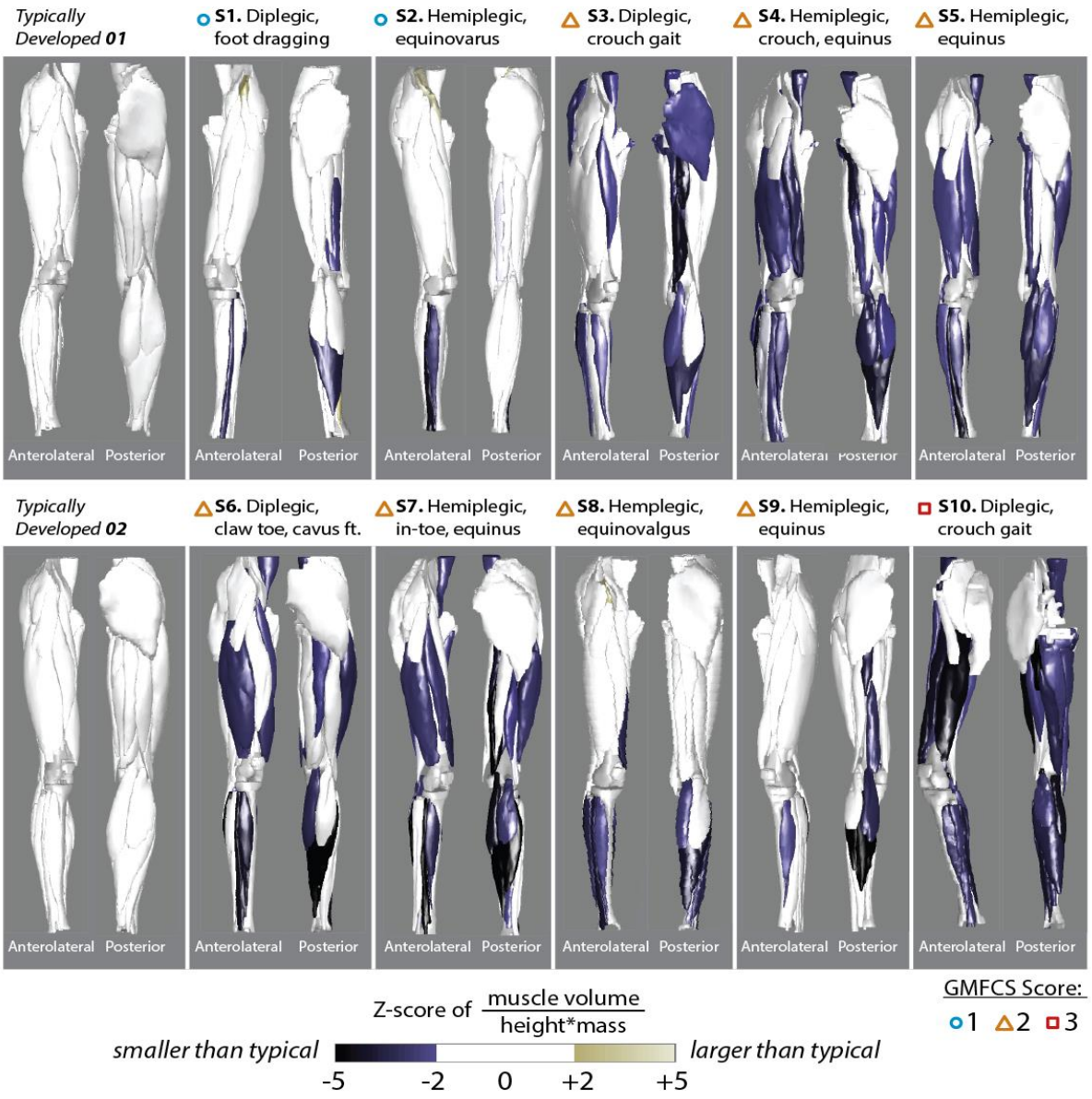

Figure 4.1: Z-score colormaps of individual subjects' musculature

Deviations in muscle volume between subjects with cerebral palsy and typically developed subjects are identified with Z-scores, defined as the number of standard deviations that a CP muscle is from the typically developed mean. Values between ±2 represent the 95% confidence interval for typically developed muscles and Z-scores outside of ±2 are considered significantly abnormal. Volumes were normalized by height·mass to account for differences in body size.

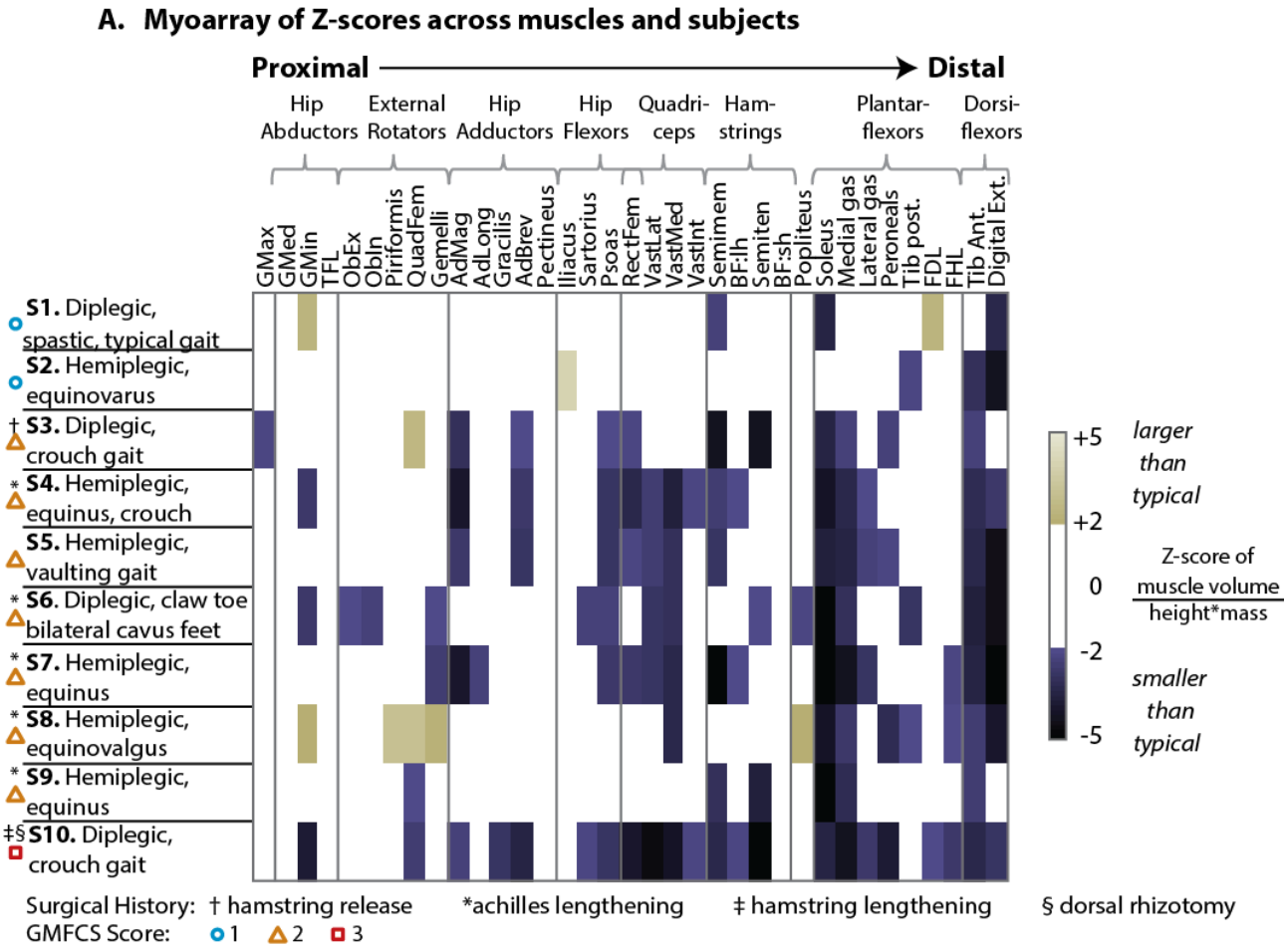

B. Summary: number of subjects for whom each muscle has Z-score < -2

muscles in which **0-2** subjects display Z<-2			muscles in which **3-6** subjects display Z<-2			muscles in which **7-10** subjects display Z<-2
GMax	QuadFem	Sartorius	GMin	VastLat	Peroneals	Semimem
GMed	Gemelli	BF:sh	AdMag	VastMed	Tib post.	Soleus
TFL	AdLong	Popliteus	AdBrev	BF:lh	FHL	Medial gas
ObEx	Gracilis	FDL	Psoas	Semiten		Tib Ant.
ObIn	Pectineus	VastInt	RectFem	Lateral gas		Digital Ext.
Piriformis	Iliacus					

Figure 4.2: Grid of Z-scores allows visual comparisons across subjects or across muscles

A. Patterns of muscle smallness differ across subjects, but size deficits in the hamstrings, plantarflexors, and dorsiflexors are common. B: A summary table was made by binning muscles by the number of subjects in which they are abnormally small. The semimembranosus, soleus, medial gastrocnemius, tibialis anterior, and the digital extensors were significantly small in at least seven of the ten subjects.

Eight subjects with cerebral palsy in this study have reduced total lower limb muscle volume based on their height and mass (Fig. 4.3A). Total limb muscle per height-mass varies across the CP population and is stratified by GMFCS score (Fig. 4.3B). The 2 CP subjects who are classified as GMFCS 1 have muscle volume per height-mass that is consistent with typically developed subjects from Handsfield et al.(Ch. 3, Handsfield et al., 2014). The hip abductors and external rotators are the only 2 functional muscle groups out of 9 that are not small in the CP group compared to the TD group (Fig. 4.4). The ratios of muscle size for agonist-antagonist pairs for the CP group are similar to the TD sample except for the abductor-adductor ratio, which is markedly smaller for the CP group.

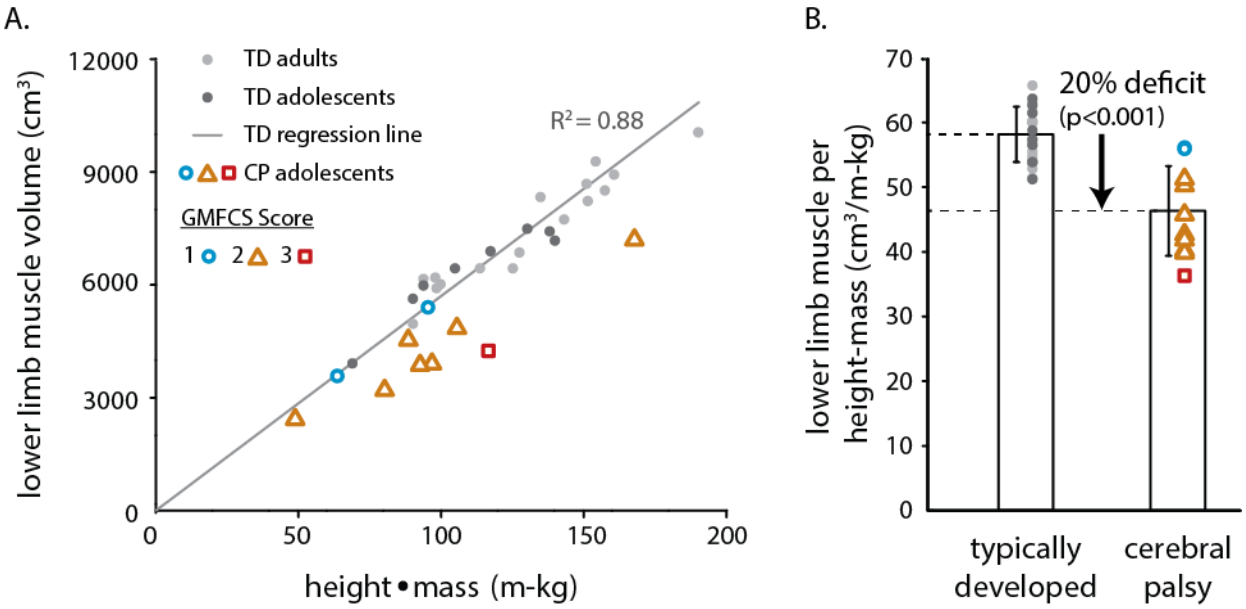

Figure 4.3: Muscle volume per height-mass in typically developed (TD) and CP subjects

A.Total muscle volume in the lower limb scales with height·mass in typically developed subjects but is reduced in subjects with cerebral palsy. B. Lower limb muscle volume per height-mass is 20% lower in subjects with cerebral palsy and is stratified by GMFCS score. Error bar displays standard deviation; individual data points are overlaid.

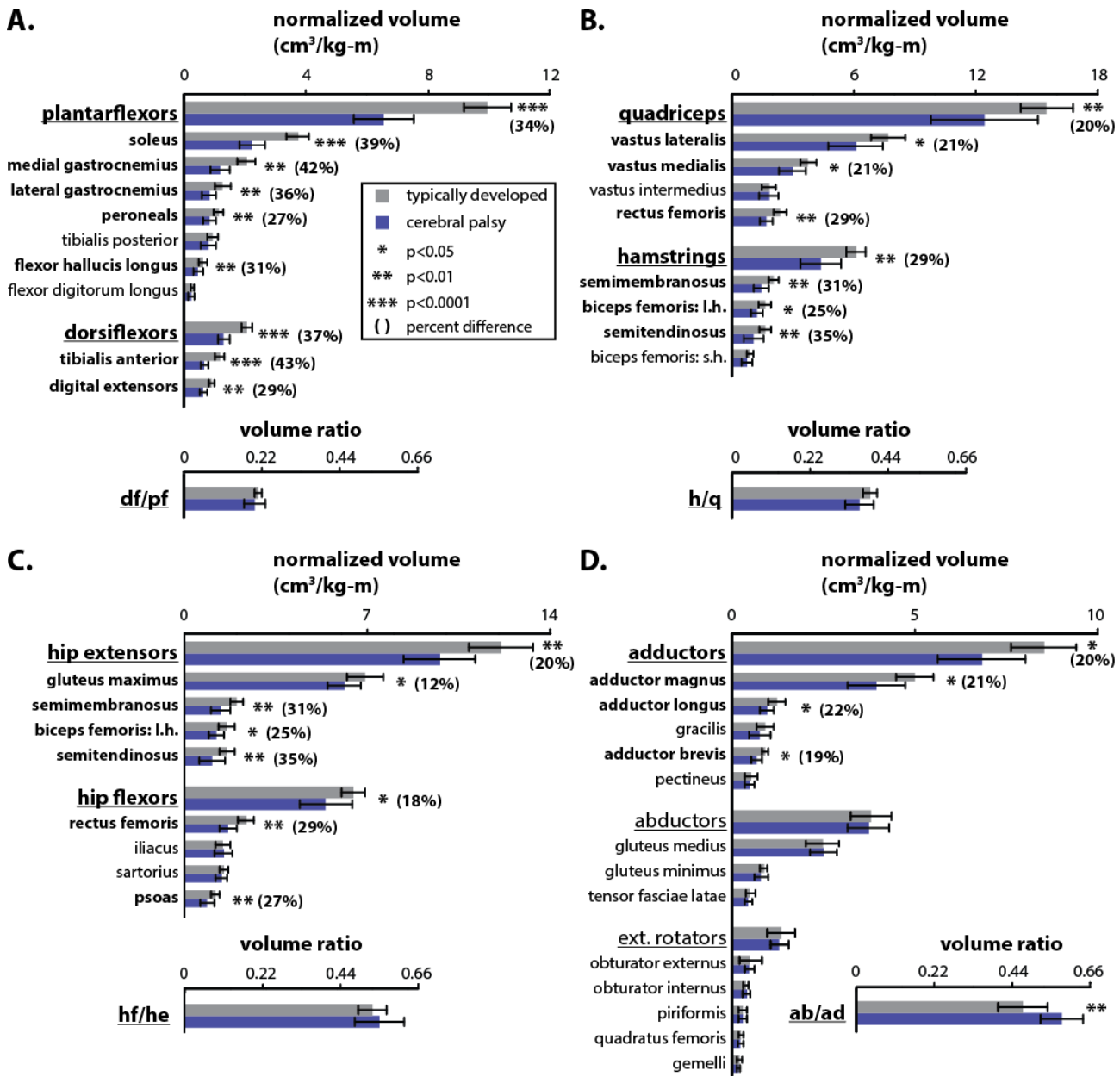

Figure 4.4: Comparison of muscle volumes and muscle group volumes between TD and CP subjects

Height-mass normalized muscle volumes are reduced in subjects with cerebral palsy for muscles and muscle groups crossing the ankle (A), knee (B), hip sagittal plane (C), and hip frontal plane (D). Antagonist volume ratios for muscle groups are only significantly different for the Abduction/Adduction ratio. Muscle groups are underlined and muscles displaying significant differences are shown in bold.

Population means of muscle volume deficits in many cases are not consistent with individual muscle volume deficits. For example, Z-score analysis reveals 3 CP subjects with small gluteus minimus volumes and 2 subjects with large gluteus minimus volumes (Fig. 4.2). This variance of expression is not evident from the means comparison of gluteus minimus volume per height-mass (Fig. 4.4). Similarly, the vastus lateralis displays a large variance of expression (Fig. 4.2): 5 subjects have smaller vastus lateralis while 5 subjects are within the normal range. The population-wise means comparison does not illuminate this variance of expression.

The majority of muscles displaying volume deficits also presents deficits in PCSA, while fewer muscles display deficits in length (Fig. 4.5 & Appendix II, Table 4.2). The few muscles displaying significant length deficits include muscles involved in plantarflexion, dorsiflexion, knee flexion, and hip adduction especially the gastrocnemius, semitendinosus, and gracilis muscles (App. II, Table 4.2). Muscles within the same functional group do not necessarily display similar strength and length deficits. For example, the semimembranosus is significantly weak but not short in 7 subjects while the semitendinosus is significantly short in 4 subjects and the gracilis is significantly short in 7 subjects (Fig. 4.5). CP subjects are not homogeneous in their expression of weakness and shortness of muscles—muscles exhibit a range of levels of weakness and shortness in this population.

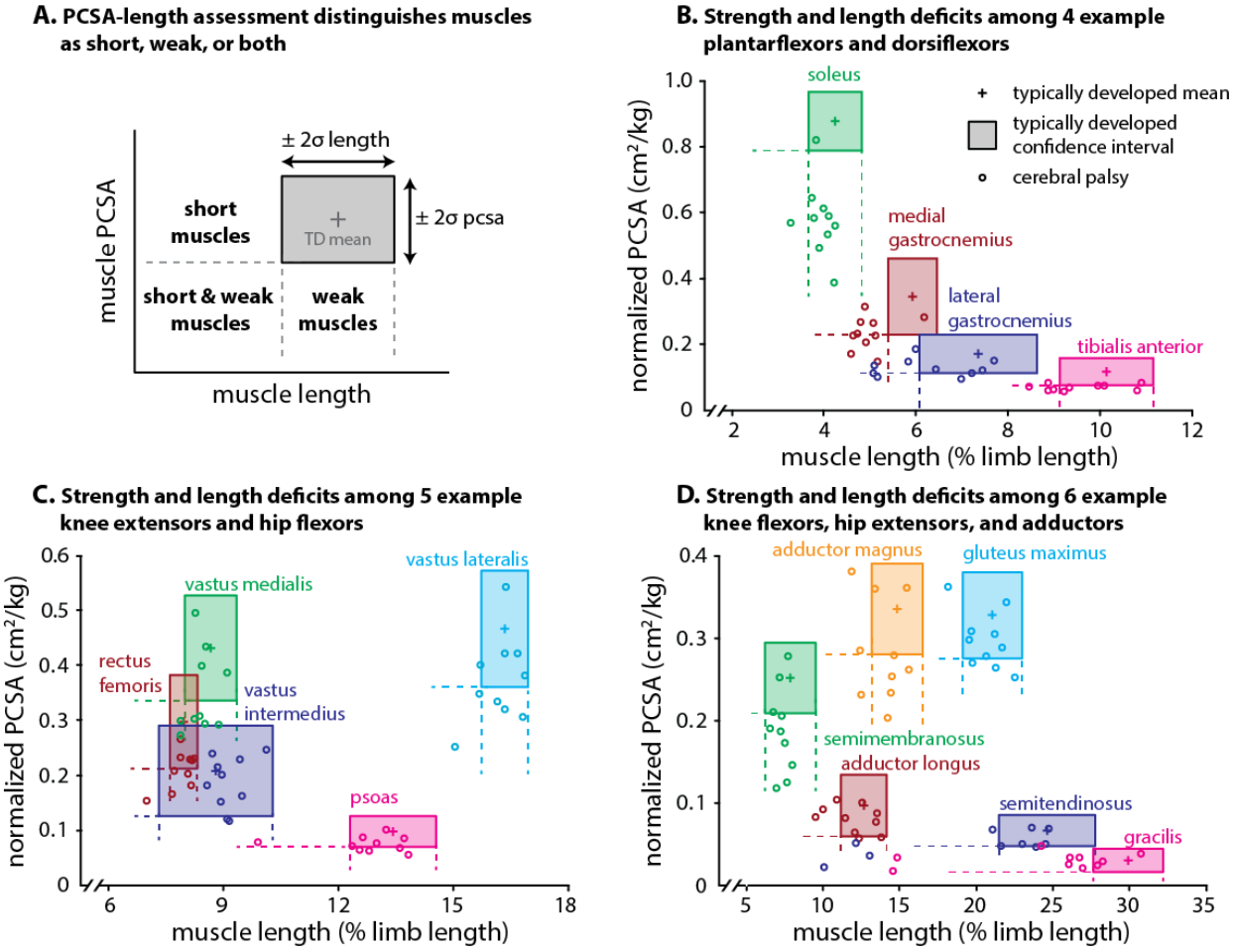

Figure 4.5: Muscle volume deficits may be due to deficits of PCSA or deficits of length

PCSA deficits indicate functional weakness. Length deficits indicate impaired range of motion. The mean and 2σ confidence interval for PCSA and length are shown for the typically developed group. Regions outside of the 2σ bounding box identify CP muscles as short, weak, or short and weak (A). Example muscles are shown in B, C, and D. PCSA and length were normalized according to Equations A4.1 and A5 (Appendix).

4.5 Discussion

In this study, we employed MRI to comprehensively assess muscle deviations in the lower limbs of children with cerebral palsy compared to muscle measurements derived from a database of healthy muscles. Using a Z-score assessment and several visualizations for identifying muscle size abnormality across muscles and subjects, our results show that muscles in subjects with CP are generally small, the magnitude of muscle atrophy varies across individuals, and small muscles are due mostly to small cross-sectional areas and, to a lesser extent, are due to length impairments. These results highlight the inhomogeneity of muscle architecture present across muscles and across subjects with cerebral palsy.

Previous studies have demonstrated that muscle volume is a useful parameter for assessing muscle strength capacity as it is related to joint torque(Akagi et al., 2009; Fukunaga et al., 2001; Holzbaur et al., 2007a; Reid et al., 2014; Trappe et al., 2001) and muscle force(Brand et al., 1986; Lieber and Friden, 2000), and can be acquired robustly from medical imaging. Several seminal studies have demonstrated the utility of MRI to quantify muscle volumes in individuals with CP (Elder et al., 2003; Noble et al., 2014; Oberhofer et al., 2010). These studies have focused their analysis to a few muscles and reported population means but have not highlighted the extent of inter-subject variability in muscle architecture. For example, Elder et al. (Elder et al., 2003) reported mean deficits in volumes and CSAs of the anterior and posterior leg compartment and the CSA of the soleus, Oberhofer et al. (Oberhofer et al., 2010) reported mean volume and length differences of 6 lower limb muscle structures, and Noble et al. (Noble et al., 2014) reported mean muscle volumes in 9 muscles in the lower limb. The present study builds upon this work by providing a holistic analysis of volume, length, and PCSA deficits in 35 lower limb muscles and illustrates inter-subject variability in muscle architecture.

The findings from previous MRI-based measurements of muscle volumes in children with CP all demonstrate diminished muscle volumes overall; however, these studies are not consistent regarding which muscles are most involved. For example, while Oberhofer et al. (Oberhofer et al., 2010) found substantially diminished volumes in the hamstrings and vasti but not in the plantarflexors, Noble et al. (Noble et al., 2014) found substantially diminished volumes in the hamstrings and plantar flexors but not in the vasti. We found diminished volumes in the hamstrings, vasti, and plantarflexors. Because all of these studies, as well as the present one, were based on relatively low sample sizes due to the cost and time of MRI and segmentation, it would be expected that we would find somewhat disparate results given the inter-subject variability in muscle size patterns observed in the present study. Therefore, generalizations based on sample means of muscle volume deficits in children with CP should be interpreted with caution. The mean values may differ if another CP population is sampled, and, even so, the mean will most likely not represent patterns of muscle deficit in a given individual subject.

Differences in muscle volume may be due either to physiological cross-sectional area (PCSA), a surrogate of muscle strength (Lieber and Friden, 2000), or to length, a surrogate of joint range-of-motion and maximum contraction velocity (Lieber and Friden, 2000). In our population, deficits in PCSA were the dominant contributor to deficits in volume. Although deficits in length were present to a lesser degree than deficits in PCSA, for certain muscles and certain individuals, length deficits were considerable especially in the gracilis, semitendinosus, and gastrocnemius muscles. The PCSA estimates presented here are based on literature values for muscle length to optimal fiber length ratio and do not take into account inter-subject differences in pennation angle or sarcomere operating range, features which may vary in CP populations (Lieber and Friden, 2003; Mohagheghi et al., 2007; Shortland et al., 2002; Smith et al., 2011). In the future, advances in techniques for assessing subject-specific pennation angles and sarcomere lengths *in vivo*

(Cromie et al., 2013; Damon et al., 2002; Froeling et al., 2012; Llewellyn et al., 2008) will further expand the utility of imaging-based PCSA-length assessments.

The relationship between neuromotor control and muscle size is not well understood and was not specifically studied in this work. However, we did find total muscle volume per height-mass scales with level of function, indicated by GMFCS score. Rose et al. (Rose et al., 1994) previously found a structure-function association between muscle fiber-type variability and energy expenditure index during gait. Reid et al. (Reid et al., 2014) report a muscle size-strength association in TD and CP subjects but note that functional strength per muscle size is reduced and more variable in subjects with CP. Both macro- and micro-scale muscle structure are important for linking neuromotor control, skeletal gait mechanics, muscle size, and function. Future work pursuing these relationships is needed to optimize therapeutic approaches utilized in CP.

What led to decreases in muscle size in our CP population? Small muscles may be the result of a combination of many factors, including impaired motor control, neural denervation, prior muscle-tendon surgeries, skeletal deformations, altered gait mechanics, or diminished activity levels. Due to the cross-sectional design of this study, we were not able to examine the sources that led to the observed muscle impairments. In the future, the present techniques have utility in studying the longitudinal effects of surgical and non-surgical factors on the sizes of many muscles.

There are several limitations to the measurements made in this study. First, while the relationship between muscle volume and strength has been studied in both healthy subjects (Akagi et al., 2009; Fukunaga et al., 2001; Holzbaur et al., 2007a; Trappe et al., 2001) and subjects with CP (Elder et al., 2003; Moreau et al., 2010; Reid et al., 2014), a complete understanding of the relationship between muscle size, motor control, and function in cerebral palsy has not been achieved. The implication that smaller muscles generate less force and that short muscle have less

excursion is supported by the literature (Lieber and Friden, 2000; Reid et al., 2014). Secondly, we did not distinguish intramuscular fatty infiltration (Johnson et al., 2009) or fibrotic tissue (Booth et al., 2001) from healthy muscle in the computation of muscle volume. Thus, the reported CP volume measurements likely include non-contractile tissue and thus over-predict the true volume of functional muscle tissue. Thirdly, we did not account for differences in muscle fiber type between the typically developed and cerebral palsy group. Previous studies have reported variability in type I fiber distribution among children with cerebral palsy (Foran et al., 2005; Ito et al., 1996; Rose et al., 1994). Future work may illuminate if fiber type distribution is related to whole muscle volume deficiencies.

The *in vivo* muscle analysis presented here has potential to improve the pre-operative assessment by complementing and clarifying the results of gait analysis and joint motion assessments. Several studies have indicated that interpretation of muscle function from gait analysis in cerebral palsy is a challenge (Narayanan, 2012; Skaggs et al., 2000) and gait analyses are usually complemented by additional approaches to confidently identify sources of gait abnormality (Davids et al., 2003). In particular since muscle-tendon surgeries and strengthening regimes target individual muscles specifically, knowing muscle-by-muscle size information would be a valuable complement to gait data for both clinical and research approaches (Steele et al., 2012, 2010). In order to merge muscle volume data with gait analysis, physical exams, and other clinical diagnosis methods, more sophisticated statistical approaches, such as cluster analysis and machine learning (Ries et al., 2014), may be used in the future to develop data-driven categorizations of subjects with cerebral palsy that better diagnose their impairments and suggest classes of optimal treatments.

Further technical developments are required in order for the *in vivo* muscle analysis presented here to become clinically viable. The measurements presented in this study rely on a custom rapid MRI sequence (Ch. 3, Handsfield et al., 2014) that is not widely available on all MRI scanners and time-intensive post-processing approaches that would be impractical to implement clinically at this time. Current efforts to make rapid MRI sequences more widely available and to develop robust automatic approaches to segmentation of muscles (Gilles et al., 2006; Scheys et al., 2009) will enable these measurements to become clinically viable and also empower clinical research studies of much larger subject populations. The data presented here demonstrate the potential clinical utility of these measurements and therefore motivate these proposed technical developments.

In conclusion, we have used MRI and muscle size scaling approaches to show that muscles per body size are smaller among children with cerebral palsy than typically developed controls; however, patterns of muscle atrophy are non-uniform across subjects and across muscles. These data may be used to inform subject-specific therapies such as muscle strengthening approaches or muscle-tendon transfers and muscle-tendon lengthenings. The visualization approaches presented in this work may have clinical utility in demonstrating statistically significantly small muscles in individual subjects compared to a control population.

Chapter 5

Adding Muscle Where You Need It:

Non-uniform Hypertrophy Patterns in Collegiate Sprinters

"The legs feed the wolf."

- Coach Herb Brooks, U.S. Olympic Hockey Team

5.1 Abstract

Purpose: To determine which of 35 lower limb muscles are significantly larger among competitive collegiate sprinters compared to healthy non-sprinter controls, if there are bilaterally asymmetric muscles in sprinters, and if muscle sizes differ between male and female sprinters.

Methods: We used an advanced, non-Cartesian MRI sequence to rapidly acquire stacks of axial 2D images through the lower limb in competitive collegiate sprinters. We segmented 35 lower limb muscles in image sets and determined volumes, lengths, and physiological cross sectional areas. We normalized muscle measurements by height*mass, limb length, and mass, respectively. Using a previously published dataset of healthy, non-sprinter muscle sizes, we computed Z-scores of athletes' muscle sizes and made statistical comparisons between groups.

Results: Sprinters present more limb musculature per height-mass than controls, but not all muscles are uniformly larger. Muscles involved in hip flexion and extension and knee extension are disproportionately and significantly larger among the sprinters than muscles crossing the ankle joint. The tibialis posterior was the only ankle-crossing muscle significantly larger in sprinters. No muscles were significantly bilaterally asymmetric among sprinters and no muscles were significantly different between male and female sprinters when normalized by the height-mass product.

Discussion: The fact that sprinters have more muscle mass per body size but muscle size differences are not uniform suggests that sprinters may undergo non-uniform hypertrophy of their limb muscles in training for their sport or may have genetic pre-dispositions toward large muscles. Hip flexion/extension and knee extension may be more important for generating high-speed gait than ankle plantarflexion and dorsiflexion. Furthermore, these data may be used as more accurate estimates of sprinters' muscle sizes than previous data generated from cadaver dissection.

5.2 Introduction

How is it that sprinters are able to run so fast? Previous research on this question has investigated moment arms (Lee and Piazza, 2009), muscle fiber types (Costill et al., 1976; Gregor et al., 1979), oxidative capacity (Costill et al., 1976; Hirakoba and Yunoki, 2002), neuromuscular activation (Ross et al., 2001), and muscle fascicle lengths (Kumagai et al., 2000). While this question has been explored in a variety of ways, muscle volumes have not been directly assessed in a group of sprinters. This has prevented a thorough understanding of the strength capacity of the lower limb in competitive collegiate sprinters.

Previous research has utilized medical imaging to determine *in vivo* muscle sizes in athletes (Tate et al., 2006), but that study assessed recreational athletes of various sports and assessed only 13 key muscles in the lower limb. An imaging approach across all 35 of the lower limb muscles in a group of competitive sprinters would enable a greater understanding of how individual muscles are influenced by a specific sport. Coupled with information on non-athlete muscle volumes in the lower limb, such an imaging approach would also begin to illuminate the hypertrophy patterns induced by high speed sprinting.

Musculoskeletal models are promising in their ability to predict muscle and joint forces during a dynamic activity (Delp and Loan, 2000; Erdemir et al., 2007). Previous musculoskeletal models of running gait have suggested that muscle forces increase nonlinearly with increasing gait speed (Dorn et al., 2012), suggesting that as gait speed increases some muscles contribute more than others to net forces of gait. In particular, the modeling approach by Dorn et al. (2012) predicted that forces generated by the hip and knee extensors increase disproportionately during high speed sprinting. These predictions are hypothetical, however, and it is not clear how these modeling results relate to actual muscle adaptations in sprinters. It may be hypothesized that the muscles predicted to require the most force increases with running speed will demonstrate a high

degree of hypertrophy among high speed sprinters since those are muscles that are used disproportionately during fast running. A comprehensive imaging assessment of the lower limbs of sprinters compared to non-sprinter controls may indicate hypertrophy patterns among the sprint group and lend confidence to results from musculosekeletal models. Such a study would also generate valuable *in vivo* data on bilateral muscle sizes in sprint athletes so that future modeling approaches may use sprinter-specific muscle inputs for male and female runners.

The goal of this work was to conduct a large *in vivo* imaging analysis of 15 collegiate sprinters and compare their muscle sizes to a previously published database of healthy *in vivo* muscle sizes from 24 active non-sprinters. We hypothesized that i) some muscles in sprinters are hypertrophied in volume compared to controls but other muscles are not, ii) muscles associated with hip and knee extension are hypertrophied among sprinters, iii) sprinters' lower limbs are bilaterally symmetric, iv) there are not gender differences in muscle size per body size, and v) the total muscle volume per body size is greater among sprinters than non-sprinter controls.

5.3 Methods

Subject Characteristics

Fifteen competitive sprinters (eight female, seven male) from the University of Virginia varsity track team with the following subject characteristics (mean ± s.d. [range]): age: 18 ± 0.6 [18-20] years, height: 176.8 ± 8.1 [162.6-193.0] cm, body mass: 68.9 ± 8.5 [54.4-82.5] kg, body mass index: 22.0 ± 1.7 [19.4-24.7] kg/m^2 were selected for this study. All subjects were self-identified sprinters and competed in events including sprints, jumping events, and hurdles. Seven of the subjects reported prior hamstrings injury (one bilateral), but all subjects were healthy and competing at the time of this study. All subjects provided informed consent and all methods were approved by the University of Virginia Institutional Review Board. A previously published dataset of *in vivo* muscle lengths and volumes from 24 recreationally active, healthy individuals was used as a non-sprinter control dataset (Ch. 3, Handsfield et al., 2014). The subject parameters of this dataset were: age: 25.5 ± 11.1 [12-51], height: 171 ± 10 [145-188] cm, body mass: 71.8 ± 14.6 [47.5-107.0] kg, body mass index: 24.3 ± 4.0 [18.9-35.1] kg/m^2.

Imaging and Segmentation

Subjects were scanned on a 3T Siemens (Munich, Germany) Trio MRI Scanner using a 2D multi-slice gradient-echo pulse sequence with an interleaved spiral k-space trajectory (Meyer et al., 1992). The scanning parameters used were: TE/TR/α: 3.8 ms/ 800 ms/ 90°; FOV: 400 mm × 400 mm; slice thickness: 5 mm; in plane spatial resolution: 1.1 mm × 1.1 mm; body receiver coil; and 4 signal averages. Spectral-spatial excitation pulses were used for fat suppression (Meyer et al., 1990). Additionally, a Chebyshev approximation was applied for semi-automatic off-resonance correction to compensate for spatial variations of the magnetic field (Chen and Meyer, 2008).

Contiguous axial images were obtained from the twelfth thoracic vertebra to the ankle joint. Scan time varied according to subject height but was approximately 30 minutes per subject.

Each of 35 muscles in both limbs was segmented using in-house segmentation and image processing software written in Matlab (The Mathworks Inc., Natick, MA, USA). Segmentations were performed by a team of seven trained individuals, each provided with a detailed slice-by-slice segmentation atlas created from one of our data sets. A single highly trained user evaluated and refined all segmentations before further analysis to ensure consistency across users. After segmentation, the volume of each muscle was calculated by summing all of the slice-wise voxel volumes for each muscle. Lower limb muscle volume was defined as the sum of all of the 35 muscle volumes in one limb; for the sprinters, this was computed as the mean summed volume of their two limbs.

Muscle length, which is related to joint range of motion (Lieber and Friden, 2000), and muscle physiological cross sectional area (PCSA), which is related to muscle strength (Lieber and Friden, 2000), were determined from imaging volumes (see Appendix I). Muscle lengths along the muscle's line-of-action were computed from the 3D path of the centroids calculated at each imaging slice (Ch. 3, Handsfield et al., 2014). PCSA was computed by dividing muscle volume by optimal fiber length (Appendix I), where optimal fiber length was estimated by scaling muscle length by the optimal fiber length – to – muscle length ratios (L_m/L_f^0) found in the literature (Ward et al., 2009).

Data Analysis

To remove the effects of body size on muscle size differences, muscle volumes were normalized by the product of height and mass. It was shown previously that lower limb muscle volumes of healthy subjects are predicted by this product (Ch. 3, Handsfield et al., 2014). Normalizing by this product yields a functional metric—muscle volume per height-mass—that can be used to compare the gross muscle capacity per body shape and size between subjects of different populations. Muscle length was normalized by limb length as these parameters have been found to scale together (Ch. 3, Handsfield et al., 2014) and PCSA was normalized by body mass (Appendix I, Eq. A2).

Z-scores were computed for each muscle in both limbs of the sprinters. A Z-score is the difference between an individual parameter and the mean of a reference population divided by the standard deviation of the reference population:

$$Z = \frac{normalized\ volume_{sprint} - mean(normalized\ volume_{non-sprint})}{st.dev.(normalized\ volume_{non-sprint})} \qquad (5.1)$$

where $normalized\ volume_{sprint}$ is the volume per height-mass of a sprinter's muscle, $mean(normalized\ volume_{non\text{-}sprint})$ is the population mean of volume per height-mass in the reference control population, and $st.dev.(normalized\ volume_{non\text{-}sprint})$ is the control population standard deviation of volume per height-mass. In this case, Z-score is a measure of how many non-sprinter standard deviations (σ) a sprinter's muscle is away from the control population mean. Use of Z-scores provides a statistically meaningful measure of volume deviation relative to non-sprinter muscles. In this case, positive Z-scores represent the degree of muscle hypertrophy present in athletes' muscles. Z-scores were computed for height-mass normalized muscle volumes for each of the 35 muscles. For all statistical tests on normalized parameters, the Wilcoxon Rank-Sum test was used. For statistical tests applied over all 35 muscles, the alpha value of 0.05 was reduced to 0.0014 using the Bonferroni family-wise error rate correction in order to minimize Type I errors.

5.4 Results

Z-score colormapped reconstructions of sprinters' limbs reveal non-uniform hypertrophy of lower limb muscles compared to non-sprinter controls (Fig. 5.1). Muscles in the thigh and hip are consistently larger in the sprinter population, while muscles in the shank are consistently smaller among sprinters compared to the non-sprinter control population (Fig. 5.2). Assessed over the sprinter population, 18 muscles were found to be significantly larger among sprinters than in the control group, including ten hip-crossing muscles, seven knee-crossing muscles, but only one ankle-crossing muscle (Appendix Table 5.1). There were no significant differences found between the triceps surae muscles of the sprinters compared to the non-sprinter controls. Differences in physiological cross-sectional area (PCSA) between sprinters and non-sprinters across muscles are consistent with the volume differences between groups, where the largest differences are in the quadriceps, hamstrings, sartorious, gracilis, and tensor fascia latae (Fig. 5.3 and App. II, Table 5.1).

Muscles in the non-dominant legs of sprinters were not significantly different in volume than muscles in the dominant legs (Fig. 5.4). Across muscles, a range of variances was observed for the differences between dominant and non-dominant legs. The muscles exhibiting the least variability between dominant and non-dominant limb were the gluteus maximus, adductor magnus, gluteus medius, psoas, the quadriceps muscles, gracilis, and soleus. The muscles exhibiting the largest variability were the gracilis, adductor brevis, biceps femoris, semitendinosus, lateral gastrocnemius, flexor digitorum longus, and flexor hallucis longus. No muscles were found to be significantly more or less variable than the others (Kruskal-Wallis test).

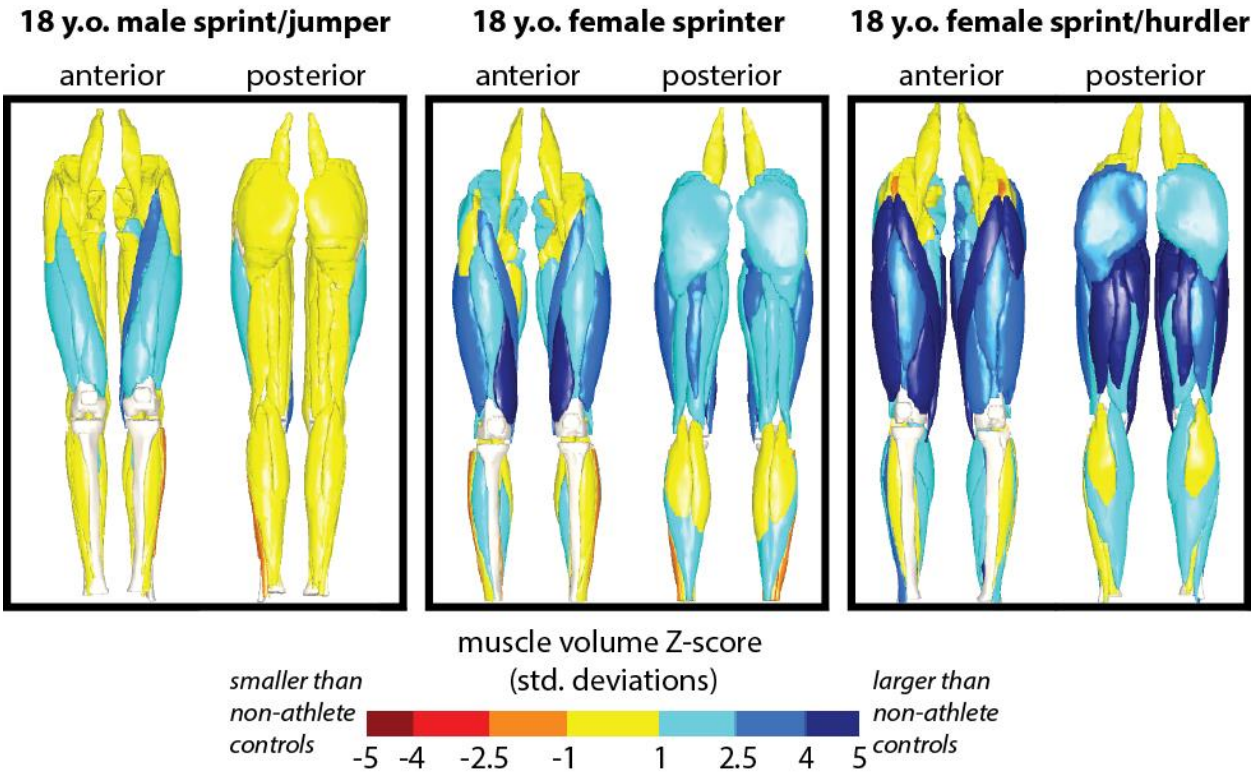

Figure 5.1: Sprinter muscle Z scores reveal large, but not uniformly large, limb muscles

Z-scores represent the number of standard deviations a muscle is from the non-athlete control mean. The three examples shown represent the range of muscle deviations observed in the sprinter dataset Muscle volumes have been normalized to the product of height and mass to remove effects of body size on muscle size.

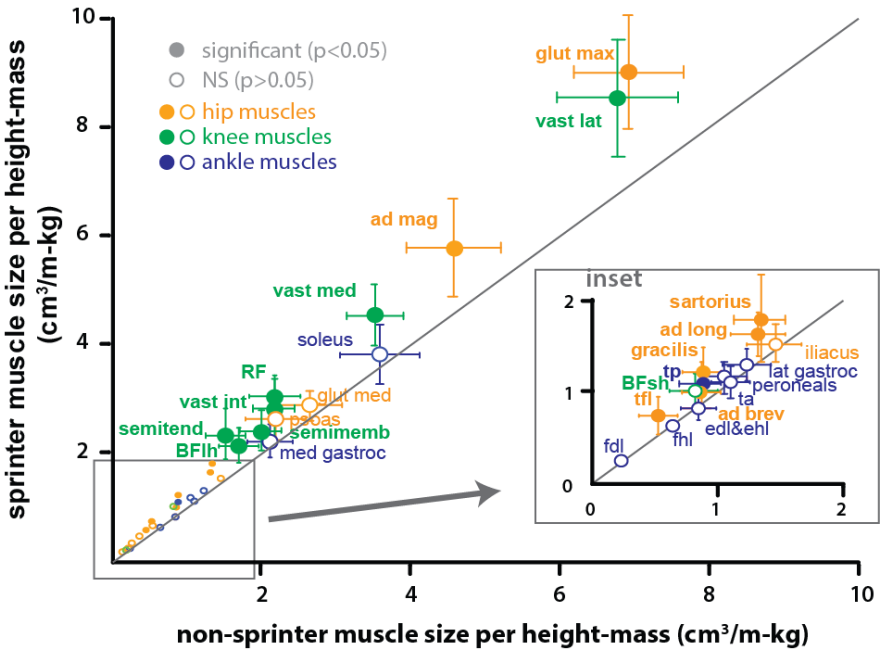

Figure 5.2: Competitive sprinters have significantly larger muscles compared to non-athlete controls for some but not all lower limb muscles.

Most of the muscles acting about the hip (orange) and knee (green) are statistically significantly larger for sprinters than controls, while most of the muscles acting about the ankle (blue) are not significantly larger for the athlete group. The per muscle alpha value of 0.05 was corrected to 0.0014 using the Bonferroni procedure.

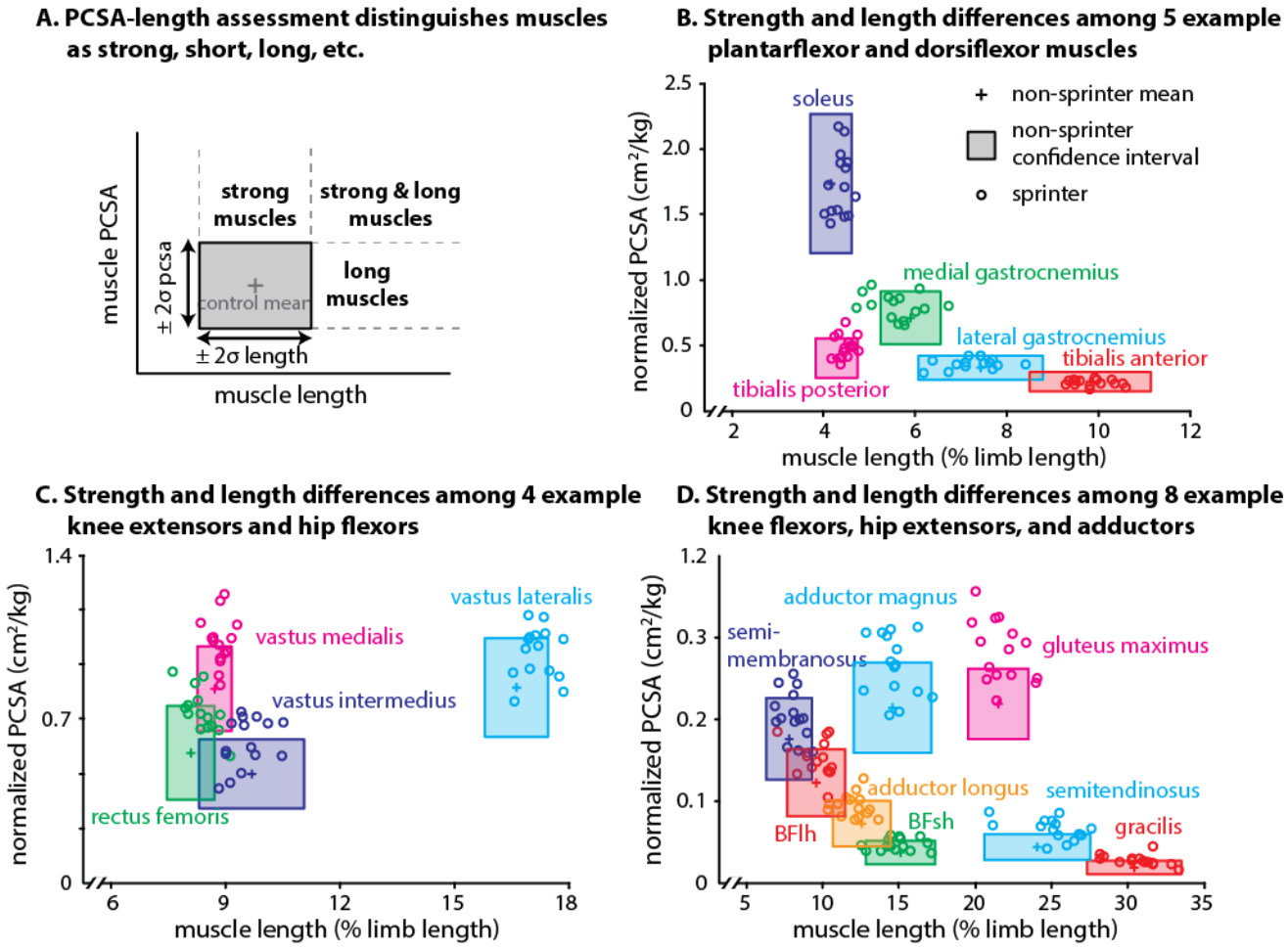

Figure 5.3: Muscle volume hypertrophy in sprinters may be due to differences in PCSA (strength) or differences in length (range of motion)

A: PCSA-length assessments are made from imaging volume and length data. Bounding boxes represent the ±2σ confidence interval for non-sprinter control group. B: Normalized muscle architectures of sprinters are similar to non-sprinter architectures for ankle-crossing muscles. C: Quadriceps muscles are stronger and slightly longer among sprinters. D: Hamstrings, hip extensors, and hip adductors of sprinters are stronger than non-sprint controls.

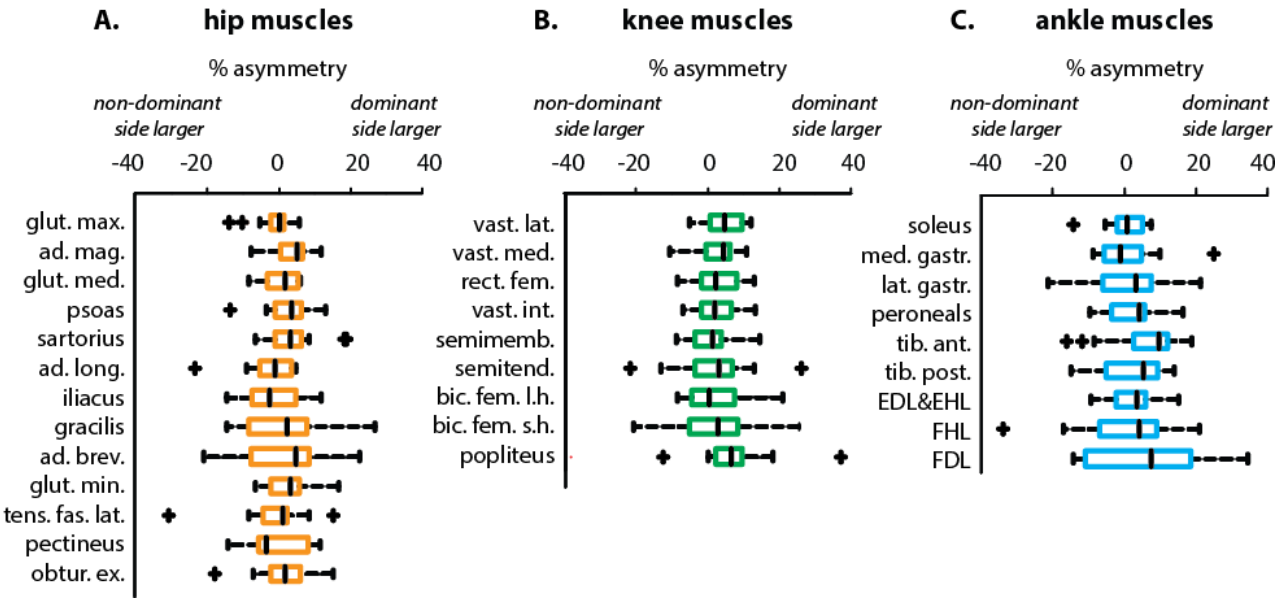

Figure 5.4: Symmetry of muscle volumes between dominant and non-dominant limb of competitive sprinters varies across muscles, but no statistically significant differences exist.

Percent asymmetry of muscle volume in dominant limb relative to non-dominant limb for 13 muscles crossing the hip (A), nine muscles crossing the knee (B), and nine muscles crossing the ankle (C) are displayed as box and whiskers plots. Solid black bars depict the median of the sprinter population, boxes represent the 25th to 75th percentile range, whiskers represent the population range, and black hashes represent population outliers as identified by the Kruskal-Wallis test.

Comparing female against male sprinters, no significant differences were found in the height-mass normalized muscle volumes across muscles (Fig. 4).There were no significant differences found between the normalized lengths of muscles of male sprinters compared to female sprinters (Wilcoxon Rank Sum Test, $p>0.0014$), where muscle lengths were normalized to limb length.

The total lower limb muscle volume per height-mass was greater for sprinters than for the non-sprinter controls (Fig. 5). On average, the total lower limb muscle volume per height-mass was 24% larger for the sprinter group ($p<10^{-5}$). Male sprinters and male controls were larger than their female counterparts in body size, but there was no significant difference in total muscle volume per height-mass between males and females within each group.

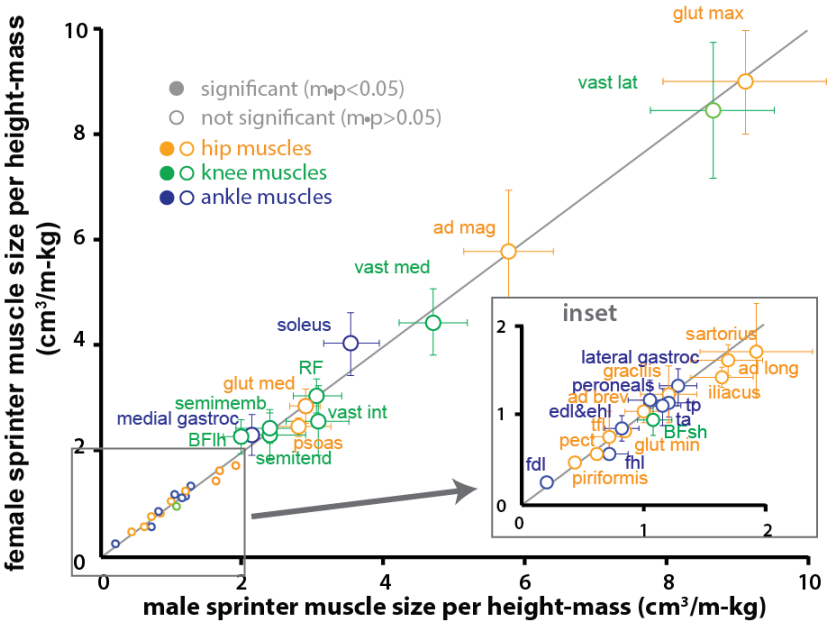

Figure 5.5: Muscle volumes were not significantly different between male and female sprinters when normalized by the product of height and mass.

Significance was tested over all 35 lower limb muscles using a Wilcoxon rank sum test. The per muscle alpha value of 0.05 was corrected to 0.0014 using the Bonferroni procedure.

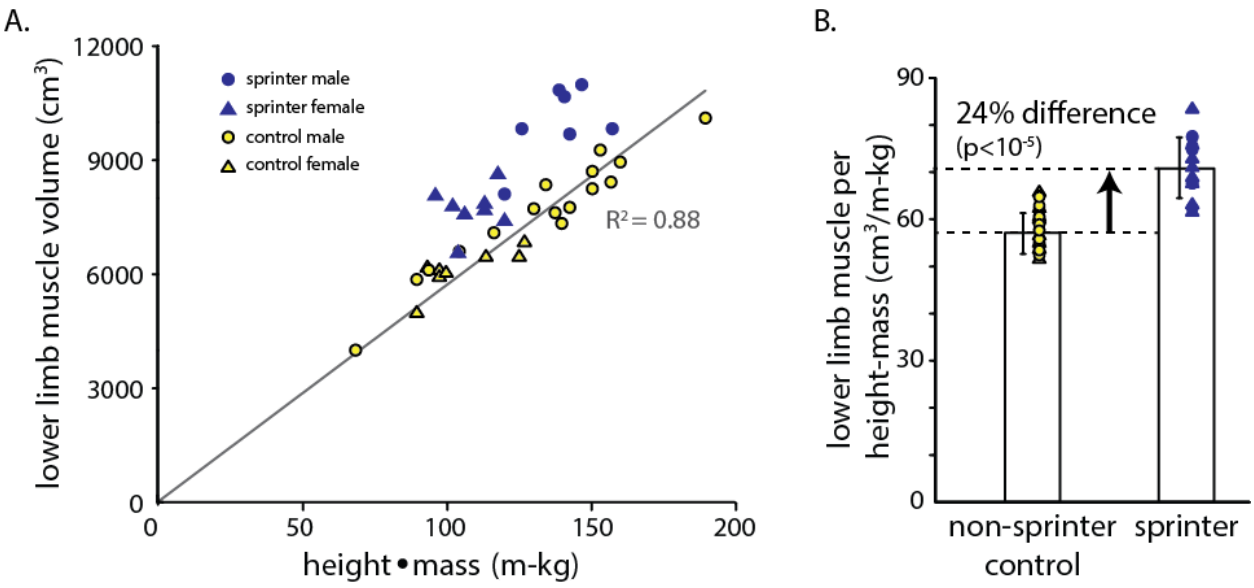

Figure 5.6: Collegiate sprinters have 24% more muscle volume per body mass and height than healthy non-sprinter controls.

A. The lower limb muscle volume of male and female non-sprinters scales linearly with the product of height and mass; male and female sprinters cluster above the non-sprinter regression line. B. The lower limb muscle volume per height-mass is significantly and substantially larger in the sprinter group compared to the controls.

5.5 Discussion

In this study, we utilized a fast non-Cartesian MRI sequence to determine *in vivo* volumes and lengths of 35 individual lower limb muscles in a population of high-speed competitive track athletes and compared those against a previously published healthy database of muscle sizes. We found that sprinters' muscles are larger but not uniformly larger than non-sprinter controls: flexors and extensors of the hip and knee are preferentially larger in sprinters. We also found no significant asymmetry of muscle sizes between limbs of sprinters, no significant differences in muscle size per body size between male and female sprinters, and significantly increased total lower limb muscle size per body size among sprinters compared to non-sprinter controls.

It was found that collegiate sprinters have muscles up to five standard deviations larger than healthy non-sprinter controls, but muscles are not all uniformly larger among sprinters. Z-scores in sprint athletes are thought to reflect the degree of hypertrophy in athletes' muscles, presumably due to their training. It is thought that at fast running speeds above seven m/s, the strategy for increasing running speed shifts from increasing stride length to increasing stride frequency. In a computational modeling study, Dorn et al. (2012) implicated the gluteus maximus, rectus femoris, hamstrings muscles, iliopsoas, and tibialis anterior in the muscular strategy for increasing speed. In the present study, we found the gluteus maximus, rectus femoris, the four hamstrings muscles, and the psoas to be significantly larger in PCSA among the sprinters compared to the non-sprinter controls. Similarly, we found no significant differences in size between sprinter gastrocnemius, soleus, or gluteus medius muscles, all of which were predicted by Dorn et al. to not contribute additional muscle force to sprinting above seven m/s.

In contrast to the predictions in Dorn et al. (2012), we did not find a significant difference in size in the tibialis anterior muscle between sprinters and controls. Furthermore, we found the vasti muscles to be significantly larger in sprinters whereas Dorn et al. did not predict large

increases in vasti force for high-speed sprinting. These discrepancies may be due to a lack of power in the present study to detect significant differences. Alternatively, they may be explained by limitations in the simulation study of Dorn et al. For example, that study only examined running at four speeds, whereas the subjects included in this study engage in a wide range of activities such as walking, running, sprinting, and weight-lifting. Non-sprinting activities such as these may require large vasti in the sprinters; this would not be apparent from examining sprinting exclusively. It is also possible that the peak force demands of movements do not correlate absolutely with muscle size (Sale et al., 1992). Muscles remodel in response to mechanical loads via physiological stimuli (Wisdom et al., 2014). Physiological signaling pathways regulating muscle size may be complex and cooperative—for example, increased force demands on one muscle may promote hypertrophy of neighboring muscles, even in the absence of explicit increased force demands. In addition to the muscles discussed above, we observed significant size increases in the gracilis, sartorius, and adductor muscles among sprinters. These muscles were not analyzed by Dorn et al. but may have a significant role in high-speed sprinting.

We examined bilateral asymmetry of muscle sizes between the dominant (largest) and non-dominant limb of the sprinters. For the sprinter population as a whole, no significant differences were found between sides for any muscle. For individual sprinters, however, bilateral size imbalances of up to 40% were present. Thus, individual sprinters present muscle size asymmetries in the lower limb, but these asymmetries are subject-specific and not reflective of the sprint population as a whole. Previous research has found significant bilateral asymmetries in the lower limbs of soccer players (Croisier et al., 2008; Rahnama et al., 2005) and other athletes (Nadler et al., 2001; Tate et al., 2006). In contrast, no common muscle asymmetries were associated with the present population of collegiate track sprinters. This is likely due to the extremely bilateral nature of sprinting. However, subject-specific muscle asymmetry of up to 40% suggests that for

individual muscles within individual subjects, there is asymmetry between some limb muscles. This may result from compensations related to previous muscle injuries. For example, a strained semitendinosus that atrophies in total volume may be accompanied by semimembranosus hypertrophy.

Some of the present population engaged in hurdle events and jumping events—long jump, high jump, and triple jump—that may promote bilaterally asymmetric muscle sizes. Other subjects engaged in running events longer than 100m that involved left-hand turns on the track. Since all of these athletes also competed in short sprinting events, it was impractical to examine bilateral asymmetries as a result of these events. Future studies with more specialized populations of hurdlers or jumpers may elucidate whether these events are associated with asymmetrical muscle sizes in athletes.

There were no significant differences in muscle size between male and female sprinters when normalized to metrics of body size. Previous work has reported that gender differences in strength are explained by differences in muscle architecture (Miller et al., 1993). The present results are consistent with the idea that muscle size per body size is not different between genders. The metric of muscle volume per height-mass is used here as a measure of muscle size per body size. Since the fundamental role of lower limb muscles is to move the body, a metric of body-normalized torque capacity is a functional measure of the capacity of the lower limb muscular system to move the body. Within the cohort of recreationally active, healthy non-sprinters utilized in this study, total lower limb muscle volume scales linearly with the product of height and mass, suggesting that those subjects are similar in their functional capacity for body movement. Subjects with cerebral palsy have been shown to have a 20% reduction in muscle volume per height-mass (Ch. 4), suggesting a reduction in the lower limb's functional capacity. In this study, it is demonstrated that the functional capacity of sprinters is increased on average compared to healthy

non-sprinters and that the functional capacity of male and female sprinters is not significantly different.

The results of the present work suggest that musculoskeletal models of athletes may underestimate athletes' muscle sizes and forces. Muscle physiological cross sectional area is often an input parameter for determining peak force of a muscle in musculoskeletal simulations. Simulations in the past have generally acquired PCSA values from cadaver dissection studies. The accuracy of muscle size data acquired from cadavers has been questioned due to concerns over the old age and pre-mortem illness of typical cadaver donors as well as the fixation process (Narici, 1999). In a previous study, it was reported that total muscle size of cadavers was less than half that of healthy control subjects of a similar body size (Ch. 3, Handsfield et al., 2014). In the present study, we have shown that the musculature of sprinters is even larger than healthy control subjects, reinforcing that cadaver data underestimates athletes' true muscle size. Moreover, we have shown that individual muscles in sprinters are not uniformly larger than in control subjects. For this reason, uniformly scaling cadaver muscle sizes to represent athletes (e.g. scaling all muscles by a factor of 2) also is not an accurate representation of athlete musculature. In the future, use of imaging-derived *in vivo* muscle size data in simulations of human movement will lend higher confidence to the predictions made by these musculoskeletal models.

In conclusion, we have used MRI and muscle size scaling approaches to show that muscles per body size are larger among sprinters but that hypertrophy patterns are non-uniform. Among the muscles that hypertrophy in sprinters are knee flexors and extensors and hip extensors but not ankle plantarflexors or dorsiflexors. It was found that muscle size per body size was not different between male and female sprinters and bilateral asymmetry of muscles occurred for individual subjects but no asymmetries were found to be common to the group as a whole.

Chapter 6

Image-Based Finite Element Modeling of the Achilles Tendon: The Role of Fascicle Morphology and Muscle Forces In Non-Uniform Tendon Displacements

"Sing, O muse, of the rage of Achilles… that brought countless ills upon the Achaeans."

- *The Iliad*, Homer

6.1 Abstract

The Achilles tendon is essential for human support and movement. It is the thickest tendon in the body and is the primary elastic energy storing component during walking and running. The incidence of Achilles tendinopathy among aging subjects, especially runners, has motivated recent experimental comparisons of Achilles deformation in young, healthy and older populations. Many of these experimental results have shown counter-intuitive displacement patterns that are difficult to understand, potentially due to the complex architecture and muscle-tendon interactions that occur in the Achilles, such as twisting tendon fascicles and inter-fascicle sliding within the tendon. The aim of the present study is to develop a novel computational model of the Achilles tendon based on ultrashort echo time magnetic resonance imaging in order to elucidate the effects of fascicle twisting, inter-fascicle sliding, post-calcaneal insertion, and differential muscle forces on tendon deformation. It was found that differential muscle forces, particularly a relatively greater passive force in the medial gastrocnemius muscle, are the primary cause of differential tissue displacements within the tendon model and that differential displacements indicate higher stretching in the medial gastrocnemius tendon fascicle. Differential displacements were reduced in the absence of the post-calcaneal insertion region, with less fascicle twisting, with lower muscle forces, and with higher tendon stiffness. These results suggest that musculotendon changes associated with aging contribute to reduced differential tissue displacements and tendinopathy in older subjects.

6.2 Introduction

Tendons are vitally important in musculoskeletal biomechanics as they transmit forces from muscles to the skeleton. Additionally, the ability for tendons to store and release elastic energy allows for energy conservation in cyclic movements like walking and running (Ishikawa et al., 2005; Sasaki and Neptune, 2006) and also allows for higher velocity movements than are permitted by systems of muscles alone (Roberts, 2002). The Achilles tendon, particularly, is important for humans as it is involved in bipedal standing, walking, and running. Recent research has suggested an importance of the meso-scale morphology, or the substructural geometry, of the Achilles tendon (Slane and Thelen, 2014; Szaro et al., 2009; Thorpe et al., 2013). Despite its potential importance, the effect of Achilles tendon meso-scale structures on Achilles deformation remain poorly understood.

Achilles meso-scale structure is complex. The tendon is composed of three to four fascicles (Screen et al., 2004) (a.k.a. tertiary fibre bundles (Wang, 2006)), each of which is controlled by a different muscle in the triceps surae muscle group (Szaro et al., 2009) (see Section 2.5). These fascicles twist ninety degrees about one another in an external direction (White, 1943), but the functional significance of this twist is not well understood. Additionally, recent work has suggested that these fascicles are capable of sliding past one another (Thorpe et al., 2013) like different cables each controlled by a different source of tension. Since this behavior is observed in young and healthy animals, but not in older animals, it has been hypothesized that sliding of the Achilles fascicles is associated with healthy tendon and loss of the sliding behavior is associated with tendon degeneration.

Recent advances in ultrasound imaging have enabled measurement of fascicle sliding *in vivo,* as demonstrated by non-uniform displacements across the Achilles tendon. These studies

have shown that fascicle sliding occurs both in controlled single joint tasks (Slane and Thelen, 2014) and during walking (Franz et al., 2014). However, the results of these experiments are challenging to interpret because of the complex three-dimensional morphology of the tendon. Many questions therefore cannot be answered with these experiments alone. For example, it is unclear what forces in the three plantarflexor muscles give rise to the tissue displacements observed experimentally. It is also unclear what role inter-fascicle sliding has in tissue displacement profiles. Lastly, the mechanical contributions of twisting fascicles and the insertion of the tendon around the posterior surface of the calcaneus remain unknown.

The goal of this work was to create a novel finite element model of the Achilles tendon in order to investigate the contributions of complex Achilles geometry, twisting fascicle morphology, and differential muscle forces on tissue displacements within the tendon. The model was built using an ultrashort echo time (UTE) MRI sequence and finite element modeling of tendon fascicles. The specific goals of this study were to: i) build a finite element model from UTE MR Imaging of the Achilles tendon, ii) predict the muscle forces necessary to replicate tissue displacements observed in the literature, iii) use the model to understand the interactions of muscle forces and fascicle sliding on fascicle displacements and strains, and iv) use the model to determine the contributions of tendon geometry on displacement profiles.

6.3 Methods

Ultrashort Echo Time Magnetic Resonance Imaging

A healthy 27 year-old female subject (height: 1.63m, mass: 52 kg) was scanned on a 3T Siemens (Munich, Germany) Trio MRI scanner using a combination 3D ultrashort echo time (UTE)/3D short echo time (shTE) sequence utilizing a radial k-space trajectory. A flex coil was placed around the subject's right ankle and the ankle was manually positioned at an angle of approximately 25° of plantarflexion. The sequence parameters for the UTE images were TE/TR/α: 0.08ms/ 6ms/10°. The sequence parameters for the shTE images were TE/TR/α: 2.54ms/6ms/10°. Field of view was 300x300x300 mm^3 and spatial resolution was 0.8mm isotropic. shTE images were subtracted from UTE images to maximize tendon signal. Osirix imaging software (Rosset et al., 2004) was used to resample images at a slice thickness of 2.4mm.

Finite Element Analysis: Geometry

The Achilles tendon was segmented in MR images from the muscle-tendon junction to the extent of its insertion on the calcaneus (Fig. 6.1). Segmentation was performed using in-house segmentation software written in Matlab (The Mathworks, Natick, MA). Control points defining tendon external geometry were exported to Autodesk Inventor Professional (Autodesk Inc, San Rafael, CA) and the tendon was reconstructed from the control points using closed contour cubic spline fits. In order to model the behavior of the Achilles fascicle bundles, we defined surfaces that subdivided the bulk tendon structure into three fascicle bundles (hereafter referred to as "fascicles" for simplicity). Each of the three fascicles corresponded to one of the three muscles of the triceps surae (Fig. 6.2). At the superior aspect of the tendon, the anterior portion of the tendon was defined as the fascicle extending from the soleus, the posterior medial portion was defined as the fascicle extending from the medial gastrocnemius, and the posterior lateral portion was defined as the

fascicle extending from the lateral gastrocnemius. The regions corresponding to each fascicle were constructed such that they twisted approximately 90° about the center of the tendon (White, 1943). The cross-sectional morphology of each fascicle at the end of the free tendon was informed by reports in the literature (Sarrafian, 1993; Szaro et al., 2009).

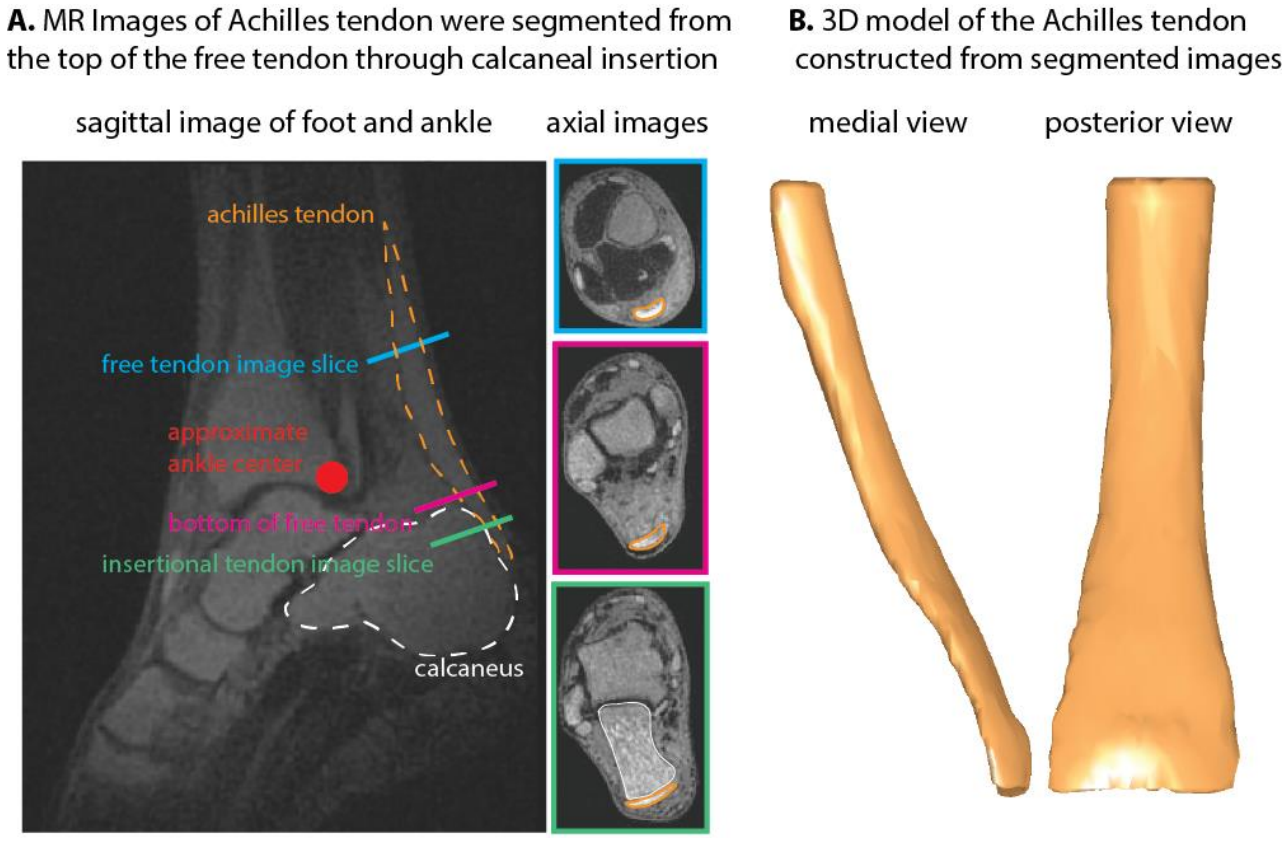

Figure 6.1: Summary of imaging and segmentation of external tendon geometry

A: Sagittal and axial 3D UTE images illustrate the location of the Achilles tendon and the process of segmentation in axial slices. B: 3D reconstruction of the segmented images reveals the gross shape of the tendon from its superior aspect to its insertion posterior to the calcaneus.

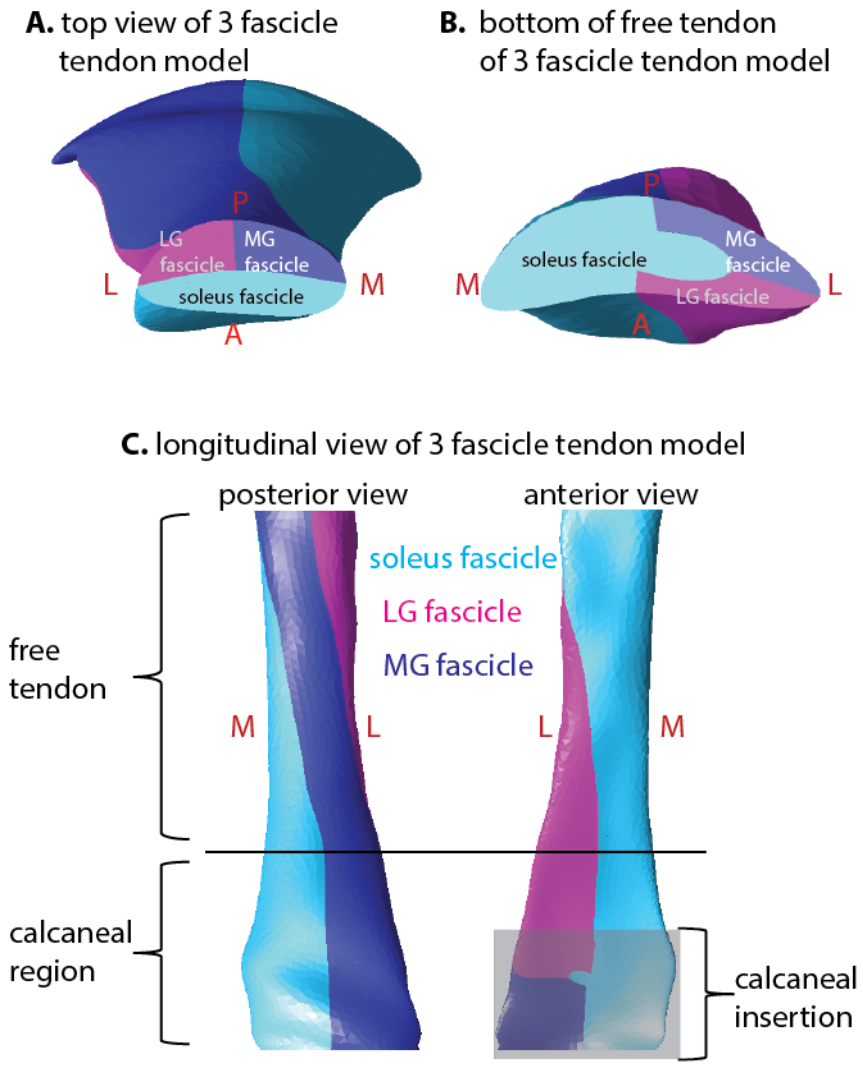

Figure 6.2: Illustration of the tendon fascicles defined in the finite element model

A: top view of model displays a tendon fascicle associated with the soleus muscle located on the anterior aspect of the tendon; the medial and lateral gastrocnemius fascicles are posteromedial and posterolateral, respectively. B: bottom view of the inferior end of the free tendon displays an orientation that is twisted 90° and is consistent with literature reports of the morphology at this level of the tendon. C: Posterior and anterior views of the tendon reveal the shape and orientation of the tendon fascicles through its calcaneal insertion.

The morphology of the Achilles fascicles in the calcaneal region is not well defined in the literature; therefore, in the present model, the cross-sectional morphology at the end of the free tendon is maintained through the tendon's insertion on the calcaneus. This morphology is consistent with sagittal imaging studies depicting collagen fibers with a longitudinal orientation in the insertional region (Milz et al., 2002) as well as photographs of the superficial collagen fiber directions of the Achilles tendon (Dalmau-Pastor et al., 2014). The model geometry was transferred to AMPSolid (AMPS Technologies, Pittsburgh, PA) and meshed into tetrahedral solid elements.

Finite Element Analysis: Constitutive Model

Each fascicle was modeled as a Neo-Hookean material. A Neo-Hookean model was able to fit literature data of *in vivo* Achilles tendon mechanical behavior (Lichtwark and Wilson, 2005). In that study, however, all of the subjects were males engaging in a high load, high frequency activity of one-legged hopping at 2 Hz. To account for velocity-dependent stiffening in the high frequency activity from Lichtwark and Wilson, we reduced the Neo-Hookean parameter by a factor of two. This reduced parameter is consistent with the Young's modulus reported for the *in vivo* Achilles tendon during low frequency experiments (Kubo et al., 2002).

Finite Element Analysis: Boundary Conditions

A frictionless contact interface was defined between the three fascicles. This boundary condition allows the three fascicles to slide past one another in order to simulate the property of fascicle sliding that has been demonstrated in healthy Achilles tendons (Thorpe et al., 2013). The superior aspect of the Achilles tendon was constrained to only move in the Y (superior-inferior) direction. The anterior and inferior aspect of the calcaneal insertion was assigned to rotate 25° to

simulate the rotation of the ankle during a dorsiflexion moment (Slane and Thelen, 2014). The center of rotation was defined by the location of the subject's malleoli from MR images.

To simulate the forces applied to the tendon by the three triceps surae muscles during a dorsiflexion motion, nodal stiffness and pressure boundaries were used on the top surface of each tendon fascicle. Nodal stiffness boundary conditions are equivalent to linear springs placed at nodes within the model. These were used to simulate the passive forces in muscle, which increase with increasing stretch (Herzog et al., 1991). Linearly ramped pressure boundaries are equivalent to a linearly increasing force applied to the top surface of the tendon. This boundary condition was used to simulate the active component of muscle forces on the ascending limb of the muscle force-length curve (Maganaris, 2003). Simulations of eccentric motion included both nodal stiffness and pressure boundary conditions; simulations of passive motion included only nodal stiffness boundary conditions.

Comparison with In Vivo Data and Muscle Force Determination

In a previous work, Slane & Thelen (2014) utilized ultrasound elastography and speckle tracking to record the displacement profiles of the Achilles tendon during controlled dorsiflexion motions. Briefly, they imaged the free Achilles tendon while subjects underwent cyclic eccentric dorsiflexion and reconstructed tissue displacements during the dorsiflexion portion of the cycles. They repeated this experiment with passive motion, where subjects remained relaxed and had their ankles moved for them.

To compare the present modeling results with these data, a region of interest in the center of the superior one-third of the tendon model was used. This region of interest was chosen to be consistent with Slane & Thelen (2014). Superior-inferior nodal displacements were recorded for finite element nodes within this region. Two-dimensional displacement profiles were calculated

by projecting nodes into the sagittal plane and smoothing with a quadratic surface fit. To compare differential displacements between the present model and those reported by Slane & Thelen (2014), nodes were binned into deep, middle, and superficial regions of the tendon and superior-inferior nodal displacements were averaged within these bins.

Muscle force determination was accomplished by tuning stiffness and pressure boundary conditions and comparing displacement profiles with Slane & Thelen (2014). Magnitudes for stiffness boundary conditions were determined using data from passive trials of that work. The stiffness boundary conditions in the passive model were varied until the nodal displacements in the Deep, Middle, and Superficial regions were within one standard deviation of experimental values reported in Slane & Thelen (2014). The stiffness boundary for the LG fascicle was set as one-half the stiffness boundary of the MG fascicle to reflect the relative PCSAs of these two muscles (Ch. 3, Handsfield et al., 2014).

Magnitudes for the pressure boundary conditions in the eccentric model were tuned using data from the eccentric trials of Slane & Thelen (2014). Maintaining the stiffness boundary conditions that were determined from passive tuning, the pressure boundary conditions in the model were varied until the nodal displacements in the Deep, Middle, and Superficial regions were within one standard deviation of experimental values for eccentric trials. The pressure boundary for the LG fascicle was set as one-half the pressure boundary of the MG fascicle, reflective of their relative PCSAs.

In addition to the passive and eccentric tuned models, we ran an additional simulation with no force boundary conditions on the tendon fascicles. The purpose of these simulations was to understand the effects of muscle forces on non-uniform tissue displacements in the tendon.

Variation of Model Morphology

In order to explore the contributions of the calcaneal insertion region, the twisting fascicles, and the sliding between fascicles, we created additional models that eliminated each of these features. The first model variation—"No Insertion"—was identical to the full model in the free tendon region, but did not include the calcaneal region of the tendon. The second model variation—"No Insertion No Twist"— similarly did not include the calcaneal region, but also lacked any twisting of the tendon fascicles. The third model variation—"Non Sliding"— included the full tendon morphology but did not allow sliding between fascicles. All boundary conditions were maintained across the model variations.

6.4 Results

Muscle Force Determination and Comparison with Experimental Results

After muscle force determination through boundary condition tuning, sagittal plane displacement profiles in the model were similar to those reported in Slane & Thelen, replicating the result that distal displacements were greater in the deep portion of the tendon than in the middle and superficial portions (Fig. 6.3). Displacement magnitudes in the simulations were within one standard deviation of the experimental ultrasound data and the profile of the displacements shows the same trend as the data in Slane & Thelen for both passive and eccentric cases (Fig. 6.4).

The maximum muscle forces determined to replicate the experimental ultrasound results are given in Table 6.1. For the passive simulations, the total force from all of the triceps surae muscles was 555N and is consistent with literature estimates of muscle forces during daily activities (Mian et al., 2007). The passive muscle force in the soleus was 34% of the total triceps surae passive forces, the medial gastrocnemius passive force was 39% of the total, and the lateral gastrocnemius passive force was 27% of the total (Table 6.1). For the eccentric simulations, the total force from all of the triceps surae muscles was 1843N; soleus muscle force was 63% of the total triceps surae force, the medial gastrocnemius force was 23% of the total, and the lateral gastrocnemius force was 14% of the total (Table 6.1).

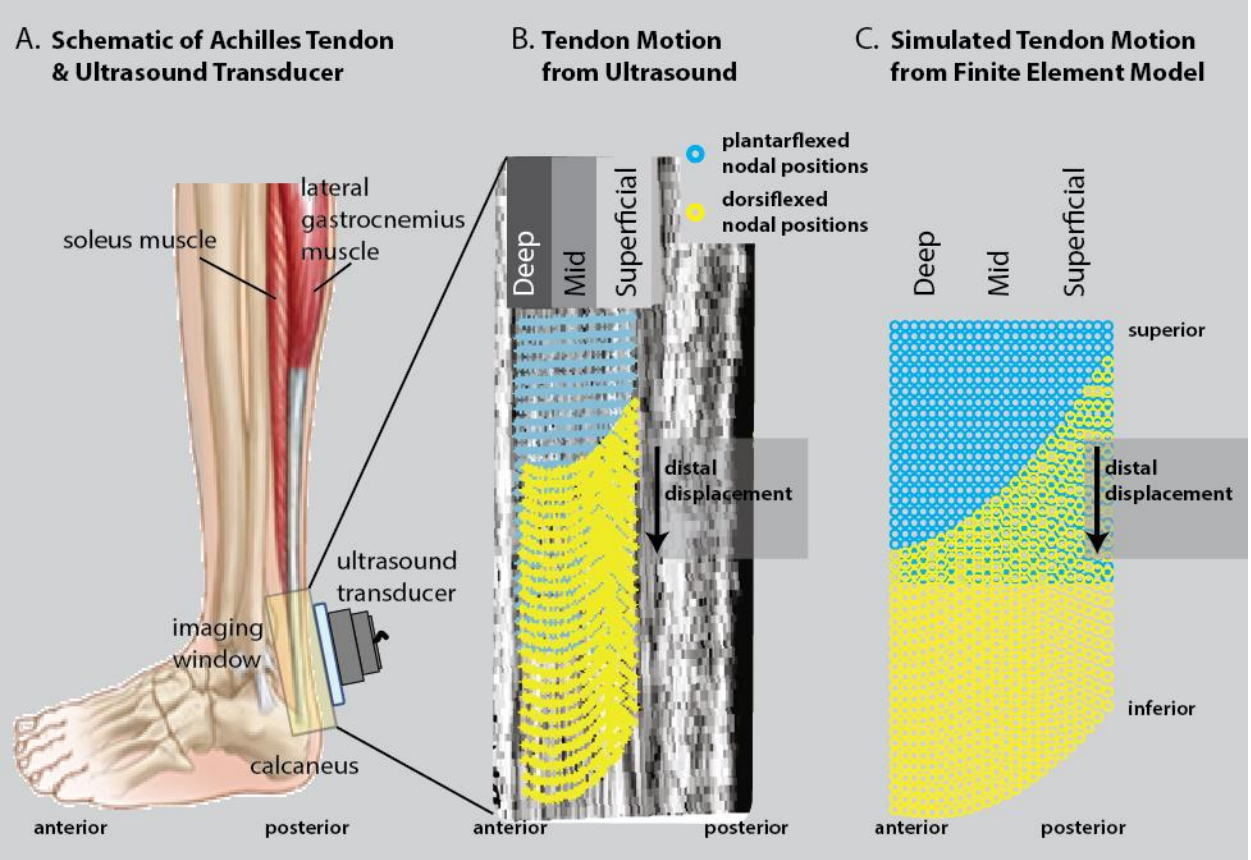

Figure 6.3: Comparison between experimental and finite element model displacement profiles

A: In (Slane and Thelen, 2014), the Achilles tendon was imaged using ultrasound while subjects went through cyclic dorsiflexion motion. (image adapted from (Slane and Thelen, 2014)) B: From plantarflexion to dorsiflexion, Achilles tissue displaced distally, but there was more displacement in the deep regions of the tendon compared to the superficial regions. (image adapted from (Slane and Thelen, 2014)) C: With appropriate force boundary conditions, nodes in the deep region of the finite element model displace more than nodes in the superficial region.

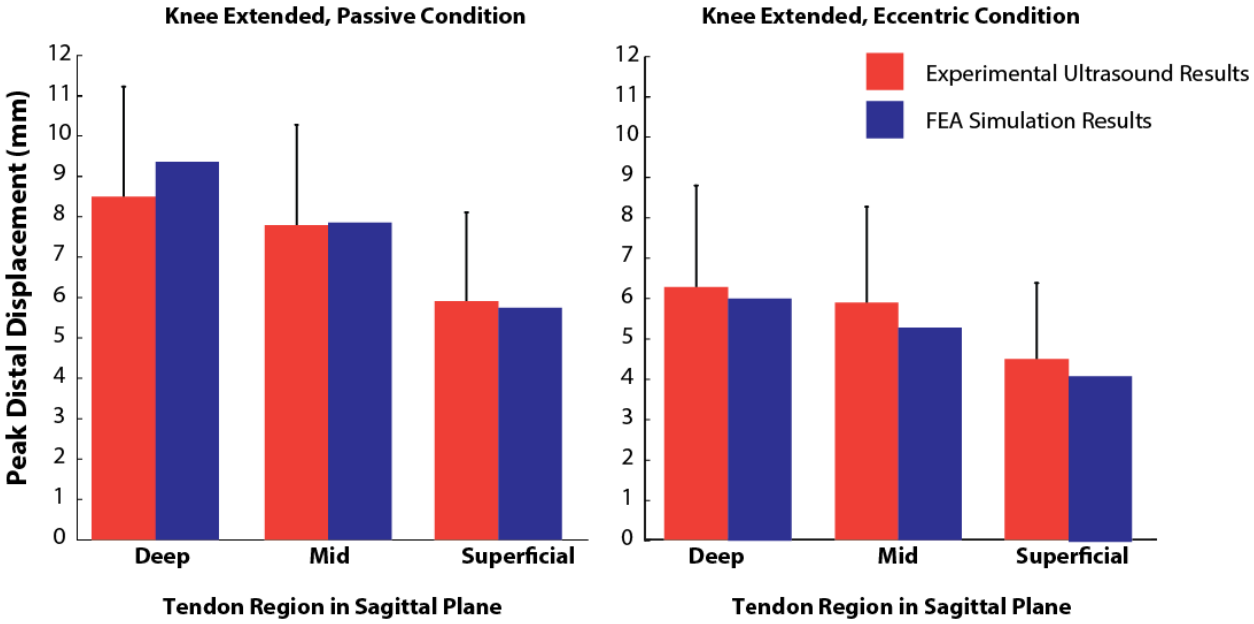

Figure 6.4: Comparison of regional displacements between experiment and finite element model

The peak distal displacements occurring in the deep, middle, and superficial regions are shown for ultrasound experiments(Slane and Thelen, 2014) and the present finite element model. For both passive and eccentric cases, finite element simulations were able to predict regional displacements within one standard deviation of experimental results.

Table 6.1: Maximum muscle forces on Achilles fascicle in FE model

	Maximum Forces During Simulation (Passive Forces) [% of total]		
Condition	**Soleus Fascicle**	**MG Fascicle**	**LG Fascicle**
Passive	189 N [34%]	217 N [39%]	149 N [27%]
Eccentric	1157 N (111 N) [63%]	423 N (132 N) [23%]	263 N (118 N) [14%]

Maximum muscle forces in the passive and eccentric models are tabulated. Total force in each fascicle are given in Newtons; percent of total Achilles force is given in brackets. For eccentric condition, passive forces are given in parentheses.

Strains, displacements, and forces in tendon

With increasing force boundary conditions in the models, distal displacements in the proximal free tendon decreased and average strains in the fascicles increased (Fig. 6.5). For both the passive and eccentric simulations in the sliding fascicle model, strains were highest in the medial gastrocnemius fascicle followed by the soleus fascicle and lateral gastrocnemius fascicle (Fig. 6.5A). Differential displacements between fascicles were the greatest for the passive force sliding fascicle models (Fig. 6.5A). Differential displacements were negligible for the non-sliding models at all force conditions (Fig. 6.5B). MG fascicle strains were lower in the non-sliding models than the sliding models; LG fascicle strains were higher in the non-sliding models than in the sliding models (Fig. 6.5B).

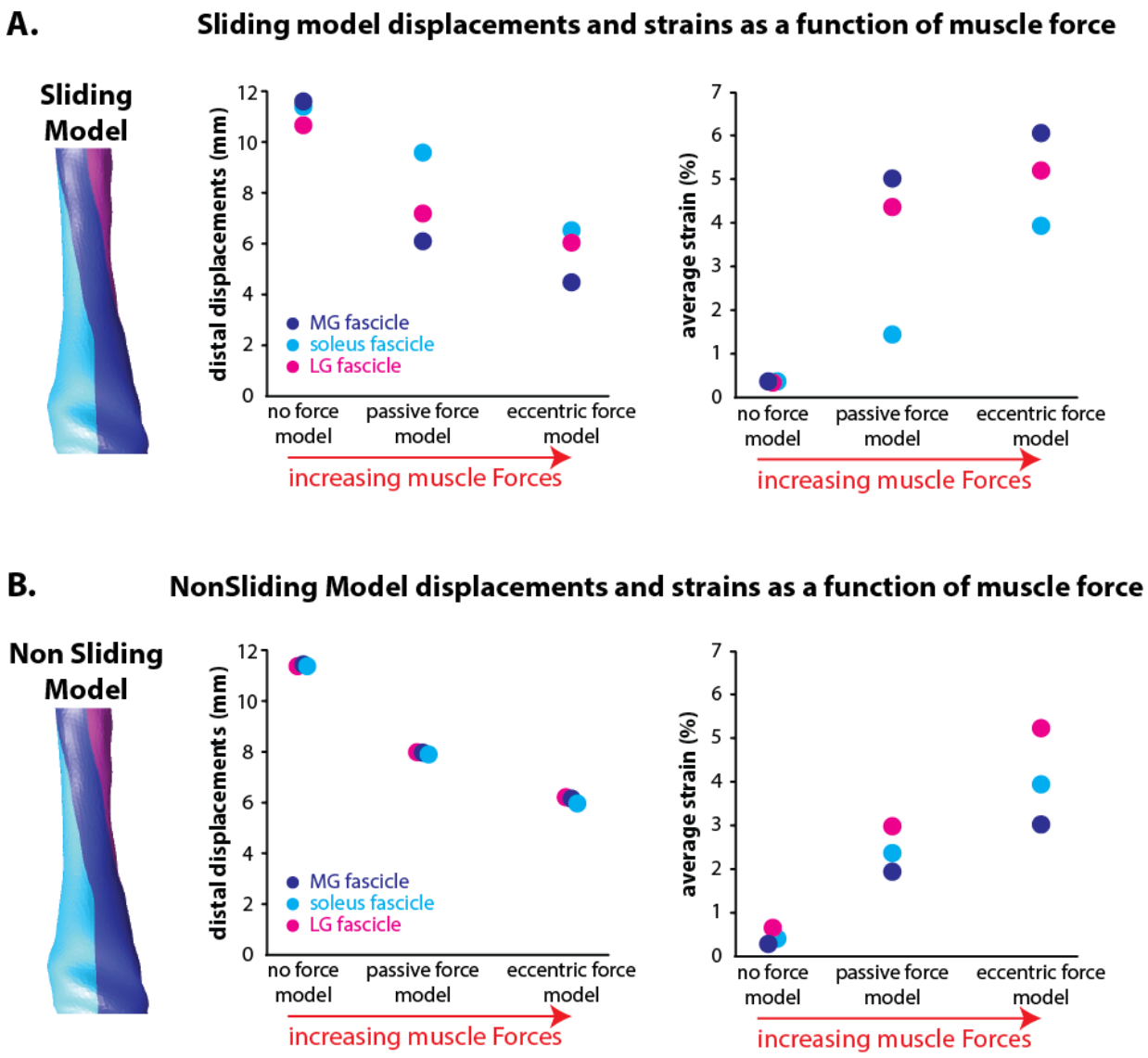

Figure 6.5: Relationship between force condition, tissue displacement, and strain in FE models

A: In the sliding model, distal displacements in the proximal free tendon decreased with increasing muscle forces and equivalent strains increased with muscle force. B: In the absence of sliding fascicles, differential displacements were negligible and strains were reduced for the MG fascicle.

Differential displacements in tendon:

Differential displacements in the Achilles tendon varied throughout the length of the tendon and were greatest near the superior aspect. Toward the inferior aspect of the tendon, differential displacements between fascicles approached zero (Fig. 6.6, top row). When no forces were applied to the fascicles, differences in fascicle displacements were negligible. Fascicle displacement differences in the sliding models were non-negligible when muscle forces were applied and were the greatest in the passive condition (Fig. 6.6, top row).

Mechanical contribution of insertion, twisting fascicles, and sliding

In the absence of the post-calcaneal tendon insertion, distal displacements increased throughout the entire free tendon but differential displacements between the fascicles were not considerably different (Fig. 6.6). In the absence of both the post-calcaneal tendon insertion and the twisting fascicles, displacements decreased in the soleus fascicle but increased in the gastrocnemius fascicles, resulting in a decrease in differential displacements (Fig. 6.6). For all of the sliding models, variations in the force boundary conditions had a greater effect on differential displacements than any of the morphological variations. In the absence of the ability for fascicles to slide, differential displacements were reduced dramatically (Fig. 6.6, bottom row).

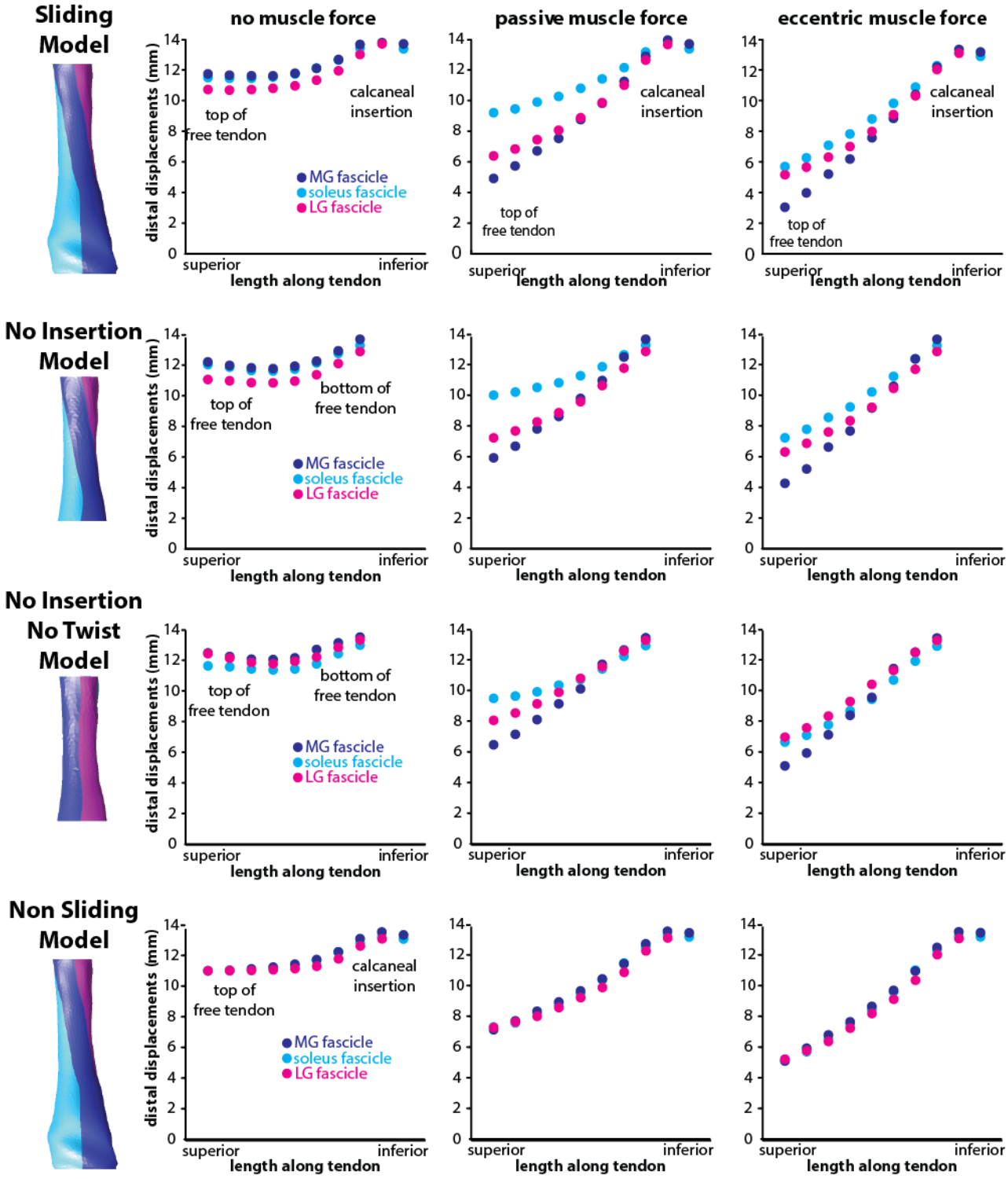

Figure 6.6: Displacement profiles across morphological variations of the Achilles tendon

The full Achilles model includes twisted fascicles, inter-fascicle sliding, and a post-calcaneal insertion. Without this insertion, the model displays slightly higher displacements but no dramatic differences in relative displacements. Without twisted fascicles, the differential displacements in the free tendon are reduced. In the absence of sliding, differential displacements between fascicles are substantially reduced.

6.5 Discussion

In this study, we used a finite element modeling approach to understand the roles of twisting fascicle morphology, inter-fascicle sliding, and muscle forces in the phenomenon of non-uniform tissue displacements in the Achilles tendon. It was found that *i)* differential tissue displacements could be replicated with realistic muscle forces and a sliding boundary between tendon fascicles, *ii)* decreasing distal displacements of muscle fascicles were associated with increasing muscle forces, *iii)* increasing muscle forces were associated with increasing fascicle strains, and *iv)* inter-fascicle sliding and muscle forces contribute more to differential displacements than the morphological features of a sub-calcaneal insertion region and twisting fascicles.

Reasonable values for active and passive muscle forces were found to predict the displacement profiles observed in previous ultrasound elastography experiments in humans (Slane and Thelen, 2014). The peak soleus forces simulated in this study are on the order of 200N passive and 1200N active and correspond to a neutral ankle position. These values are in the range of forces observed in the plateau region of the soleus force-length curve *in vivo* (Rubenson et al., 2012), which is consistent with forces anticipated at a neutral ankle position. There are fewer literature sources for the *in vivo* behavior of the gastrocnemius muscles. However, the total peak passive forces in the Achilles tendon simulated in this study are on the order of 500 N and 1800 N for passive and eccentric forces. Previous studies have estimated *in vivo* Achilles tendon forces of 440N during the knee extended swing phase of walking and 1300N during stance (Mian et al., 2007). Slane & Thelen (2014) recorded net plantarflexion moments of 25 Nm during the eccentric portion of their experiment, suggesting plantarflexion muscle forces on the order of 1000N. Thus,

the forces estimated in this study are similar or slightly higher than literature estimates of *in vivo* muscle forces during typical activities.

It is possible that we over-estimated the material stiffness of the Achilles tendon in the present model since we did not compute subject-specific material properties. In this case, the muscle forces determined in this study would have been reduced due to the demonstrated relationship between muscle force and fascicle strain. The material parameters chosen were based on literature reports of *in vivo* Achilles tendon material properties during hopping (Lichtwark and Wilson, 2005) and were reduced from that study's mean to account for velocity differences between studies. In that study a range of tendon moduli are presented with a minimum of 610MPa. Literature reports of elastic moduli of tendon are often greater than 1GPa (Maganaris and Paul, 2002). However, this modulus refers to the tangent modulus beyond the toe region of the tendon material curve and is thus too large to represent stress at low levels of strain. Additionally, literature reports of elastic moduli for ligaments are as low as 100MPa (Siegler et al., 1988) and a range of tendon moduli (400-1700 MPa) have been reported for animals (Zajac, 1989). Taken together, this suggests that effective Achilles tendon moduli below 600MPa may not be unreasonable. Variations of tendon stiffness in the present model changed the muscle forces necessary to replicate experimental ultrasound results, but the fascicle strains associated with the replicated ultrasound results were not affected by tendon stiffness once the model forces were tuned. Thus, high fascicle stretch was insensitive to material properties.

Interestingly, the passive forces in the medial gastrocnemius necessary to replicate the experimental data were higher than the passive forces in the soleus muscle. The stiffness (force per unit stretch) boundary condition used in the MG fascicle to produce these passive forces was nearly two-and-a-half times the stiffness applied to the soleus. It may be that the gastrocnemius muscles have a steeper passive curve than the soleus in order to promote high stretching and elastic storage of energy in the superficial aspect of the tendon. Previous work has shown that the Achilles

tendon stretches much more than previously thought (Lichtwark and Wilson, 2005; Maganaris and Paul, 2002). Other research has suggested that the MG aponeurosis-tendon complex is especially extensible, especially in humans (Roberts, 2002). The present work reinforces the extensibility of the gastrocnemius tendon fascicle and implicates passive gastrocnemius muscle forces in its stretch function. Further work is needed to examine the passive properties of the gastrocnemius muscles with respect to those of the soleus.

In this work we set the passive stiffness of the lateral gastrocnemius to half that of the medial gastrocnemius, consistent with the relative PCSAs of these muscles (Ch. 3, Handsfield et al., 2014). Since it is thought that previous ultrasound experiments were imaging the medial gastrocnemius and soleus, but not the lateral gastrocnemius tendon fascicle (Bojsen-Møller et al., 2004; Slane and Thelen, 2014), we did not use the LG fascicle in comparisons with experimental data and so it is uncertain if the forces and displacements we modeled in the LG are accurate.

The present model reveals an association between distal displacement and muscle forces. Higher muscle force led to reduced distal displacements. Results between passive (higher distal displacements and lower forces) and eccentric (lower distal displacements and higher forces) are consistent with this idea. Variations of morphology, such as elimination of the post-calcaneal insertion region and elimination of twisting fascicles, imposed only small changes on the differential displacements between tendon fascicles. Differential displacements in the tendon were much more sensitive to muscle forces than they were to variations in morphology, suggesting a role of muscles in the experimentally observed tendon displacements in the literature. Additionally, sliding between fascicles was necessary in order to recapitulate the displacement profiles from the literature. Elimination of sliding between fascicles severely inhibited the differential displacements in the tendon and could not be overcome even with high muscle forces. The idea that sliding and muscle forces are necessary to observe non-uniform tendon displacements is consistent with reports of sliding in the tendons of healthy young horses and not

in the tendons of older horses (Thorpe et al., 2013) and further suggests a role of the triceps surae muscles for driving the motion of the fascicles.

There are several limitations to our model that should be considered. We used an isotropic Neo-Hookean material model. Transversely isotropic material models for tendon (Weiss et al., 1996) may be a more appropriate constitutive relationship . Since our results primarily relate force, longitudinal strain, and displacement, it is not expected that a transversely isotropic material model would significantly change the quality of these results. Use of a transversely isotropic tendon material model may alter the particular muscle forces necessary to replicate experimental results and is worth pursuing in the future. The moment arm in the present model was small compared to most literature estimates of Achilles moment arm (Maganaris et al., 2000) and the ankle joint center was modeled as a pin joint. Further work on adequate modeling of the ankle joint may be able to incorporate additional complexities of ankle motion. In the present work, muscles were modeled by imposing length-dependent passive muscle forces and active muscle forces on the tendon fascicles. Since muscle tissue is in series and in parallel with connective tissue, which inserts into tendon, our model oversimplifies the true morphology of muscle-tendon interaction (Epstein et al., 2006). Future work incorporating the entire muscle-tendon unit in a finite element model will be an important next step at furthering our understanding of the role of muscles in Achilles deformation.

How do these results relate to an understanding of age-related tendon changes and tendinopathy? Aging is related to a progression of the Achilles insertion from the posterior calcaneus to the superior calcaneus (Kim et al., 2011). With aging there is also thought to be a reduction in inter-fascicle sliding behavior due to collagen cross-linking (Thorpe et al., 2013). Both of these changes to the tendon would result in reductions in differential displacements with the same force inputs. Additionally, aging is also related to strength losses in the muscles (Doherty, 2003) and may be related to stiffening of the material properties of the tendon (Narici et al., 2008).

These changes would further contribute to reductions in differential displacements in the Achilles tendon. While it is unclear whether the changing location of the Achilles insertion and changes to the material properties of the tendon can be prevented, it is well-established that age-related changes to the muscles can be counteracted with resistance training of the muscles (Fiatarone et al., 1990). This may be the simplest and most effective precaution that can be taken to promote differential displacement in the tendon with aging, a phenomenon believed to be associated with healthy, non-tendinopathic tendons. Further study of this will determine to what extent strength training may prevent age-related tendinopathy.

The phenomenon of non-uniform displacements in the Achilles tendon has been reported only recently in the last decade (Bojsen-Møller et al., 2004; Franz et al., 2014; Slane and Thelen, 2014). An understanding of the functional significance of this phenomenon remains hypothetical. Previous authors have suggested that an optimal amount of tenocyte stimulation is required for maintenance of tendon health (Wang, 2006). It may be that differential displacement between tendon fascicles is important for adequately stimulating tendon cells. If this is the case, it seems that processes associated with aging—collagen cross-linking in the tendon, tendon stiffening, and loss of muscle strength—may all have a role in tendon degeneration via reduction of tenocyte stimulation. These mechanisms may be the link between aging and Achilles tendinopathy. Tendinopathy is also associated with distance running. It may be that similar mechanisms—collagen cross-linking, tendon stiffening, muscle loss or neuromuscular changes—occur with high volume distance running and may explain the incidence of tendinopathy in runners. Further study is needed in order to understand the role of individual fascicle motion for healthy movement and in pathological cases.

Chapter 7

Conclusion

7.1 Summary

Prior to this dissertation, the scientific community's understanding of muscle structure and tendon mechanics did not take advantage of the full capabilities of medical imaging for elucidating *in vivo* architecture and mechanics. Instead, previous knowledge on muscle size was based largely on cadaver dissection measurements; similarly, previous understanding of tendon mechanics was based on simplified conceptual models of muscle-tendon interaction. In this dissertation, it was shown that cadaver muscles do not accurately represent the muscles of healthy living humans, let alone those of pathological populations or elite athletes (Fig. 7.1). Additionally, previous models of the Achilles tendon that did not incorporate the meso-scale morphology of tendon fascicle structure have failed to acknowledge the role of differential muscle forces on tendon deformation during movement and have led to confusion in understanding Achilles deformation. **For the cases of lower limb skeletal muscle and the Achilles tendon, this dissertation leveraged non-Cartesian magnetic resonance imaging modalities to advance our understanding of the structure of these tissues, and leveraged image-based modeling approaches to gain deeper insight into muscle and tendon function in *in vivo* populations.**

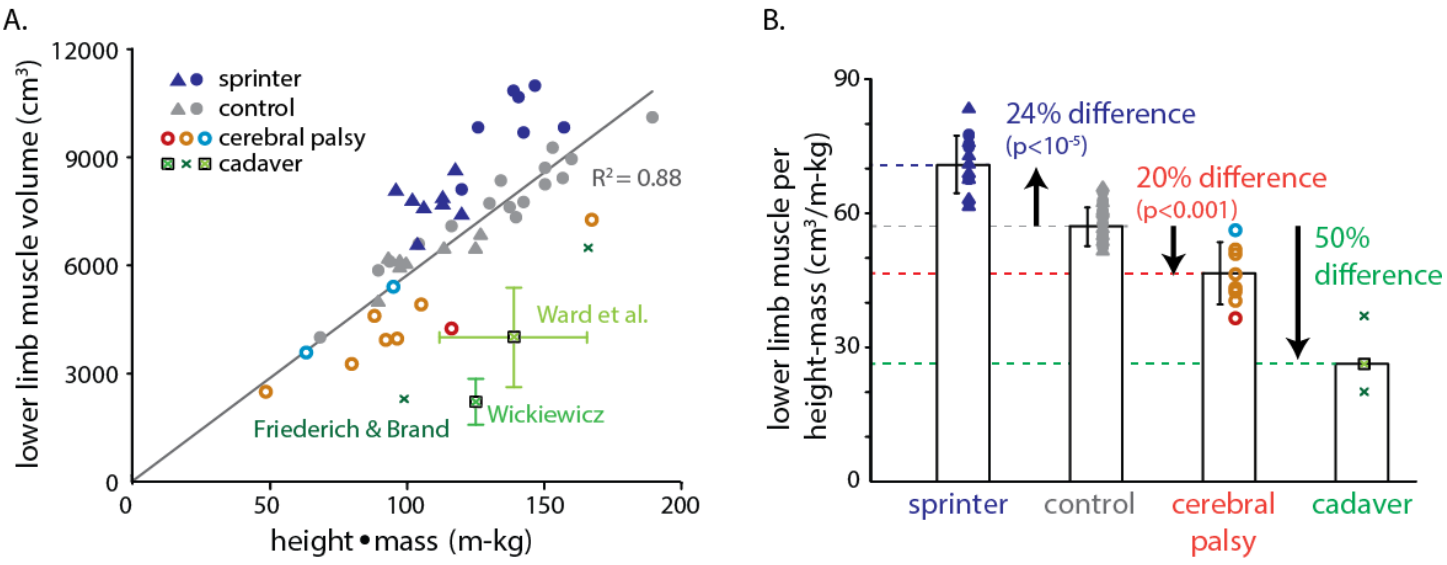

Figure 7.1: Lower limb muscle volume scaling across populations

A. The lower limb muscle volume of recreationally active control subjects scaled with the height-mass product. Sprinters fall above the control line while children with cerebral palsy and cadaver data (Friederich and Brand, 1990; Ward et al., 2009; Wickiewicz et al., 1983) fall below the line. B: Muscle volume per height-mass is significantly different between functionally different groups.

7.2 Contributions

The work presented in this dissertation spans three broad areas of interest in biomechanics: use of imaging for determining muscle size parameters *in vivo*, exploration of scaling relationships in human muscles, and image-based modeling approaches for elucidating muscle-tendon mechanics. In these areas of interest, I have published valuable data for use in future research, proposed novel metrics and analyses for assessing muscle size in populations, and offered new insights into previously unexplained phenomena. Specific contributions made in this dissertation are enumerated in the following subsections.

The first in vivo database of healthy lower limb muscle sizes

In this dissertation, I have presented an *in vivo* volume and length assessment of 35 lower limb muscles in 24 healthy subjects ranging in age, gender, and body size. These data can be used in the future for computational models requiring muscle size inputs, baseline values for estimating muscle sizes and size distributions in human populations, and as a normative database for comparing populations of interest such as subjects with disease, athletes, aging populations, etc.

A novel scaling metric for muscle sizes

In this dissertation, I show that the product of height and mass predicts lower limb muscle volume in a healthy, recreationally active population. The fact that this population ranged in BMI motivated the use of height and mass as covariates, since the relationship between height and mass was not consistent across the population. To my knowledge, this scaling approach for muscle volumes is novel and it suggests that mechanical torque balance in the musculoskeletal system may be a principle by which muscle tissue remodels. As has been demonstrated here, this scaling metric is useful for normalizing muscle volumes in populations that differ in body size.. In the

future, this scaling metric may be further explored in order to understand the mechanical stimuli that promote muscle size maintenance in humans.

An atlas of individual muscles in cross-section

A major challenge in determining individual muscle sizes from cross-sectional images is the difficulty of identifying the location of muscle boundaries within an image. Current atlases of muscle anatomy do not typically define muscle boundaries, instead identifying a center point within each muscle. Additionally, cross sections are usually displayed only for key slices in a few locations along the limb. These traditional atlases are not especially helpful for segmenting individual muscles in which knowledge of muscle boundaries throughout the limb is important.

In the pursuit of this dissertation, I have developed an atlas of cross-sectional muscle anatomy that details the boundaries of 35 muscles in 5mm increments throughout the lower limb. I anticipate that this atlas will be used by future researchers to assist in identifying muscle boundaries within axial images. Additionally, widespread use of a single atlas, such as that developed here, will provide a standard template for identifying muscles. While there is currently no gold standard for imaging-based muscle volume assessment, use of a standard atlas as a template will promote internal consistency among imaging-based assessments and will serve as a standard moving forward.

A novel functional metric for assessing muscle's mechanical capacity

Physical activity is increasingly implicated in long-term good health, especially in aging populations. For example, physical activity prevents the development of Type II diabetes and osteoporosis (Holten et al., 2004; Sayer et al., 2005; Shimegi et al., 1994). Recently, physical activity has been associated with longevity (Studenski et al., 2011). In populations that undergo intensive surgery, levels of physical strength are related to recovery time and the likelihood of survival (de Brito et al., 2012; Hunt et al., 1985). While the importance of physical activity and fitness are clear, few simple metrics exist that summarize the physical fitness of humans.

In this work, I normalized lower limb muscle volumes by the product of height and mass in order to compare muscle sizes across subjects varying in body size. This metric, muscle volume per height-mass, is hypothesized to be a gross metric of the lower limb's capacity to move the body. While much work remains in rigorously evaluating whether this metric is robust for clinical applications, it is promising that three populations with notable differences in their capacity for mobility—normal subjects, subjects with cerebral palsy, and elite athletes—were significantly stratified by this metric. Thus, muscle volume per height-mass may be a satisfactory metric for evaluating a subject's mobility capacity so that surgical and treatment decisions can be objectively tailored based on a subject's level of physical activity.

The first comprehensive assessment of lower limb muscle sizes in children with cerebral palsy

Children with cerebral palsy have neurological impairments which manifest in abnormalities of the musculoskeletal system. Previous researchers have used imaging to show that muscles in children with cerebral palsy are smaller than their typically developed counterparts, but the extent of muscle weakness across the lower limb has not been shown in detail. In this work, I show that children with cerebral palsy have extreme muscle size impairments in the lower limb

but size impairments differ across muscles and across subjects. Further research may promote the utility of medical imaging for subjects with cerebral palsy to promote targeted muscle strengthening or inform muscle-tendon orthopaedic decision making.

A novel use of Z scores to assess muscle abnormality on a subject-by-subject basis

This work utilized Z scores of muscle volume per height-mass to assess the degree of abnormality of cerebral palsy subjects' individual muscles compared to a healthy standard. In the past, this statistically-based approach has not been applied to muscle sizes. Since cerebral palsy has a panoply of symptoms, the use of Z scores is well-suited for cerebral palsy where patient-specific diagnostics and treatment planning is important. This approach is also applicable to assessment of athletes' muscles. This metric may be used in the future for individualized assessments of muscles in any population of interest.

The first comprehensive assessment of lower limb muscle sizes in sprint athletes

Competitive collegiate sprinters are able to perform greater functional tasks with their lower limbs compared to healthy non-athletes, generating high muscle forces in order to produce high speed running gaits. In this dissertation, I conduct the first comprehensive assessment of the muscle sizes of competitive sprinters' lower limbs. It was found that competitive sprinters had a 24% greater volume per height-mass than non-sprinter controls and that volume hypertrophy was greater in sprinters' hip extensor and knee extensor muscles. This volume assessment in sprinters lends further credence to the need for having population-specific *in vivo* muscle size data for building musculoskeletal models of athletes.

SUTE&TIE: A 3D Ultrashort TE imaging approach for Achilles tendon modeling

Ultrashort echo time (UTE) MRI has been demonstrated as a technique in 2D imaging of tendon. For utility in 3D modeling of tendon, 2D stacks or 3D imaging that are optimized for tendon are needed in order to construct a full anatomical model. In this dissertation, a combined ultrashort echo time/ short echo time 3D radial sequence was optimized for tendon imaging. Nicknamed SUTE&TIE (Subtraction Ultrashort TE & Tendon Intensity Enhancement), this optimized 3D sequence is well-suited for model building of the Achilles tendon. SUTE&TIE may be used in the future for modeling and clinical tendon applications.

A novel finite element model of Achilles tendon including meso-scale fascicle structure

Previous finite element models of the Achilles tendon have not included the internal fascicle structures of the tendon and consequently have failed to consider the role of differential muscle forces on tendon deformation. The model presented here includes these meso-scale structures and models the interfaces between these fascicles. From a clinical perspective, the consideration of sub-tendon structures in this model may shift the current clinical thinking about Achilles tendinopathy to include more study of the role of the plantarflexor muscles and interfascicle sliding as contributors to tendon degradation. From a modeling perspective, the approach undertaken in this dissertation represents a move toward multi-scale modeling of the tendon, which is an ongoing goal in biomechanical modeling and bioengineering communities.

Novel insights into differential stretching of fascicles in the Achilles tendon

In chapter 6 of this dissertation, finite element modeling revealed that experimentally observed non-uniform displacements in the Achilles tendon were associated with differential stretching of Achilles fascicles. Specifically, it was found that the medial gastrocnemius tendon fascicle undergoes high stretching, likely as a result of high passive forces in the medial gastrocnemius muscle. Conventional understanding does not account for non-uniform stretching within tendons. Furthermore, conventional understanding of muscle passive forces does not articulate differences in passive muscle properties across muscles. The current dissertation challenges these ideas and motivates further study of the properties of individual muscle-tendon units with respect to their functional contributions to the musculoskeletal system.

7.3 Applications of this Work

The insights gained from this dissertation challenge current assumptions in biomechanics and motivate the undertaking of new research directions. Specifically, the determination of *in vivo* muscle size parameters across populations offer new data sets with which to build musculoskeletal models, the insights into muscle size scaling offers new ways of assessing strength impairment that may be applied to clinical populations, and the revealed impact of tendon meso-scale structure suggest the incorporation of these features into future models and clinical research. Detailed descriptions of applications stemming from this dissertation are enumerated in the following subsections.

Imaging-derived muscle sizes in computational musculoskeletal models

The data presented in this dissertation represent a shift in accessible muscle size parameters from cadaver muscle data to *in vivo* data from reasonably large human datasets. The volumes, lengths, and PCSAs reported for normal subjects, children with CP, and sprint athletes can now be implemented into musculoskeletal models of these populations to better understand relative contributions of muscles to movement across populations and add increased accuracy to modeling approaches of these subject groups.

Use of CP muscle volumes in pre-treatment planning for CP therapies

In vivo muscle sizes acquired from subjects with cerebral palsy may add new dimensions to conventional pre-treatment assessments for this pathology. Gait analysis via motion capture has been used for decades as a quantitative method for assessing gait abnormality in CP subjects. While gait analysis can determine net joint torques during walking, the relative contributions of individual muscles cannot be determined. Combining *in vivo* muscle volumes with joint torques

determined from gait analysis may begin to solve this problem. Dividing net joint torques by *in vivo* muscle volumes for subjects with cerebral palsy yields a metric that grossly indicates how much effort is required by each muscle in order to produce movement. This metric is hypothesized to relate to fatigue in cerebral palsy and thus has clinical utility. Further studies of this metric and other integrations of imaging data with traditional treatment assessments in cerebral palsy are needed.

Extension of in vivo muscle volumes to other populations

The existence of a normative database of muscle sizes makes it feasible to conduct imaging studies of the lower limb musculature of various populations of interest. Just as the normative data were used to assess the abnormality of subjects with cerebral palsy and the hypertrophy patterns of track athletes, they can be used to assess the abnormality of the muscles of any other pathological or athletic group. Furthermore, imaging assessments of muscles in the feet, torso, arms, neck, and head may be made with the same techniques presented here.

Muscle volume per height-mass as a fitness metric: application to obesity

Obesity is often defined as having a body mass index (BMI) greater than 30 kg/m^2, but this definition of obesity is not consistent across ethnicities, ages, and levels of physical activity. Healthy Polynesians and healthy athletes, for example, are often identified as overweight or obese by the BMI definition despite having a healthy level of physical activity and body fat percentage. The BMI definition of obesity is also problematic when applied to children who have different body proportions than adult populations. Most researchers use population percentiles of BMI to define childhood obesity, but this definition is inherently sensitive to incidence of obesity—

increases in body fat percentages of an entire population over time, for example, would not be identified by this definition of childhood obesity.

There are two primary health concerns associated with obesity: excessive body fat and physical inactivity. BMI is problematic as a measure of obesity because it does not specifically reflect either of these two primary concerns. While body fat percentage may be used as a metric of obesity that specifically relates to excessive body fat, there is no clinical metric that measures obese subjects' capacity for physical activity.

The metric of muscle volume per height-mass may be ideal for measuring the mobility potential of overweight or obese subjects. This metric is hypothesized to be far more specific than BMI for identifying pathological obesity. For example, a highly mobile athlete with a BMI near 30 kg/m^2 would be falsely labeled as obese by the BMI definition, since their muscle volume per height-mass is high, indicating that high mobility capacity. Coupling of this metric with body fat percentage would indicate directly whether mobility potential, body fat percentage, or both are health concerns for a subject. The metric of BMI does not indicate either of these.

Muscle volume per height-mass as a fitness metric: application to aging

Aging is related to a loss of muscle mass known as sarcopenia. As muscle tissue is lost over time, musculoskeletal function declines and physical activity becomes increasingly difficult. Recent research has suggested a strong association between walking speed and longevity among the elderly. The present dissertation has indicated a possible link between muscle size per height-mass and step length. It is possible that walking speed is related to muscle quantity per body size and that longevity is thus associated with muscle quantity in the lower limb. Lower limb muscle quantity is associated with peripheral vascular health, glucose uptake, and recovery from surgery, as well as levels of activity. It is proposed here that use of muscle volume per height-mass as a

measurement applied to aging populations may help to indicate levels of functional capacity among the elderly. This may influence the prescription of exercise regimes designed to increase muscle size and promote long-term health.

Implications of tendon model on musculoskeletal modeling approaches

The work presented here is at the scale of the Achilles tendon. While this model has revealed new insights into Achilles function, it is difficult to precisely extend this modeling approach to motion of the whole body. Understanding the role of tendon fascicles and individual triceps surae muscles in whole body movement would be better served with whole body musculoskeletal models. Current musculoskeletal modeling approaches of the Achilles tendon treat this important tendon as three independent nonlinear springs actuated by the triceps surae muscles (Delp et al., 1990; Zajac, 1989). The advancement of these modeling approaches to include fascicle twisting and sliding and the possible incorporation of muscle-specific passive force curves may allow more precise understanding of the interaction between the plantarflexor muscles, the Achilles tendon, and whole body movement.

7.4 Future Work

DTI and two photon microscopy of lower limb muscles

In this work, I used non-Cartesian MRI to determine volumes and lengths of lower limb muscles *in vivo.* Using cadaver data for muscle length to optimal fiber length ratios, I estimated muscle physiological cross-sectional area (PCSA). Recent advances in imaging approaches have made it feasible to determine muscle fiber directions and muscle sarcomere length *in vivo* (Cromie et al., 2013; Damon et al., 2002; Llewellyn et al., 2008). The combination of non-Cartesian static MRI, diffusion tensor imaging (DTI), and two photon muscle microscopy make it possible to fully estimate the force-generating capacity and operating range of muscles *in vivo*. This approach is ideal for assessing populations for which pennation angle and sarcomere length may differ substantially from one another. Use of these techniques in athletes and subjects with cerebral palsy is promising for full determination of muscle force-generating parameters *in vivo*.

High resolution imaging of the meso-scale structure of the Achilles tendon

SUTE&TIE (Subtraction Ultrashort TE & Tendon Intensity Enhancement) imaging was used in this dissertation to create a 3D Achilles tendon model. Fascicle structural morphology within the tendon was inferred from literature studies of cadaver tendons. With improved coil design, it is possible that SUTE&TIE imaging and related approaches may be able to image the fascicle structure within the tendon, offering the opportunity to accurately determine meso-scale tendon structure with MRI. This advancement would have implications for modeling and may offer clinical benefits for exploring the role of fascicle morphology in Achilles tendinopathy.

Patient specific imaging based rigid body models

Rigid body musculoskeletal models and continuum level finite element models of muscle are often considered as two different scales of muscle modeling. While rigid body modeling can indicate joint- and limb-level pathologies or abnormalities, they are not built with sufficient muscle shape detail to assess force or strain irregularities at the muscle tissue level. Finite element models, while possessing the ability to model local stress and strain behavior within the muscle, are limited in that it is difficult to relate the finite element simulation back to a realistic human movement. Bridging these two models is a goal in the biomechanics community as it may be able to link whole body motion with muscle tears (such as in athletics) and chronic muscle degeneration (such as in muscular dystrophy). For cerebral palsy, such integrated models may suggest what specific muscle pathology—shortness, weakness, spasticity—is contributing to an observed gait abnormality. The work presented here represents the first comprehensive assessment of lower limb muscle sizes in cerebral palsy and is a valuable step in the integration of continuum and rigid body models.

Dynamic mechanical model of lower limb muscle size

In this dissertation, it was found that the product of height and mass predicted lower limb muscle volume better than mass or height alone. While I hypothesized that mechanical torque balance was the fundamental principle behind this scaling relationship, a model of lower limb function is an important next step for verifying the validity of this relationship. Such a model will allow for the variation of mass and height independently across physiologically reasonable values while lower limb forces are input in order to generate scalable function. This will help to elucidate whether torque balance or some other mechanical relationship is primarily involved in muscle maintenance in the lower limb.

Extension of torque-balance hypothesis to muscle moment arms

Moment arm is the distance between a muscle's line of action and the joint center on which it operates (Fig. 7.2). Joint torque has heuristically been correlated to muscle volume in the past (Fukunaga et al., 2001; Holzbaur et al., 2007a; Trappe et al., 2001). The more direct definition of joint torque defines it as the product of muscle force (related to PCSA) with moment arm. If torque balance is a major principle by which muscle remodels, inclusion of moment arms with muscle PCSAs may improve the scaling relationship between muscle size and the height-mass product. Pilot work into this relationship is promising (Fig. 7.2) but is limited in its use of static MR images to define Achilles moment arm. Future work in defining moment arms dynamically is needed to add further credence to the hypothesis of musculoskeletal torque balance.

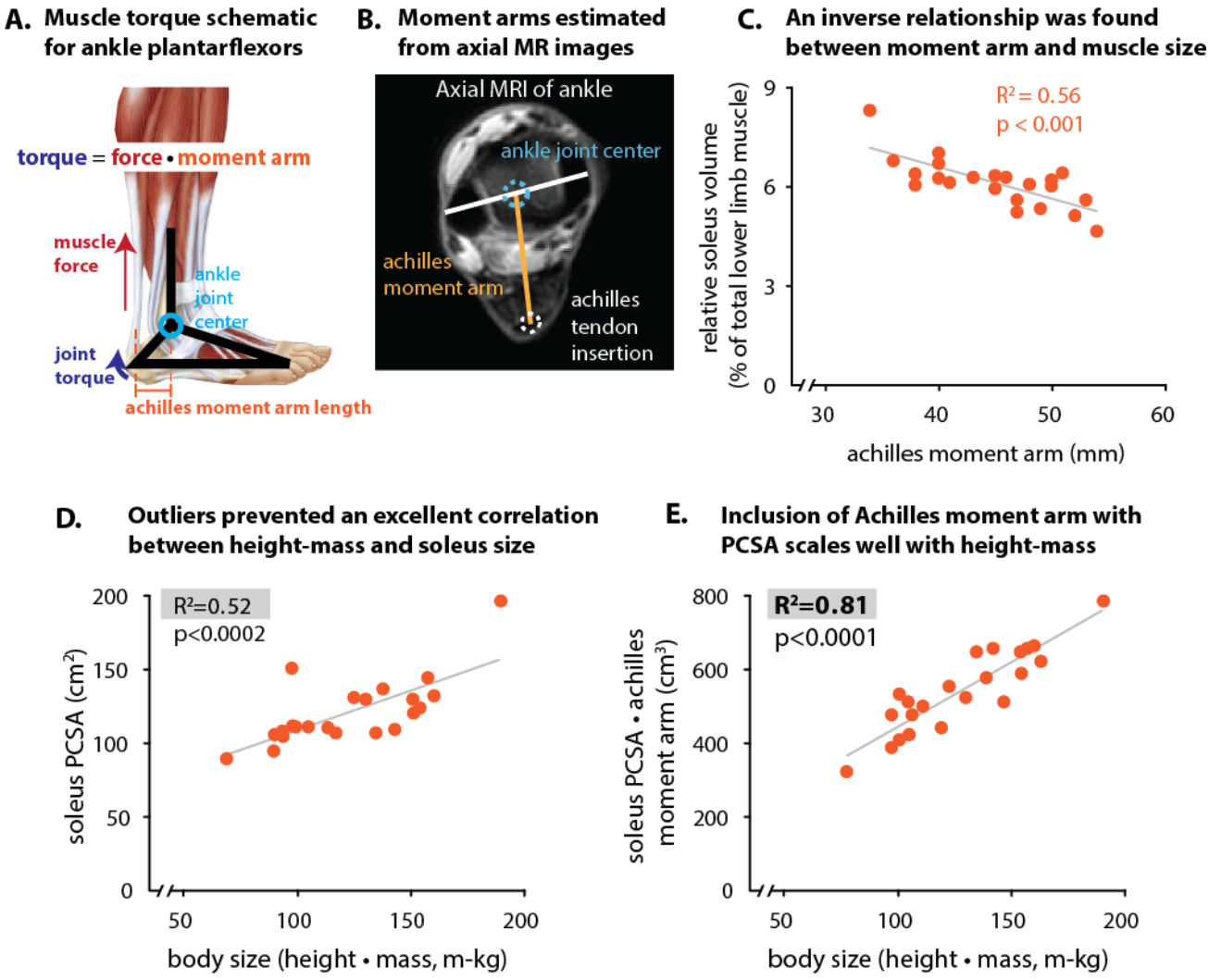

Figure 7.2: The inclusion of moment arms with muscle size parameters may improve scaling relationships and reinforce that torque balance is related to height-mass scaling

A: Moment arms are the distance between a muscle line of action and the joint center and relate joint torque to muscle force. B: In a pilot study, Achilles moment arms were determined from static axial MR images. C: An inverse relationship was found between muscle size and moment arm length, suggesting that torque balance may exist in muscles: subjects with longer moment arms need less muscle force to generate the same torques. D: The soleus PCSA did not scale well with the height-mass product. E: Inclusion of Achilles moment arm significantly improved the scaling relationship for height-mass as a predictor of muscle size.

Determination of muscle sizes and scaling relationships across ethnicities

The normative database presented here was limited in that the convenience sample of subjects at the University of Virginia who were willing to volunteer for an MRI scan were overwhelmingly of Caucasian descent. It is not known whether ethnic differences will be related to variations in lower limb muscle sizes. For this reason, investigation of healthy, recreationally active subjects from other ethnic backgrounds may be useful in the creation of a large, ethnically diverse database of normative muscle sizes.

Future explicit modeling of tendinopathy

The modeling approaches in this dissertation suggests that alterations in muscle forces, tendon material properties, and the inter-fascicle interface in the tendon affects the displacement profile of tissue within the tendon during motion. Aging is associated with changes to all three of these factors and tendinopathy is thought to be related to mechanical changes within the tendon. Future explicit models of aging tendons and of tendons associated with tendinopathic changes may further the present work and suggest more specifically how muscles, aging, tissue properties, and tendinopathy relate to one another. Furthermore, clinical studies focusing on the role of the muscles and intra-tendon cross-linking are indicated by the work presented in this dissertation. Lastly, modeling approaches of Achilles lengthening surgeries in subjects with cerebral palsy may benefit from the insights on tendon substructure suggested in this work.

7.5 Conclusion

Biomedical Engineering is the field of designing, building, and utilizing techniques and technology that advance the understanding of human health and the treatment of human disease. In the present dissertation, I utilized non-Cartesian MRI and computational modeling approaches in order to determine muscle sizes and scaling relationships for skeletal muscle in healthy subjects *in vivo*. I extended this analysis to two populations: children with cerebral palsy in order to understand muscle size abnormality in a pathological group, and collegiate sprinters in order to understand muscle hypertrophy patterns in an athlete group. Lastly, I used advanced imaging and modeling to create the first meso-scale model of the Achilles tendon from 3D non-Cartesian UTE MRI and finite element modeling. In the pursuit of these aims, I have discovered previously unknown phenomena and innovated new metrics for contextualizing muscle size abnormalities in humans. With this data, I offer previously unavailable information on the human musculoskeletal system *in vivo* that will open the possibility for more accurate modeling approaches of human muscle and tendon for future researchers. Hopefully, this work will be viewed in the broader context of advancing an understanding of human health and disease through scientific and technological advancement and a paradigm shift toward imaging-based subject-specific medicine.

"And in the end/ the love you take/ is equal to the love/ you make."

-*The Beatles*, "The End"

Appendix I

Equations for Computing Muscle Parameters from Imaging Volumes and Lengths

Physiological cross sectional area, PCSA, is calculated by dividing the imaging-based volume by the centroid length(Ch. 3, Handsfield et al., 2014) and multiplying by the ratio of muscle length to optimal fiber length from literature(Ward et al., 2009):

$$\boldsymbol{PCSA} = \frac{\boldsymbol{volume}}{\boldsymbol{length}} \cdot \frac{\boldsymbol{L_m}}{\boldsymbol{L_f^0}} \quad \textbf{(A1)}$$

Muscle volume is normalized by subject height and subject body mass:

$$\boldsymbol{normalized\ volume} = \frac{\boldsymbol{volume}}{\boldsymbol{height \cdot mass}} \quad \textbf{(A2)}$$

Normalized muscle length is defined as the muscle centroid length divided by limb length, where limb length is the summed linear length of the tibia and femur:

$$\boldsymbol{normalized\ length} = \frac{\boldsymbol{length}}{\boldsymbol{limb\ length}} = \frac{\boldsymbol{length}}{\boldsymbol{tibia\ length + femur\ length}} \quad \textbf{(A3)}$$

Normalized PCSA is defined as the normalized volume (A2) divided by the normalized length (A3) and scaled by the $\frac{L_m}{L_f^0}$ ratio, which may be written as:

$$\boldsymbol{normalized\ PCSA}\ (\mathbf{1}) = \frac{\boldsymbol{volume}}{\boldsymbol{length}} \cdot \frac{\boldsymbol{limb\ length}}{\boldsymbol{height \cdot mass}} \cdot \frac{\boldsymbol{L_m}}{\boldsymbol{L_f^0}} \quad \textbf{(A4.1)}$$

This equation is equivalent to PCSA divided by mass and scaled by the ratio of limb length to height:

$$\boldsymbol{normalized\ PCSA}\ (\mathbf{1}) = \frac{\boldsymbol{PCSA}}{\boldsymbol{mass}} \cdot \frac{\boldsymbol{limb\ length}}{\boldsymbol{height}}$$

In populations where the $\frac{limb\ length}{height}$ ratio may be considered to not vary across subjects, this ratio may not be needed for PCSA normalization. In this case, equation A4.1 may be replaced with the simpler equation:

$$\boldsymbol{normalized\ PCSA}\ (\mathbf{2}) = \frac{\boldsymbol{volume}}{\boldsymbol{length}} \cdot \frac{\mathbf{1}}{\boldsymbol{mass}} \cdot \frac{\boldsymbol{L_m}}{\boldsymbol{L_f^0}} = \frac{\boldsymbol{PCSA}}{\boldsymbol{mass}} \quad \textbf{(A4.2)}$$

Optimal muscle length along the muscle fiber direction, $\boldsymbol{muscle\ length_f^o}$, may be needed for understanding muscle range of motion. The normalized form of this parameter may be found as the normalized length scaled by the $\frac{L_m}{L_f^0}$ ratio:

$$\boldsymbol{normalized\ muscle\ length_f^o} = \frac{\boldsymbol{length}}{\boldsymbol{limb\ length}} \div \frac{\boldsymbol{L_m}}{\boldsymbol{L_f^0}} \quad \textbf{(A5)}$$

Appendix II

Tables

Table 3.2: Coefficients for linear best fit for muscle volumes in normal subjects

	total muscle volume		mass		height*mass	
muscle	**b_1 (cm^3/cm^3)**	**b_2 (cm^3)**	**b_1 (cm^3/kg)**	**b_2 (cm^3)**	**b_1 (cm^3/kg-m)**	**b_2 (cm^3)**
gluteus maximus	0.123	-25.4	11.9	-3.91	6.01	105
adductor magnus	0.0793	-4.70	6.93	62.3	3.64	109
gluteus medius	0.0478	-16.9	4.14	26.3	2.17	54.8
psoas	0.0550	-117	4.45	-44.7	2.43	-26.3
iliacus	0.0248	0.383	2.08	27.6	1.11	39.4
sartorius	0.0256	-18.2	2.34	-4.47	1.19	15.9
adductor longus	0.0259	-21.9	2.27	-0.48	1.19	14.3
gluteus minimus	0.0129	12.6	1.08	27.0	0.576	33.1
adductor brevis	0.0137	6.20	1.13	22.9	0.622	27.1
gracilis	0.0138	6.07	1.08	26.5	0.580	32.1
pectineus	0.0107	-9.94	0.946	-1.59	0.481	6.7
tensor fasciae latae	0.0136	-31.5	1.12	-15.6	0.620	-11.8
obturator externus	0.00349	28.3	0.279	33.1	0.146	35.1
piriformis	0.00372	16.2	0.203	28.1	0.137	25.7
quadratus femoris	0.00475	-1.45	0.409	3.01	0.228	4.2
obturator internus	0.00252	8.68	0.228	10.3	0.120	11.7
small ext. rotators	0.00172	3.85	0.139	6.11	0.0688	7.56
vastus lateralis	0.125	-55.7	11.5	6.15	5.89	102
vastus medialis	0.0631	-16.3	6.12	-6.22	3.03	57.6
vastus intermedius	0.0273	76.5	2.49	91.5	1.29	111
rectus femoris	0.0371	4.97	3.15	43.2	1.71	56.9
semimembranosus	0.0319	18.2	2.96	33.3	1.54	54.5
biceps femoris: l.h.	0.0256	24.3	2.31	40.8	1.24	53.0
semitendinosus	0.0285	-16.8	2.37	15.9	1.27	29.1
biceps femoris: s.h.	0.0160	-13.8	1.38	1.02	0.738	8.64
popliteus	0.00298	2.11	0.245	5.75	0.133	6.84
soleus	0.0507	78.2	5.26	61.1	2.57	120
med gastrocnemius	0.0348	9.42	3.41	12.6	1.71	46.2
lat gastrocnemius	0.0199	8.21	2.19	-7.59	1.08	15.7
tibialis anterior	0.0161	20.3	1.56	22.9	0.796	36.7
peroneals (brev/long)	0.0194	-7.43	1.91	-6.58	0.956	12.5
tibialis posterior	0.0104	30.8	0.835	44.8	0.451	48.9
extensors (EDL/EHL)	0.0132	8.70	1.21	15.5	0.619	25.6
flexor hallucis longus	0.0137	-18.9	1.14	-2.95	0.622	1.85
flexor digit. longus	0.00259	11.6	0.245	12.4	0.130	13.9

Coefficients are given for linear fits of muscle volume against the metrics of total lower limb muscle volume, mass, and height*mass. Values are for equations of the form: $Volume = b_1 * metric + b_2$.

Table 3.3: Volumes, lengths, and R^2 values for muscle correlations in normal subjects

muscle	action group	average volume (cm^3) (±S.D.)	average volume fraction (%) (±S.D.)	length (cm) (±S.D.)	mass R^2	height* mass R^2	total muscle volume R^2
gluteus maximus†	HE	849.0 (194.7)	11.93 (1.02)	29.0 (2.1)	**0.79**	**0.82**	**0.83**
adductor magnus	HAd	559.8 (129.4)	7.86 (0.86)	31.4 (2.9)	**0.61**	**0.68**	**0.78**
gluteus medius†	HAb	323.2 (81.1)	4.54 (0.62)	19.1 (1.9)	**0.55**	**0.61**	**0.72**
psoas*	HF	274.8 (89.9)	3.80 (0.61)	32.9 (2.4)	**0.52**	**0.63**	**0.78**
iliacus*	HF	176.8 (41.6)	2.48 (0.31)	25.2 (1.9)	**0.53**	**0.61**	**0.74**
sartorius	HF	163.7 (41.9)	2.29 (0.29)	52.6 (3.7)	**0.67**	**0.70**	**0.77**
adductor longus	HAd	162.1 (43.7)	2.26 (0.34)	21.0 (2.1)	**0.57**	**0.64**	**0.73**
gluteus minimus†	HAb	104.5 (23.0)	1.47 (0.19)	12.9 (1.7)	0.47	**0.54**	**0.65**
adductor brevis	HAd	104.0 (25.8)	1.47 (0.23)	13.6 (1.8)	0.41	**0.50**	**0.59**
gracilis	HAd	104.0 (24.8)	1.46 (0.23)	32.3 (2.3)	0.40	0.47	**0.64**
pectineus	HAd	66.3 (21.6)	0.92 (0.22)	12.8 (1.8)	0.41	0.43	**0.51**
tensor fasciae latae	HAb, HF	64.9 (26.3)	0.89 (0.27)	15.9 (2.2)	0.39	0.48	**0.55**
obturator externus	HER	53.2 (12.7)	0.76 (0.16)	9.9 (1.4)	0.10	0.11	0.16
piriformis	HER	42.7 (12.9)	0.61 (0.17)	9.5 (2.3)	0.05	0.10	0.17
quadratus femoris	HER	32.4 (10.7)	0.45 (0.11)	7.3 (1.1)	0.31	0.39	0.41
obturator internus	HER	26.6 (7.1)	0.38 (0.09)	8.0 (1.4)	0.22	0.25	0.26
small ext. rotators	HER	16.1 (5.8)	0.23 (0.07)	8.2 (2.1)	0.12	0.12	0.18
vastus lateralis‡	KE	830.9 (194.3)	11.66 (1.06)	36.7 (2.7)	**0.74**	**0.79**	**0.85**
vastus medialis‡	KE	432.6 (100.1)	6.06 (0.56)	33.0 (2.3)	**0.79**	**0.79**	**0.82**
vastus intermedius ‡	KE	270.5 (56.6)	3.84 (0.60)	33.2 (3.3)	0.41	0.45	0.48
rectus femoris‡	KE, HF	269.0 (64.3)	3.79 (0.51)	32.1 (1.7)	**0.51**	**0.61**	**0.69**
semimembranosus§	KF, HE	245.4 (54.2)	3.46 (0.43)	27.2 (2.6)	**0.63**	**0.70**	**0.72**
biceps femoris: l.h. §	KF, HE	206.5 (48.4)	2.92 (0.43)	28.4 (3.1)	0.48	**0.56**	**0.58**
semitendinosus§	KF, HE	186.0 (47.0)	2.60 (0.34)	30.9 (2.2)	**0.54**	**0.63**	**0.76**
biceps femoris: s.h.§	KF	100.1 (32.0)	1.40 (0.30)	25.8 (2.7)	0.40	0.46	**0.52**
popliteus		23.3 (5.0)	0.33 (0.04)	9.6 (1.5)	**0.51**	**0.61**	**0.73**
soleus¶	APF	438.2 (91.6)	6.21 (0.80)	32.1 (2.2)	**0.69**	**0.67**	**0.62**
medial gastrocnemius¶	APF, KF	257.4 (61.8)	3.62 (0.48)	26.9 (1.8)	**0.65**	**0.65**	**0.66**
lateral gastrocnemius¶	APF, KF	150.0 (42.2)	2.11 (0.42)	24.1 (2.3)	**0.58**	**0.58**	0.47
tibialis anterior	ADF	135.2 (27.5)	1.91 (0.23)	31.7 (2.9)	**0.69**	**0.72**	**0.71**
peroneals (brev/long)	APF	130.8 (34.3)	1.83 (0.28)	35.5 (2.7)	**0.66**	**0.67**	**0.66**
tibialis posterior	APF	104.8 (22.3)	1.49 (0.24)	30.6 (2.7)	0.30	0.35	0.45
extensors (EDL/EHL)	PE, ADF	102.3 (21.6)	1.44 (0.14)	36.3 (2.8)	**0.67**	**0.71**	**0.77**
flexor hallucis longus	PF, APF	78.8 (23.1)	1.09 (0.19)	23.0 (3.3)	**0.52**	**0.62**	**0.73**
flexor digit. longus	PF, APF	30.0 (8.2)	0.43 (0.11)	24.9 (3.7)	0.19	0.22	0.21
**Iliopsoas*	*HF*	451.6 (124.1)	6.28 (0.67)		**0.59**	**0.70**	**0.86**
†*Gluteals*	*HE*	1,276.7 (281.4)	17.94 (1.24)		**0.79**	**0.83**	**0.88**
‡*Quadriceps*	*KE*	1,803.0 (380.5)	25.35 (1.66)		**0.79**	**0.84**	**0.91**
§*Hamstrings*	*KF*	737.9 (156.3)	10.38 (0.75)		**0.71**	**0.81**	**0.88**
¶*Triceps Surae*	*APF*	845.6 (183.1)	11.94 (1.38)		**0.75**	**0.74**	**0.69**

Major action(s) of muscles are given (HE—Hip Extensor, HF—Hip Flexor, HAd—Hip Adductor, HAb—Hip Abductor, HER—Hip External Rotator, KE—Knee Extensor, KF—Knee Flexor, APF—Ankle Plantarflexor, ADF—Ankle Dorsiflexor, PE – Phalangeal Extensor, PF – Phalangeal Flexor). Absolute muscle volume, muscle volume fraction (muscle volume divided by total lower limb muscle volume), and anatomical length means and standard deviations are reported. R^2 values are reported for the relationship between muscle volume and mass, between muscle volume and the height-mass product, and between muscle volume and total limb muscle volume. R^2 values that indicate a predictive power of 50% or greater are in bold. In three cases, more than one muscle were grouped into a single anatomical structure—'extensors' is composed of the extensor digitorum longus, the extensor hallucis longus, and the peroneus tertius; 'peroneals' is the peroneus longus and peroneus brevis; 'small ext. rotators' is the gemellus superior, gemellus inferior, and the posterior part of the obturator internus.

Table 3.4: Relative volume and length, and PCSA in normal vs. cadaver muscles

muscle	volume fraction (%) (±S.D.)	cadaver volume fraction (%) ‖	length fraction(%) (±S.D.)	cadaver length fraction (%) ‖	PCSA (cm^2) (±S.D.) ††	cadaver PCSA (cm^2) ‖	PCSA fraction (%) (±S.D.)
gluteus maximus	11.93 (1.02)	13.88	34.8 (1.7)	33.5	46.8 (8.7)	36.0	5.79 (0.42)
adductor magnus	7.86 (0.86)	8.23	37.6 (2.7)	47.1	45.5 (8.5)	21.3	5.62 (0.56)
gluteus medius	4.54 (0.62)	6.94	22.9 (1.8)	24.9	45.6 (10.2)	36.1	5.64 (0.82)
psoas	3.80 (0.61)	2.48	39.4 (2.1)	30.2	16.5 (4.4)	7.8	2.02 (0.34)
iliacus	2.48 (0.31)	2.88	30.2 (1.7)	25.6	12.4 (2.5)	10.2	1.54 (0.22)
sartorius	2.29 (0.29)	1.99	63.0 (3.3)	55.7	3.4 (0.8)	1.9	0.42 (0.06)
adductor longus	2.26 (0.34)	1.89	25.1 (1.9)	27.2	15.4 (3.6)	6.6	1.90 (0.31)
gluteus minimus	1.47 (0.19)		15.4 (1.7)		8.2 (1.8) ‡‡		1.01 (0.16)
adductor brevis	1.47 (0.23)	1.33	16.3 (1.9)	35.7	9.7 (1.9)	5.0	1.20 (0.18)
gracilis	1.46 (0.23)	1.38	38.6 (1.9)	19.1	4.7 (1.0)	2.2	0.58 (0.10)
pectineus	0.92 (0.22)		15.3 (2.1)		5.1 (1.4) ‡‡	2.9 §§	0.63 (0.13)
tensor fasciae latae	0.89 (0.27)		19.0 (2.2)		4.0 (1.3) ‡‡	2.5 §§	0.48 (0.12)
obturator externus	0.76 (0.16)		11.8 (1.6)		5.4 (1.2) ‡‡		0.68 (0.15)
piriformis	0.61 (0.17)		11.5 (2.9)		4.7 (1.7) ‡‡	5.0 §§	0.59 (0.21)
quadratus femoris	0.45 (0.11)		8.7 (1.2)		4.4 (1.1) ‡‡	4.2 §§	0.55 (0.12)
obturator internus	0.38 (0.09)		9.5 (1.6)		3.3 (0.5) ‡‡		0.42 (0.07)
small ext. rotators	0.23 (0.07)		9.9 (2.4)		2.0 (0.7) ‡‡	1.8 §§	0.25 (0.09)
vastus lateralis	11.66 (1.06)	9.53	43.9 (1.5)	34.0	59.3 (12.1)	37.0	7.33 (0.75)
vastus medialis	6.06 (0.56)	6.07	39.5 (1.4)	54.6	59.1 (11.4)	23.7	7.30 (0.67)
vastus intermedius	3.84 (0.60)	4.36	39.7 (3.3)	51.2	39.0 (8.0)	16.8	4.85 (0.84)
rectus femoris	3.79 (0.51)	2.80	38.4 (1.4)	45.1	34.8 (7.4)	13.9	4.31 (0.63)
semimembranosus	3.46 (0.43)	3.41	32.6 (3.0)	36.5	37.8 (9.1)	19.1	4.65 (0.62)
biceps femoris: l.h.	2.92 (0.43)	2.88	34.0 (3.4)	43.2	25.9 (4.9)	11.5	3.22 (0.46)
semitendinosus	2.60 (0.34)	2.53	37.0 (2.6)	36.9	9.3 (2.3)	4.9	1.14 (0.19)
biceps femoris: s.h.	1.40 (0.30)	1.52	30.8 (2.3)	27.8	7.8 (1.8)	5.2	0.96 (0.16)
popliteus	0.33 (0.04)		11.5 (1.5)		2.5 (0.6) ‡‡	7.9 §§	0.31 (0.06)
soleus	6.21 (0.80)	6.99	38.4 (2.0)	50.4	124.1 (24.9)	58.8	15.39 (1.86)
med gastrocnemius	3.62 (0.48)	2.88	32.2 (1.8)	33.5	50.1 (10.0)	21.4	6.19 (0.67)
lat gastrocnemius	2.11 (0.42)	1.58	28.8 (2.6)	27.8	23.0 (6.0)	9.9	2.84 (0.45)
tibialis anterior	1.91 (0.23)	2.03	37.9 (2.5)	32.3	15.8 (2.9)	11.1	1.96 (0.22)
peroneals (brev/long)	1.83 (0.28)	2.08	42.5 (1.3)	33.7**	19.3 (4.4)	15.7	2.38 (0.34)
tibialis posterior	1.49 (0.24)	1.48	36.6 (2.1)	38.6	28.4 (4.7)	14.8	3.55 (0.54)
extensors (EDL/EHL)	1.44 (0.14)	1.57	43.4 (1.4)	36.1**	10.2 (1.7)	8.4	1.27 (0.13)
flexor hallucis longus	1.09 (0.19)	0.99	27.5 (3.2)	33.4	16.9 (3.6)	7.2	2.09 (0.31)
flexor digit. longus	0.43 (0.11)	0.51	29.8 (3.7)	34.0	7.5 (1.5)	4.5	0.94 (0.20)

Values obtained in this study and in literature cadaver studies for 35 lower limb muscles. Volume fractions are given as a percentage of the total lower limb muscle volume. Length fractions are given as a percentage of the summed linear superior-inferior lengths of the tibia and femur. PCSA fractions are reported as a percentage of the total PCSA, which is the summation of the PCSAs of all 35 muscles.

See Following Page for Footnotes

‖ Average values for muscle parameters reported in Ward et al., 2009 are reproduced here. In the case of muscle volumes, values were obtained by dividing muscle masses reported in Ward et al. by muscle density, ρ, reported in

Ward et al. as ρ =1.056 *g/cm*^{3}. Values from Ward et al. were normalized by a weighted sum of the muscle volumes in order to compute cadaver muscle volume fraction. Muscles that were not reported in Ward et al. were assigned the same relative muscle volume as the present study's average so that the summed total muscle volume of cadavers would be represented by the same set of 35 muscles as in this study. For muscle length, values from Ward et al. were normalized by the sum of the reported femur and tibia length to compute muscle length fractions. For PCSA, reported values were divided by the cosine of the reported pennation angle so that the value given here represents the value: $= \frac{V_m}{L_m} / \frac{L_f^0}{L_m}$.

** Ward et al. reported peroneus longus and brevis separately, whereas our study combined those muscles into one structure. Similarly, this study combined the extensor digitorum longus and the extensor hallucis longus. This may account for differences between the Ward et al. length data and the length data reported here.

†† PCSA or Physiological Cross Sectional Area was computed by dividing the muscle volume, V_m, by the anatomical muscle belly length, L_m, and dividing by literature values for optimal fiber length to muscle length ratios ($PCSA = \frac{V_m}{L_m} / \frac{L_f^0}{L_m}$). Optimal fiber length to muscle length ratios ($\frac{L_f^0}{L_m}$) were obtained from Ward et al., 2009.

‡‡ In cases where no optimal fiber length to muscle length ratios were reported by Ward et al., this ratio was set equal to 1. For these muscles the value reported as PCSA is a mean cross sectional area with respect to the muscle's line of action which does not take into account pennation angle.

§§ In cases where Ward et al. did not report PCSA for muscles, the literature PCSA value was obtained from Wickiewicz et al., 1983 or Brand et al., 1982. Reported PCSA values were divided by reported pennation angle so that the value given here represents the value: $= \frac{V_m}{L_m} / \frac{L_f^0}{L_m}$.

Table 4.2: Mean deficits in muscle volume, PCSA, and length in subjects with CP

lower limb muscle	**% volume difference** of CP group (*p<0.05 † p<0.01 ‡p<0.001)	**% PCSA difference** of CP group (*p<0.05 †p<0.01 ‡p<0.001)	**% length difference** of CP group (*p<0.05 †p<0.01 ‡p<0.001)	# of CP muscles small in volume (Z_V < -2)	# of CP muscles small in PCSA (Z_{PCSA} < -2)	# of CP muscles short in length (Z_L < -2)	# of CP muscles small in PCSA and short in length
tibialis anterior	**-43.4‡**	**-40.1‡**	-6.0	9	7	4	3
med. gastrocnemius	**-42.2‡**	**-32.2‡**	**-15.5†**	8	5	9	5
soleus	**-39.3‡**	**-34.0‡**	**-7.5***	9	9	1	1
lat. gastrocnemius	**-35.8‡**	**-24.8†**	**-14.4***	4	4	5	2
semitendinosus	**-35.3†**	**-23.5***	**-19.5***	4	3	4	2
semimembranosus	**-30.5†**	**-25.2***	-7.2	8	7	0	0
flexor hallucis longus	**-30.5†**	**-33.5†**	3.7	3	3	2	1
rectus femoris	**-29.2‡**	**-28.9‡**	-0.9	5	4	1	1
digital ext. (EDL&EHL)	**-28.6‡**	**-24.2†**	**-5.6†**	8	6	1	0
psoas	**-27.4†**	**-23.7†**	-4.9	6	4	1	0
peroneals	**-27.3†**	**-24.1***	**-4.9***	5	3	4	2
biceps femoris: l.h.	**-24.6***	**-22.9†**	-3.5	3	1	0	0
adductor longus	**-22.3***	-17.4	-5.5	2	2	3	0
biceps femoris: s.h.	-22.2	**-16.9***	-5.4	1	2	2	1
vastus medialis	**-21.4***	**-19.3***	-3.0	6	6	2	2
adductor magnus	**-20.8***	-15.1	-6.3	5	6	3	1
vastus lateralis	**-20.6***	**-20.2***	-0.8	5	5	3	2
obturator externus	-20.4	-14.5	-12.7	2	0	0	0
adductor brevis	**-19.2***	-16.7	-2.3	4	3	1	0
gracilis	-16.0	0.8	**-17.7†**	1	0	7	0
tibialis posterior	-14.3	-12.3	-3.4	3	1	1	1
pectineus	-14.1	-5.9	-6.8	0	0	1	0
gluteus maximus	**-11.5***	-9.3	-2.1	1	3	1	0
tensor fasciae latae	-11.3	-11.9	2.5	0	3	0	0
flexor digit. longus	-10.5	-6.1	-6.2	1	3	0	0
popliteus	-9.8	-9.6	-0.2	1	1	0	0
gluteus minimus	-9.2	-8.1	-2.2	3	3	0	0
sartorius	-6.7	-3.3	-4.3	2	0	1	0
vastus intermedius	-6.6	-10.4	3.5	2	2	0	0
obturator internus	-6.2	-6.2	-1.5	1	4	0	0
gemelli	-6.0	-10.5	0.8	2	0	0	0
quadratus femoris	-0.7	-11.8	10.0	2	0	1	0
iliacus	-0.1	0.4	-0.8	0	0	1	0
gluteus medius	1.4	-2.1	3.8	0	0	0	0
piriformis	2.0	6.4	4.0	0	0	0	0

Volumes, PCSAs, and lengths were normalized to height, mass, and leg length according to Supplementary Equations 1-4. Statistical significance is denoted, based on rank-sum testing. Number of muscles outside of 2σ confidence interval are tabulated.

Table 5.1a: Muscle volumes and PCSAs of sprinters and non-sprinters

muscle	sprinter muscle volume (cm^3)	sprinter normalized volume (cm^3/kg-m)	control normalized volume (cm^3/kg-m)	vol. % diff	sprinter muscle pcsa (cm^2)	sprinter normalized pcsa (cm^2/kg)	control normalized pcsa (cm^2/kg)	pcsa % diff
semitend.	289±71 [194-423]	2.3±0.5 [1.5-3.3]	1.5±0.3 [1-2.1]	**54%**	13±3 [9-19]	0.19±0.04 [0.12-0.26]	0.13±0.02 [0.08-0.17]	**47%**
gracilis	149±30 [90-205]	1.2±0.3 [0.8-2.1]	0.9±0.2 [0.6-1.3]	**42%**	6±1 [4-8]	0.08±0.02 [0.05-0.13]	0.06±0.01 [0.04-0.09]	**40%**
tensor fasciae latae	91±24 [43-129]	0.7±0.2 [0.4-1.3]	0.5±0.2 [0.3-0.9]	**41%**	5±1 [3-8]	0.08±0.02 [0.05-0.12]	0.06±0.01 [0.03-0.08]	**41%**
rectus femoris	375±60 [276-497]	3±0.3 [2.4-3.7]	2.2±0.3 [1.5-2.8]	**40%**	52±8 [35-68]	0.74±0.09 [0.54-0.93]	0.56±0.1 [0.34-0.78]	**34%**
sartorius	224±67 [115-364]	1.8±0.5 [1.1-2.7]	1.3±0.2 [0.9-1.8]	**37%**	5±1 [3-8]	0.06±0.02 [0.04-0.1]	0.05±0.01 [0.04-0.07]	**35%**
gluteus maximus	1114±206 [856-1523]	9±1 [7.3-10.5]	6.9±0.7 [5.8-8.6]	**31%**	59±10 [46-85]	0.85±0.12 [0.66-1.11]	0.66±0.06 [0.55-0.81]	**29%**
vastus medialis	562±110 [413-804]	4.6±0.6 [3.6-5.6]	3.5±0.4 [2.7-4.3]	**30%**	73±12 [57-99]	1.04±0.11 [0.85-1.26]	0.83±0.09 [0.66-1.02]	**26%**
vastus intermedius	348±102 [194-520]	2.8±0.6 [1.6-3.5]	2.2±0.3 [1.7-2.8]	**29%**	41±10 [24-58]	0.59±0.11 [0.37-0.73]	0.46±0.07 [0.34-0.72]	**28%**
tibialis posterior	135±24 [80-187]	1.1±0.2 [0.8-1.6]	0.9±0.2 [0.5-1.2]	**28%**	33±6 [23-46]	0.48±0.09 [0.35-0.68]	0.4±0.08 [0.25-0.57]	20%
adductor magnus	707±124 [489-929]	5.8±0.9 [4.1-7.7]	4.6±0.6 [3.5-5.7]	**26%**	56±9 [38-73]	0.81±0.12 [0.58-1.02]	0.64±0.08 [0.49-0.76]	**25%**
vastus lateralis	1049±180 [737-1420]	8.5±1.1 [6.1-10.5]	6.8±0.8 [5.2-8.3]	**26%**	69±10 [51-90]	1±0.11 [0.78-1.19]	0.83±0.11 [0.62-1]	**20%**
biceps femoris: l.h.	262±41 [170-342]	2.1±0.3 [1.6-2.9]	1.7±0.3 [1.3-2.2]	**26%**	31±6 [21-48]	0.45±0.07 [0.3-0.63]	0.37±0.06 [0.25-0.48]	**24%**
biceps femoris: s.h.	127±32 [79-194]	1±0.2 [0.7-1.4]	0.8±0.2 [0.5-1.2]	26%	10±2 [6-14]	0.14±0.02 [0.09-0.18]	0.11±0.02 [0.07-0.15]	**28%**
adductor longus	202±43 [151-330]	1.6±0.2 [1.4-2.3]	1.3±0.2 [0.9-1.8]	**25%**	19±3 [16-29]	0.28±0.04 [0.23-0.38]	0.22±0.042 [0.13-0.29]	**28%**
pectineus	83±21 [57-141]	0.7±0.1 [0.5-1]	0.5±0.1 [0.3-0.8]	24%	6±1 [4-9]	0.09±0.02 [0.06-0.12]	0.07±0.01 [0.05-0.11]	**19%**
adductor brevis	127±24 [76-173]	1±0.1 [0.6-1.4]	0.8±0.1 [0.6-1.2]	**21%**	13±2 [8-16]	0.18±0.02 [0.13-0.21]	0.16±0.03 [0.12-0.23]	**16%**
semimembr.	297±61 [191-420]	2.4±0.4 [1.8-3.3]	2±0.3 [1.7-2.9]	**20%**	42±7 [32-58]	0.61±0.09 [0.47-0.82]	0.53±0.07 [0.42-0.68]	**15%**

All values given as mean ± s.d. [range]. Normalized volumes are muscle volumes divided by the product of height and mass. PCSA was computed by dividing volumes by lengths and multiplying by muscle length to optimal fiber length ratios found in the literature. Normalized pcsa was computed by dividing PCSA by body mass.

Table 5.1b: Muscle volumes and PCSAs of sprinters and non-sprinters

muscle	sprinter muscle volume (cm^3)	sprinter normalized volume (cm^3/kg-m)	control normalized volume (cm^3/kg-m)	vol. % diff	sprinter muscle pcsa (cm^2)	sprinter normalized pcsa (cm^2/kg)	control normalized pcsa (cm^2/kg)	pcsa % diff
psoas	325±78 [210-502]	2.6±0.4 [2-3.6]	2.2±0.4 [1.6-3.2]	19%	20±4 [13-29]	0.28±0.04 [0.21-0.37]	0.23±0.04 [0.17-0.33]	**25%**
peroneals	144±33 [88-228]	1.2±0.2 [0.9-1.6]	1.1±0.2 [0.8-1.4]	11%	20±4 [14-32]	0.29±0.04 [0.21-0.41]	0.27±0.04 [0.19-0.35]	8%
gluteus medius	353±58 [257-450]	2.9±0.3 [2.5-3.5]	2.6±0.4 [1.7-3.7]	8%	49±7 [39-63]	0.71±0.07 [0.58-0.84]	0.64±0.12 [0.41-0.95]	10%
lateral gastroc.	161±30 [89-220]	1.3±0.2 [0.8-1.6]	1.2±0.2 [0.9-1.8]	7%	24±3 [16-32]	0.35±0.04 [0.25-0.42]	0.32±0.04 [0.25-0.45]	9%
soleus	466±77 [313-595]	3.8±0.6 [2.9-4.8]	3.6±0.5 [2.8-5.2]	6%	119±18 [82-154]	1.72±0.24 [1.31-2.17]	1.73±0.26 [1.33-2.65]	-1%
iliacus	190±43 [141-274]	1.5±0.2 [1.2-2.1]	1.4±0.2 [1.1-1.9]	6%	13±3 [9-19]	0.19±0.03 [0.15-0.27]	0.18±0.03 [0.13-0.23]	5%
medial gastroc.	273±50 [178-351]	2.2±0.3 [1.7-2.9]	2.1±0.3 [1.5-2.7]	4%	54±9 [35-74]	0.78±0.11 [0.58-0.96]	0.71±0.1 [0.52-0.93]	10%
tibialis anterior	139±32 [69-213]	1.1±0.2 [0.7-1.5]	1.1±0.1 [0.8-1.4]	2%	15±3 [8-22]	0.22±0.03 [0.14-0.28]	0.22±0.03 [0.16-0.3]	0%
obturator externus	73±17 [46-109]	0.6±0.1 [0.4-0.8]	0.4±0.1 [0.3-0.6]	**32%**	13±3 [7-22]	0.19±0.04 [0.11-0.34]	0.19±0.08 [0.08-0.35]	1%
piriformis	56±12 [29-80]	0.5±0.1 [0.3-0.7]	0.4±0.1 [0.2-0.6]	28%	7±1 [3-9]	0.1±0.02 [0.04-0.13]	0.08±0.03 [0.05-0.16]	18%
quadratus femoris	40±10 [23-62]	0.3±0.1 [0.2-0.5]	0.3±0.1 [0.2-0.4]	22%	7±1 [4-10]	0.11±0.02 [0.05-0.15]	0.09±0.02 [0.06-0.13]	18%
gemelli	20±4 [11-30]	0.2±0 [0.1-0.2]	0.1±0 [0.1-0.2]	18%	9±3 [5-19]	0.13±0.04 [0.07-0.24]	0.08±0.06 [0.02-0.29]	57%
obturator internus	30±6 [15-40]	0.2±0 [0.1-0.3]	0.2±0.1 [0.1-0.4]	7%	4±1 [2-5]	0.05±0.01 [0.04-0.07]	0.05±0.01 [0.03-0.06]	12%
popliteus	24±6 [13-39]	0.2±0 [0.1-0.3]	0.2±0 [0.1-0.3]	4%	2±1 [2-4]	0.04±0.01 [0.02-0.05]	0.03±0.01 [0.02-0.05]	2%
flexor halluc. longus	80±23 [45-124]	0.6±0.14 [0.4-1]	0.6±0.1 [0.4-0.8]	-1%	16±3 [10-22]	0.23±0.04 [0.16-0.34]	0.24±0.036 [0.16-0.29]	-3%
digital ext. (EDL&EHL)	102±19 [63-140]	0.8±0.13 [0.6-1.1]	0.8±0.1 [0.7-1]	-1%	10±2 [6-13]	0.14±0.02 [0.09-0.18]	0.14±0.02 [0.11-0.18]	-2%
gluteus minimus	103±22 [65-155]	0.8±0.09 [0.6-1]	0.9±0.15 [0.6-1.1]	-3%	8±1 [6-12]	0.11±0.01 [0.09-0.16]	0.12±0.023 [0.07-0.18]	-2%

All values given as mean ± s.d. [range]. Normalized volumes are muscle volumes divided by the product of height and mass. PCSA was computed by dividing volumes by lengths and multiplying by muscle length to optimal fiber length ratios found in the literature. Normalized pcsa was computed by dividing PCSA by body mass.

References

Abel, M.F., Damiano, D.L., Pannunzio, M., Bush, J., 1999. Muscle-tendon surgery in diplegic cerebral palsy: functional and mechanical changes. J. Pediatr. Orthop. 19, 366–375.

Akagi, R., Takai, Y., Ohta, M., Kanehisa, H., Kawakami, Y., Fukunaga, T., 2009. Muscle volume compared to cross-sectional area is more appropriate for evaluating muscle strength in young and elderly individuals. Age Ageing 38, 564–569.

Akima, H., Kawakami, Y., Kubo, K., Sekiguchi, C., Ohshima, H., Miyamoto, A., Fukunaga, T., 2000. Effect of short-duration spaceflight on thigh and leg muscle volume. Med. Sci. Sports Exerc. 32, 1743–1747.

Albright, A.L., 1996. Baclofen in the treatment of cerebral palsy. J. Child Neurol. 11, 77–83.

Alexander, R., Jayes, A.S., Maloiy, G.M.O., Wathuta, E.M., 1979. Allometry of the limb bones of mammals from shrews (Sorex) to elephant (Loxodonta). J. Zool. 189, 305–314.

Alexander, R.M., Jayes, A.S., Maloiy, G.M.O., Wathuta, E.M., 1981. Allometry of the leg muscles of mammals. J. Zool. 194 (4), 539–552.

Anderson, J., Schjerling, P., Saltin, B., 2000. Muscle, Genes and Athletic Performance. Sci. Am. 283: 48–55.

Arnold, E.M., Ward, S.R., Lieber, R.L., Delp, S.L., 2010. A model of the lower limb for analysis of human movement. Ann. Biomed. Eng. 38, 269–279.

Barbour, K.E., Zmuda, J.M., Strotmeyer, E.S., Horwitz, M.J., Boudreau, R., Evans, R.W., Ensrud, K.E., Petit, M.A., Gordon, C.L., Cauley, J.A., Group, O.F. in M. (MrOS) R., 2010. Correlates of trabecular and cortical volumetric bone mineral density of the radius and tibia in older men: the Osteoporotic Fractures in Men Study. J. Bone Miner. Res. 25, 1017–1028.

Barrett, R.S., Lichtwark, G. a, 2010. Gross muscle morphology and structure in spastic cerebral palsy: a systematic review. Dev. Med. Child Neurol. 52, 794–804.

Bax, M., 1964. Terminology and classification of cerebral palsy. Dev. Med. Child Neurol. 6, 295–297.

Bax, M., Goldstein, M., Rosenbaum, P., Leviton, A., Paneth, N., Dan, B., Jacobsson, B., Damiano, D., Palsy, E.C. for the D. of C., 2005. Proposed definition and classification of cerebral palsy, April 2005. Dev. Med. Child Neurol. 47, 571–576.

Biewener, A.A., 1989. Scaling body support in mammals: limb posture and muscle mechanics. Science (80-.). 245, 45–48.

Blemker, S.S., Asakawa, D.S., Gold, G.E., Delp, S.L., 2007. Image-based musculoskeletal modeling: applications, advances, and future opportunities. J. Magn. Reson. Imaging 25, 441–51.

Blemker, S.S., Pinsky, P.M., Delp, S.L., 2005. A 3D model of muscle reveals the causes of nonuniform strains in the biceps brachii. J. Biomech. 38, 657–665.

Bloomfield, S.A., 1997. Changes in musculoskeletal structure and function with prolonged bed rest. Med. Sci. Sport. Exerc. 29(2), 197–206.

Bojsen-Møller, J., Hansen, P., Aagaard, P., Svantesson, U., Kjaer, M., Magnusson, S.P., 2004. Differential displacement of the human soleus and medial gastrocnemius aponeuroses during isometric plantar flexor contractions in vivo. J. Appl. Physiol. 97, 1908–14.

Booth, C.M., Cortina-Borja, M.J.F., Theologis, T.N., 2001. Collagen accumulation in muscles of children with cerebral palsy and correlation with severity of spasticity. Dev. Med. Child Neurol. 43, 314.

Borelli, G., Bernoulli, J., Elinger, N., Joannes a Jesu, C., 1743. De motu animalium. Petrum Gosse.

Boyd, R.N., Hays, R.M., 2001. Current evidence for the use of botulinum toxin type A in the management of children with cerebral palsy: a systematic review. Eur. J. Neurol. 8, 1–20.

Brand, R.A., Crowninshield, R.D., Wittstock, C.E., Pedersen, D.R., Clark, C.R., Van Krieken, F.M., 1982. A model of lower extremity muscular anatomy. J. Biomech. Eng. 104, 304–310.

Brand, R.A., Pedersen, D.R., Friederich, J.A., 1986. The sensitivity of muscle force predictions to changes in physiologic cross-sectional area. J. Biomech. 19, 589–596.

Brooks, S. V, Faulkner, J.A., 1994. Skeletal muscle weakness in old age: underlying mechanisms. Med. Sci. Sports Exerc. 26, 432–439.

Brown, M., Ross, T.P., Holloszy, J.O., 1992. Effects of ageing and exercise on soleus and extensor digitorum longus muscles of female rats. Mech. Ageing Dev. 63, 69–77.

Buford, T.W., Lott, D.J., Marzetti, E., Wohlgemuth, S.E., Vandenborne, K., Pahor, M., Leeuwenburgh, C., Manini, T.M., 2012. Age-related differences in lower extremity tissue compartments and associations with physical function in older adults. Exp. Gerontol. 47, 38–44.

Butler, C., Campbell, S., Adams, R., Abel, M., Chambers, H., Goldstein, M., Leach, J., Darrah, J., Msall, M., Edgar, T., McLaughlin, J., Damiano, D., Stott, N.S., Samson-Fang, L., Logan, L., Albright, L., Armstrong, R., O'Donnell, M., 2000. Evidence of the effects of intrathecal baclofen for spastic and dystonic cerebral palsy. Dev. Med. Child Neurol. 42, 634–645.

Chen, B.B., Shih, T.T., Hsu, C.Y., Yu, C.W., Wei, S.Y., Chen, C.Y., Wu, C.H., 2011. Thigh muscle volume predicted by anthropometric measurements and correlated with physical function in the older adults. J. Nutr. Health Aging 15, 433–438.

Chen, W., Meyer, C.H., 2008. Semiautomatic off-resonance correction in spiral imaging. Magn. Reson. Med. 59, 1212–1219.

Chen, W., Sica, C.T., Meyer, C.H., 2008. Fast conjugate phase image reconstruction based on a Chebyshev approximation to correct for B0 field inhomogeneity and concomitant gradients. Magn. Reson. Med. 60, 1104–1111.

Correa, T.A., Pandy, M.G., 2011. A mass-length scaling law for modeling muscle strength in the lower limb. J. Biomech. 44, 2782–2789.

Costill, D.L., Daniels, J., Evans, W., Fink, W., Krahenbuhl, G., Saltin, B., 1976. Skeletal muscle enzymes and fiber composition in male and female track athletes. J. Appl. Physiol. 40, 149–154.

Croisier, J.-L., Ganteaume, S., Binet, J., Genty, M., Ferret, J.-M., 2008. Strength imbalances and prevention of hamstring injury in professional soccer players: a prospective study. Am. J. Sports Med. 36, 1469–75.

Cromie, M.J., Sanchez, G.N., Schnitzer, M.J., Delp, S.L., 2013. Sarcomere lengths in human extensor carpi radialis brevis measured by microendoscopy. Muscle Nerve 48, 286–92.

Dalmau-Pastor, M., Fargues-Polo, B., Casanova-Martínez, D., Vega, J., Golanó, P., 2014. Anatomy of the Triceps Surae: A Pictorial Essay. Foot Ankle Clin.

Damiano, D.L., 2006. Activity, activity, activity: rethinking our physical therapy approach to cerebral palsy. Phys. Ther. 86, 1534–1540.

Damon, B.M., Ding, Z., Anderson, A.W., Freyer, A.S., Gore, J.C., 2002. Validation of diffusion tensor MRI-based muscle fiber tracking. Magn. Reson. Med. 48, 97–104.

Davids, J.R., Ounpuu, S., DeLuca, P.A., Davis, R.B., 2003. Optimization of walking ability of children with cerebral palsy [WWW Document]. J. Bone Jt. Surg.

De Brito, L.B.B., Ricardo, D.R., de Araújo, D.S.M.S., Ramos, P.S., Myers, J., de Araújo, C.G.S., 2012. Ability to sit and rise from the floor as a predictor of all-cause mortality. Eur. J. Prev. Cardiol. 21, 892–898.

Delp, S.L., Loan, J.P., 2000. A Computational Framework for Simulating and Analyzing Human and Animal Movement. Comput. Sci. Eng. 2, 46–55.

Delp, S.L., Loan, J.P., Hoy, M.G., Zajac, F.E., Topp, E.L., Rosen, J.M., 1990. An Interactive Graphics-Based Model of the Lower Extremity to Study Orthopaedic Surgical Procedures. IEEE Trans. Biomed. Eng. 37, 757–767.

Doherty, T.J., 2003. Invited review: Aging and sarcopenia. J. Appl. Physiol. (Bethesda, Md. 1985) 95, 1717–1727.

Donahue, T.L., Hull, M.L., Rashid, M.M., Jacobs, C.R., 2002. A Finite Element Model of the Human Knee Joint for the Study of Tibio-Femoral Contact. J. Biomech. Eng. 124, 273.

Dorn, T.W., Schache, A.G., Pandy, M.G., 2012. Muscular strategy shift in human running: dependence of running speed on hip and ankle muscle performance. J. Exp. Biol. 215, 1944–56.

Duda, G.N., Brand, D., Freitag, S., Lierse, W., Schneider, E., 1996. Variability of femoral muscle attachments. J. Biomech. 29, 1185–1190.

Elder, G.C., Kirk, J., Stewart, G., Cook, K., Weir, D., Marshall, A., Leahey, L., 2003. Contributing factors to muscle weakness in children with cerebral palsy. Dev. Med. Child Neurol. 45, 542–550.

Epstein, M., Wong, M., Herzog, W., 2006. Should tendon and aponeurosis be considered in series? J. Biomech. 39, 2020–5.

Erdemir, A., McLean, S., Herzog, W., van den Bogert, A.J., 2007. Model-based estimation of muscle forces exerted during movements. Clin. Biomech. (Bristol, Avon) 22, 131–54.

Erskine, R.M., Jones, D.A., Maffulli, N., Williams, A.G., Stewart, C.E., Degens, H., 2011. What causes in vivo muscle specific tension to increase following resistance training? Exp. Physiol. 96, 145–155.

Ferretti, J.L., Cointry, G.R., Capozza, R.F., Capiglioni, R., Chiappe, M.A., 2001. Analysis of biomechanical effects on bone and on the muscle-bone interactions in small animal models. J. Musculoskelet. Neuronal Interact. 1, 263–274.

Fiatarone, M.A., Marks, E.C., Ryan, N.D., Meredith, C.N., Lipsitz, L.A., Evans, W.J., 1990. High-Intensity Strength Training in Nonagenarians. 1Journal Am. Med. Assoc. 263, 3029–3034.

Fiorentino, N.M., Blemker, S.S., 2013. Computational models predict larger muscle tissue strains at faster sprinting speeds. Med.Sci.Sports Exerc. In review.

Foran, J.R.H., Steinman, S., Barash, I., Chambers, H.G., Lieber, R.L., 2005. Review Structural and mechanical alterations in spastic skeletal muscle. Dev. Med. Child Neurol. 47, 713–717.

Franz, J.R., Slane, L.C., Rasske, K., Thelen, D.G., 2014. Non-uniform in vivo deformations of the human Achilles tendon during walking. Gait Posture 1–6.

Friederich, J.A., Brand, R.A., 1990. Muscle fiber architecture in the human lower limb. J. Biomech. 23, 91–95.

Froeling, M., Nederveen, A.J., Heijtel, D.F.R., Lataster, A., Bos, C., Nicolay, K., Maas, M., Drost, M.R., Strijkers, G.J., 2012. Diffusion-tensor MRI reveals the complex muscle architecture of the human forearm. J. Magn. Reson. Imaging 36, 237–48.

Frontera, W.R., Hughes, V.A., Fielding, R.A., Fiatarone, M.A., Evans, W.J., Roubenoff, R., 2000. Aging of skeletal muscle : a 12-yr longitudinal study. J. Appl. Physiol. 88, 1321–1326.

Frost, H.M., 1997. Defining osteopenias and osteoporoses: another view (with insights from a new paradigm). Bone 20, 385–391.

Frost, H.M., 2000. The Utah paradigm of skeletal physiology: an overview of its insights for bone, cartilage and collagenous tissue organs. J. Bone Miner. Metab. 18, 305–316.

Fry, N.R., Gough, M., McNee, A.E., Shortland, A.P., 2007. Changes in the volume and length of the medial gastrocnemius after surgical recession in children with spastic diplegic cerebral palsy. J. Pediatr. Orthop. 27, 769–74.

Fukunaga, T., Miyatani, M., Tachi, M., Kouzaki, M., Kawakami, Y., Kanehisa, H., 2001. Muscle volume is a major determinant of joint torque in humans. Acta Physiol. Scand. 172, 249–255.

Fukunaga, T., Roy, R.R., Shellock, F.G., Hodgson, J.A., Day, M.K., Lee, P.L., Kwong-Fu, H., Edgerton, V.R., 1992. Physiological cross-sectional area of human leg muscles based on magnetic resonance imaging. J. Orthop. Res. 10, 928–934.

Fukunaga, T., Roy, R.R., Shellock, F.G., Hodgson, J.A., Edgerton, V.R., 1996. Specific tension of human plantar flexors and dorsiflexors. J. Appl. Physiol. (Bethesda, Md. 1985) 80, 158–165.

Gage, J.R., 1994. The role of gait analysis in the treatment of cerebral palsy. J. Pediatr. Orthop. 14, 701–702.

Gans, C., 1982. Fiber architecture and muscle function. Exerc. Sport Sci. Rev. 10, 160–207.

Gilles, B., Moccozet, L., Magnenat-Thalmann, N., 2006. Anatomical modelling of the musculoskeletal system from MRI. Med. Image Comput. Comput. Interv., Lecture Notes in Computer Science 4190, 289–296.

Gopalakrishnan, R., Genc, K.O., Rice, A.J., Lee, S.M., Evans, H.J., Maender, C.C., Ilaslan, H., Cavanagh, P.R., 2010. Muscle volume, strength, endurance, and exercise loads during 6-month missions in space. Aviat. Space. Environ. Med. 81, 91–102.

Graham, H.K., Aoki, K.R., Autti-Rämö, I., Boyd, R.N., Delgado, M.R., Gaebler-Spira, D.J., Gormley, M.E., Guyer, B.M., Heinen, F., Holton, A.F., Matthews, D., Molenaers, G., Motta, F., García Ruiz, P.J., Wissel, J., 2000. Recommendations for the use of botulinum toxin type A in the management of cerebral palsy. Gait Posture 11, 67–79.

Gregor, J., Reggie, V., Perrine, J., 1979. Torque-velocity relationships and muscle fiber composition in elite female athletes. J. Appl. Physiol. 47, 388–392.

Handsfield, G.G., Meyer, C.H., Hart, J.M., Abel, M.F., Blemker, S.S., 2014. Relationships of 35 lower limb muscles to height and body mass quantified using MRI. J. Biomech. 47, 631–638.

Herzog, W., Read, L.J., Ter Keurs, H.E., 1991. Experimental determination of force-length relations of intact human gastrocnemius muscles. Clin. Biomech. (Bristol, Avon) 6, 230–8.

Hill, A.V., 1938. The heat of shortening and the dynamic constants of muscle. Proc. R. Soc. London 126, 136–195.

Hirakoba, K., Yunoki, T., 2002. Blood Lactate Changes during Isocapnic Buffering in Sprinters and Long Distance Runners. J. Physiol. Anthropol. Appl. Human Sci. 21, 143–149.

Holten, M.K., Zacho, M., Gaster, M., Juel, C., Wojtaszewski, J.F.P., Dela, F., 2004. Uptake , GLUT4 Content , and Insulin Signaling in Skeletal Muscle in Patients With Type 2 Diabetes. Diabetes 53, 294–305.

Holzbaur, K.R., Delp, S.L., Gold, G.E., Murray, W.M., 2007a. Moment-generating capacity of upper limb muscles in healthy adults. J. Biomech. 40, 2442–2449.

Holzbaur, K.R., Murray, W.M., Gold, G.E., Delp, S.L., 2007b. Upper limb muscle volumes in adult subjects. J. Biomech. 40, 742–749.

Hunt, D.R., Rowlands, B.J., Johnston, D., 1985. Hand Grip Strength-- A Simple Prognostic Indicator in Surgical Patients. J. Parenter. Enter. Nutr. 9, 701–704.

Infantolino, B.W., 2012. Pennation angle variability in human whole muscle. In: Challis, John H.

Ishikawa, M., Komi, P. V, Grey, M.J., Lepola, V., Bruggemann, G.-P., 2005. Muscle-tendon interaction and elastic energy usage in human walking. J. Appl. Physiol. 99, 603–8.

Ito, J., Araki, A., Tanaka, H., Tasaki, T., 1996. Muscle histopathology in spastic cerebral palsy. Brain Dev. 18, 299–303.

Johnson, D.L., Miller, F., Subramanian, P., Modlesky, C.M., 2009. Adipose Tissue Infiltration of Skeletal Muscle in Children with Cerebral Palsy. J. Pediatr. 154, 715–720.e1.

Kastelic, J., Galeski, A., Baer, E., 1978. The multicomposite structure of tendon. Connect. Tissue Res. 6, 11–23.

Kawakami, Y., Akima, H., Kubo, K., Muraoka, Y., Hasegawa, H., Kouzaki, M., Imai, M., Suzuki, Y., Gunji, A., Kanehisa, H., Fukunaga, T., 2001. Changes in muscle size, architecture, and neural activation after 20 days of bed rest with and without resistance exercise. Eur. J. Appl. Physiol. 84, 7–12.

Kawakami, Y., Muraoka, Y., Kubo, K., Suzuki, Y., Fukunaga, T., 2000. Changes in muscle size and architecture following 20 days of bed rest. J. Gravit. Physiol. 7, 53–59.

Kim, P.J., Martin, E., Ballehr, L., Richey, J.-M., Steinberg, J.S., 2011. Variability of insertion of the Achilles tendon on the calcaneus: an MRI study of younger subjects. J. Foot Ankle Surg. 50, 41–3.

Kramer, P.A., Sylvester, A.D., 2013. Humans, geometric similarity and the Froude number: is reasonably close'' really close enough? Biol. Open 2, 111–120.

Kubo, K., Kawakami, Y., Kanehisa, H., Fukunaga, T., 2002. Measurement of viscoelastic properties of tendon structures in vivo. Scand. J. Med. Sci. Sport. 12, 3–8.

Kumagai, K., Abe, T., Brechue, W.F., Ryushi, T., Takano, S., Mizuno, M., 2000. Sprint performance is related to muscle fascicle length in male 100-m sprinters. J. Appl. Physiol. 88, 811–816.

LeBlanc, A., Lin, C., Shackelford, L., Sinitsyn, V., Evans, H., Belichenko, O., Schenkman, B., Kozlovskaya, I., Oganov, V., Bakulin, A., Hedrick, T., Feeback, D., 2000. Muscle volume, MRI relaxation times (T2), and body composition after spaceflight. J Appl Physiol 89, 2158–2164.

Lee, R.C., Wang, Z., Heo, M., Ross, R., Janssen, I., Heymsfield, S.B., 2000. Total-body skeletal muscle mass: development and cross-validation of anthropometric prediction models. Am. J. Clin. Nutr. 72, 796–803.

Lee, S.S., Piazza, S.J., 2009. Built for speed: musculoskeletal structure and sprinting ability. J. Exp. Biol. 212, 3700–3707.

Lichtwark, G. a, Wilson, a M., 2005. In vivo mechanical properties of the human Achilles tendon during one-legged hopping. J. Exp. Biol. 208, 4715–25.

Lieber, R.L., 2002. Skeletal Muscle Structure, Function, and Plasticity: The Physiological Basis of Rehabilitation. Lippincott Williams and Wilkin, Baltimore, Philadelphia.

Lieber, R.L., Friden, J., 2000. Functional and clinical significance of skeletal muscle architecture. Muscle Nerve 23, 1647–1666.

Lieber, R.L., Friden, J., 2003. Spastic Muscle Cells are Shorter and Stiffer than Normal Cells. Muscle Nerve 27, 157–164.

Liu, M.Q., Anderson, F.C., Pandy, M.G., Delp, S.L., 2006. Muscles that support the body also modulate forward progression during walking. J. Biomech. 39, 2623–2630.

Llewellyn, M.E., Barretto, R.P.J., Delp, S.L., Schnitzer, M.J., 2008. Minimally invasive high-speed imaging of sarcomere contractile dynamics in mice and humans. Nature 454, 784–8.

Maffulli, N., 1999. Current Concepts Review Rupture of the Achilles Tendon *. J. Bone Jt. Surg. 81, 1019–1036.

Maffulli, N., Sharma, P., Luscombe, K.L., 2004. Achilles tendinopathy: aetiology and management. JRSM 97, 472–476.

Maganaris, C.N., 2003. Force-length characteristics of the in vivo human gastrocnemius muscle. Clin. Anat. 16, 215–23.

Maganaris, C.N., Baltzopoulos, V., Ball, D., Sargeant, A.J., 2001. In vivo specific tension of human skeletal muscle. J. Appl. Physiol. (Bethesda, Md. 1985) 90, 865–872.

Maganaris, C.N., Baltzopoulos, V., Sargeant, A.J., 2000. In vivo measurement-based estimations of the human Achilles tendon moment arm. Eur. J. Appl. Physiol. 83, 363–369.

Maganaris, C.N., Paul, J.P., 2002. Tensile properties of the in vivo human gastrocnemius tendon. J. Biomech. 35, 1639–1646.

Malaiya, R., McNee, A.E., Fry, N.R., Eve, L.C., Gough, M., Shortland, A.P., 2007. The morphology of the medial gastrocnemius in typically developing children and children with spastic hemiplegic cerebral palsy. J. Electromyogr. Kinesiol. 17, 657–63.

McLaughlin, J., Bjornson, K., Temkin, N., Steinbok, P., Wright, V., Reiner, A., Roberts, T., Drake, J., O'Donnell, M., Rosenbaum, P., Barber, J., Ferrel, A., 2002. Selective dorsal rhizotomy: meta-analysis of three randomized controlled trials. Dev. Med. Child Neurol. 44, 17.

McLaughlin, J.F., Bjornson, K.F., Astley, S.J., Graubert, C., Hays, R.M., Roberts, T.S., Price, R., Temkin, N., 2008. Selective dorsal rhizotomy: efficacy and safety in an investigator-masked randomized clinical trial. Dev. Med. Child Neurol. 40, 220–232.

McMahon, T., 1973. Size and shape in biology: Elastic criteria impose limits on biological proportions, and consequently on metabolic rates. Science (80-.). 179, 1201–1204.

Meyer, C.H., Hu, B.S., Nishimura, D.G., Macovski, A., 1992. Fast spiral coronary artery imaging. Magn. Reson. Med. 28, 202–213.

Meyer, C.H., Pauly, J.M., Macovski, A., Nishimura, D.G., 1990. Simultaneous spatial and spectral selective excitation. Magn. Reson. Med. 15, 287–304.

Mian, O.S., Thom, J.M., Ardigò, L.P., Minetti, a E., Narici, M. V, 2007. Gastrocnemius muscle-tendon behaviour during walking in young and older adults. Acta Physiol. (Oxf). 189, 57–65.

Miller, A.E.J., MacDougall, J.D., Tarnopolsky, M.A., Sale, D.G., 1993. Gender differences in strength and muscle fiber characteristics. J. Appl. Physiol. 66, 254–262.

Milz, S., Rufai, a., Buettner, a., Putz, R., Ralphs, J.R., Benjamin, M., 2002. Three-dimensional reconstructions of the Achilles tendon insertion in man. J. Anat. 200, 145–152.

Mitsiopoulos, N., Baumgartner, R.N., Heymsfield, S.B., Lyons, W., Gallagher, D., Ross, R., 1998. Cadaver validation of skeletal muscle measurement by magnetic resonance imaging and computerized tomography. J. Appl. Physiol. 85, 115–122.

Mohagheghi, A. a, Khan, T., Meadows, T.H., Giannikas, K., Baltzopoulos, V., Maganaris, C.N., 2007. Differences in gastrocnemius muscle architecture between the paretic and non-paretic legs in children with hemiplegic cerebral palsy. Clin. Biomech. 22, 718–24.

Moreau, N.G., Simpson, K.N., Teefey, S.A., Damiano, D.L., 2010. Muscle architecture predicts maximum strength and is related to activity levels in cerebral palsy. Phys. Ther. 90, 1619–1630.

Mutch, L., Alberman, E., Hagberg, B., Kodama, K., Perat, M.V., 1992. Cerebral palsy epidemiology: where are we now and where are we going? Dev. Med. Child Neurol. 34, 547–551.

Nadler, S.F., Malanga, G. a., Feinberg, J.H., Prybicien, M., Stitik, T.P., DePrince, M., 2001. Relationship Between Hip Muscle Imbalance and Occurrence of Low Back Pain in Collegiate Athletes. Am. J. Phys. Med. Rehabil. 80, 572–577.

Narayanan, U.G., 2007. The role of gait analysis in the orthopaedic management of ambulatory cerebral palsy. Curr. Opin. Pediatr. 19, 38–43.

Narayanan, U.G., 2012. Management of children with ambulatory cerebral palsy: an evidence-based review. J. Pediatr. Orthop. 32, S172–S181.

Narici, M., 1999. Human skeletal muscle architecture studied in vivo by non-invasive imaging techniques: functional significance and applications. J. Electromyogr. Kinesiol. 9, 97–103.

Narici, M. V, Maffulli, N., Maganaris, C.N., 2008. Ageing of human muscles and tendons. Disabil. Rehabil. 30, 1548–54.

Narici, M. V, Maganaris, C.N., Reeves, N.D., Capodaglio, P., 2003. Effect of aging on human muscle architecture. J. Appl. Physiol. (Bethesda, Md. 1985) 95, 2229–2234.

Nevill, A.M., 1994. The need to scale for differences in body size and mass: an explanation of Kleiber's 0.75 mass exponent. J. Appl. Physiol. (Bethesda, Md. 1985) 77, 2870–2873.

Nevill, A.M., Stewart, A.D., Olds, T., Holder, R., 2004. Are adult physiques geometrically similar? The dangers of allometric scaling using body mass power laws. Am. J. Phys. Anthropol. 124, 177–182.

Nishimura, D.G., 2010. Principles of Magnetic Resonance Imaging.

Noble, J.J., Fry, N.R., Lewis, A.P., Keevil, S.F., Gough, M., Shortland, A.P., 2014. Lower limb muscle volumes in bilateral spastic cerebral palsy. Brain Dev. 36, 294–300.

Oberhofer, K., Stott, N.S., Mithraratne, K., Anderson, I. a, 2010. Subject-specific modelling of lower limb muscles in children with cerebral palsy. Clin. Biomech. (Bristol, Avon) 25, 88–94.

Rahnama, N., Lees, A., Bambaecichi, E., 2005. A comparison of muscle strength and flexibility between the preferred and non-preferred leg in English soccer players. Ergonomics 48, 1568–75.

Ramsay, J.W., Barrance, P.J., Buchanan, T.S., Higginson, J.S., 2011. Paretic muscle atrophy and non-contractile tissue content in individual muscles of the post-stroke lower extremity. J. Biomech. 44, 2741–2746.

Rashevsky, N., 1955. Organic form as determined by function. Ann. NY Acad. Sci. 63, 442–453.

Rehorn, M.R., Blemker, S.S., 2010. The effects of aponeurosis geometry on strain injury susceptibility explored with a 3D muscle model. J. Biomech. 43, 2574–2581.

Reid, S.L., Pitcher, C.A., Williams, S.A., Licari, M.K., Valentine, J.P., Shipman, P.J., Elliott, C.M., 2014. Does muscle size matter? The relationship between muscle size and strength in children with cerebral palsy. Disabil. Rehabil.

Ries, A.J., Novacheck, T.F., Schwartz, M.H., 2014. A data driven model for optimal orthosis selection in children with cerebral palsy. Gait Posture 40, 539–544.

Roberts, T.J., 2002. The integrated function of muscles and tendons during locomotion . Comp. Biochem. Physiol. 133, 1087–1099.

Roberts, T.J., Kram, R., Weyand, P.G., Taylor, C.R., 1998. Energetics of bipedal running. I. Metabolic cost of generating force. J. Exp. Biol. 201, 2745–2751.

Robling, A.G., 2009. Is bone's response to mechanical signals dominated by muscle forces? Med. Sci. Sports Exerc. 41, 2044–2049.

Rose, J., Haskell, W.L., Gamble, J.G., Hamilton, R.L., Brown, D. a, Rinsky, L., 1994. Muscle pathology and clinical measures of disability in children with cerebral palsy. J. Orthop. Res. 12, 758–68.

Rosenbaum, P., Paneth, N., Leviton, A., Goldstein, M., Bax, M., Damiano, D., Dan, B., Jacobsson, B., 2007. A report: the definition and classification of cerebral palsy April 2006. Dev. Med. Child Neurol. Suppl. 109, 8–14.

Ross, A., Leveritt, M., Riek, S., 2001. Neural Influences on Sprint Running Training Adaptations and Acute Responses. Sport. Med. 31, 409–425.

Rosset, A., Spadola, L., Ratib, O., 2004. OsiriX: an open-source software for navigating in multidimensional DICOM images. J. Digit. Imaging 17, 205–16.

Rubenson, J., Pires, N.J., Loi, H.O., Pinniger, G.J., Shannon, D.G., 2012. On the ascent: the soleus operating length is conserved to the ascending limb of the force-length curve across gait mechanics in humans. J. Exp. Biol. 215, 3539–51.

Sacks, R.D., Roy, R.R., 1982. Architecture of the hind limb muscles of cats: functional significance. J. Morphol. 173, 185–195.

Sale, D.G., Martin, J.E., Moroz, D.E., 1992. Hypertrophy without increased isometric strength after weight training. Eur. J. Appl. Physiol. 64, 51–55.

Sarrafian, S.K., 1993. Calcaneal (achilles) tendon. In: Anatomy of the Foot and Ankle: Descriptive Topographic Functional. J.B. Lippincott Company, Philadelphia, pp. 280–282.

Sasaki, K., Neptune, R.R., 2006. Muscle mechanical work and elastic energy utilization during walking and running near the preferred gait transition speed. Gait Posture 23, 383–90.

Sayer, A.A., Dennison, E.M., Syddall, H.E., Gilbody, H.., Phillips, D.I.W., Cooper, C., 2005. Type 2 Diabetes, Muscle Strength, and Impaired Physical Function. Diabetes Care 28, 2541–2542.

Scheys, L., Loeckx, D., Spaepen, A., Suetens, P., Jonkers, I., 2009. Atlas-based non-rigid image registration to automatically define line-of-action muscle models: A validation study. J. Biomech. 42, 565–572.

Schoenau, E., 2005. From mechanostat theory to development of the "Functional Muscle-Bone-Unit." J. Musculoskelet. Neuronal Interact. 5, 232–238.

Screen, H.R.C., Lee, D. a, Bader, D.L., Shelton, J.C., 2004. An investigation into the effects of the hierarchical structure of tendon fascicles on micromechanical properties. Proc. Inst. Mech. Eng. Part H J. Eng. Med. 218, 109–119.

Sharafi, B., Ames, E.G., Holmes, J.W., Blemker, S.S., 2011. Strains at the myotendinous junction predicted by a micromechanical model. J. Biomech. 44, 2795–2801.

Shim, V.B., Fernandez, J.W., Gamage, P.B., Regnery, C., Smith, D.W., Gardiner, B.S., Lloyd, D.G., Besier, T.F., 2014. Subject-specific finite element analysis to characterize the influence of geometry and material properties in Achilles tendon rupture. J. Biomech. 47, 3598–3604.

Shimegi, S., Yanagita, M., Okano, H., Yamada, M., Fukui, H., Fukumura, Y., Ibuki, Y., Kojima, I., 1994. Physical Exercise Increases Bone Mineral Density in Postmenopausal Women. Endocr. J. 41, 49–56.

Shortland, A.P., Harris, C. a, Gough, M., Robinson, R.O., 2002. Architecture of the medial gastrocnemius in children with spastic diplegia. Dev. Med. Child Neurol. 44, 158.

Siegler, S., Block, J., Schneck, C.D., 1988. The Mechanical Characteristics of the Collateral Ligaments of the Human Ankle Joint. Foot Ankle 8, 234–242.

Skaggs, D.L., Rethlefsen, S.A., Kay, R.M., Dennis, S.W., Rynolds, R.A., Tolo, V.T., 2000. Variability in gait analysis interpretation. J. Pediatr. Orthop. 20, 759–764.

Slane, L.C., Thelen, D.G., 2014. Non-uniform displacements within the Achilles tendon observed during passive and eccentric loading. J. Biomech. 47, 2831–5.

Smith, L.R., Lee, K.S., Ward, S.R., Chambers, H.G., Lieber, R.L., 2011. Hamstring contractures in children with spastic cerebral palsy result from a stiffer extracellular matrix and increased in vivo sarcomere length. J. Physiol. 589, 2625–39.

Stanley, F., Alberman, E.D., Blair, E., 2000. Cerebral palsies: epidemiology and causal pathways. Mac Keith, London.

Steele, K.M., Seth, A., Hicks, J.L., Schwartz, M.S., Delp, S.L., 2010. Muscle contributions to support and progression during single-limb stance in crouch gait. J. Biomech. 43, 2099–105.

Steele, K.M., van der Krogt, M.M., Schwartz, M.H., Delp, S.L., 2012. How much muscle strength is required to walk in a crouch gait? J. Biomech. 45, 2564–9.

Studenski, S., Faulkner, K., Inzitari, M., Brach, J., Chandler, J., Cawthon, P., Connor, E.B., Kritchevsky, S., Badinelli, S., Harris, T., Newman, A.B., Ferrucci, L., Guralnik, J., 2011. Gait Speed and Survival in Older Adults. J. Am. Med. Assoc. 305, 50–58.

Szaro, P., Witkowski, G., Smigielski, R., Krajewski, P., Ciszek, B., 2009. Fascicles of the adult human Achilles tendon - an anatomical study. Ann. Anat. 191, 586–593.

Tate, C.M., Williams, G.N., Barrance, P.J., Buchanan, T.S., 2006. Lower Extremity Muscle Morphology in Young Athletes: An MRI-Based Analysis. Med. Sci. Sport. Exerc. 38, 122–128.

Thorpe, C.T., Udeze, C.P., Birch, H.L., Clegg, P.D., Screen, H.R., 2013. Capacity for sliding between tendon fascicles decreases with ageing in injury prone equine tendons: a possible mechanism for age-related tendinopathy? Eur. Cell. Mater. 25, 48–60.

Tisdale, M.J., 2010. Cancer cachexia. Curr. Opin. Gastroenterol. 26, 146–151.

Trappe, S.W., Trappe, T.A., Lee, G.A., Costill, D.L., 2001. Calf muscle strength in humans. Int. J. Sports Med. 22, 186–191.

Vidt, M.E., Daly, M., Miller, M.E., Davis, C.C., Marsh, A.P., Saul, K.R., 2011. Characterizing upper limb muscle volume and strength in older adults: A comparison with young adults. J. Biomech.

Von Forell, G. a, Bowden, A.E., 2014. A damage model for the percutaneous triple hemisection technique for tendo-achilles lengthening. J. Biomech. 47, 3354–60.

Wang, J.H.-C., 2006. Mechanobiology of tendon. J. Biomech. 39, 1563–82.

Ward, S., Eng, C., Smallwood, L., Lieber, R., 2009. Are Current Measurements of Lower Extremity Muscle Architecture Accurate? Clin. Orthop. Relat. Res. 467, 1074–1082.

Weiss, J.A., Maker, B.N., Govindjee, S., 1996. Finite element implementation of incompressible, transversely isotropic hyperelasticity. Comput. Methods Appl. Mech. Eng. 135, 107–128.

Wetzsteon, R.J., Zemel, B.S., Shults, J., Howard, K.M., Kibe, L.W., Leonard, M.B., 2011. Mechanical loads and cortical bone geometry in healthy children and young adults. Bone 48, 1103–1108.

White, J.W., 1943. Torsion of the Achilles tendon: its surgical significance. Arch. Surg. 46, 784.

White, S.C., Yack, H.J., Winter, D.A., 1989. A three-dimensional musculoskeletal model for gait analysis. Anatomical variability estimates. J. Biomech. 22, 885–893.

Wickiewicz, T.L., Roy, R.R., Powell, P.L., Edgerton, V.R., 1983. Muscle architecture of the human lower limb. Clin. Orthop. Relat. Res. (179), 275–283.

Winter, D.A., 1980. Overall principle of lower limb support during stance phase of gait. J. Biomech. 13, 923–927.

Wisdom, K.M., Delp, S.L., Kuhl, E., 2014. Use it or lose it: multiscale skeletal muscle adaptation to mechanical stimuli. Biomech. Model. Mechanobiol.

Wright, F.V., Sheil, E.M.H., Drake, J.M., Wedge, J.H., Naumann, S., 2008. Evaluation of selective dorsal rhizotomy for the reduction of spasticity in cerebral palsy: a randomized controlled trial. Dev. Med. Child Neurol. 40, 239–247.

Zajac, F.E., 1989. Muscle and tendon: properties, models, scaling, and application to biomechanics and motor control. Crit. Rev. Biomed. Eng. 17, 359–411.